Effect of *Fgf10* deficiency on mouse lung development and in a mouse model of bronchopulmonary dysplasia

Inaugural Dissertation

submitted to the

Faculty of Medicine

in partial fulfillment of the requirements

for the PhD-Degree

of the Faculties of Veterinary Medicine and Medicine

of the Justus Liebig University Giessen

by

Chao, Cho-Ming

of

Saigon, Vietnam

Giessen 2017

From the Department of Internal Medicine II and

Excellence Cluster Cardio-Pulmonary System (ECCPS)

of the Faculty of Medicine of the Justus Liebig University Giessen

Director / Chairman: Prof. Dr. Werner Seeger

First Supervisor and Committee Member: Prof. Dr. Saverio Bellusci

Second Supervisor: Prof. Dr. Emma Rawlins

Committee Member (Chair): Prof. Dr. Klaus-Dieter Schlüter

Committee Member: Prof. Dr. Klaus-Peter Zimmer

Committee Member: Prof. Dr. Robbert J. Rottier

Date of Doctoral Defense: 27th of April 2017

Dedicated to my family, my friends and my mice!

Declaration

"I declare that I have completed this dissertation single-handedly without the unauthorized help of a second party and only with the assistance acknowledged therein. I have appropriately acknowledged and referenced all text passages that are derived literally from or are based on the content of published or unpublished work of others, and all information that relates to verbal communications. I have abided by the principles of good scientific conduct laid down in the charter of the Justus Liebig University of Giessen in carrying out the investigations described in the dissertation."

_____

Cho-Ming Chao

Table of Contents

List of Tables

List of Figures

Abbreviations and Acronyms

α-SMA	α-Smooth Muscle Actin
ADRP	Adipose differentiation-related protein
AEC I	Alveolar epithelial cell type I
AEC II	Alveolar epithelial cell type II
ALSG	Aplasia of lacrimal and salivary glands
BADJ	Broncho-alveolar duct junction
BMP 4	Bone morphogenetic protein 4
BPD	Bronchopulmonary dysplasia
BSA	Bovine serum albumin
CCSP	Club cell secretary protein
COPD	Chronic obstructive pulmonary disease
E	Embryonic
ETV5	Ets Variant 5
FEV1	Forced expiratory volume in one second
FGF10	Fibroblast growth factor
FGFR	Fibroblast growth factor receptor
GFP	Green fluorescent protein
GLI1	Glioma-Associated Oncogene 1
HBSS	Hanks balanced salt solution
HOX	Hyperoxia
HRP	Horseradish peroxidase

ID2	Inhibitor of differentiation 2
ISL1	Insulin gene enhancer protein ISL-1
IVC	Inspiratory vital capacity
LADD	Lacrimo-auriculo-dento-digital syndrome
LIF	Lipofibroblast
MYF	Myofibroblast
NF-κB	Nuclear factor 'kappa-light-chain-enhancer' of activated B-cells
NOX	Normoxia
P	Postnatal
PBS	Phosphate-buffered saline
PDGF	Platelet derived growth factor
PDPN	Podoplanin
PECAM	Platelet endothelial cell adhesion molecule
PFA	Paraformaldehyde
PPARγ	Peroxisome proliferator-activated receptor gamma
PTHRP	Parathyroid hormone-related protein
RA	Retinoid acid
SCGB1A1	Secretoglobin, Family1A, Member 1
SDS	Sodium dodecyl sulfate
SEM	Subepithelial mesenchyme
SFTPC	Surfactant protein C
SFTPB	Surfactant protein B
SHH	Sonic hedgehog

SMM	Submesothelial mesenchyme
SOX 9	SRY (sex determining region Y)-box 9
SP1	Specificity Protein 1
SPRY 2	Sprouty 2
TAE	TRIS-Acetate-EDTA
TBS-T	TRIS-buffered saline with Tween 20
TGF-β1	Transforming growth factor β-1
TLR	Toll-like receptor
VEGF	Vascular endothelial growth factor
VEGFR	Vascular endothelial growth factor receptor
WNT	Wingless and int

1. Introduction

1.1. Lung development

The lung is a complex ramified organ, which develops through continuous branching during embryonic development. The elaborate interaction amongst the epithelium, mesenchyme, mesothelium and endothelium via an intricate signaling network controls the amplification, proliferation, migration and differentiation of many progenitor cells to populate these different compartments.

1.1.1. Lung development: human compared to mouse

In human and mouse, the lung arises from two germ layers during early embryonic development; the gut endoderm gives rise to the lung epithelium and the splanchnic mesoderm is the origin of the lung mesenchyme. The human lung consists of three lobes on the right and two lobes on the left side. In contrast, mice have four lobes on the right (cranial, medial, caudal and accessory lobe) and one on the left side. In human lungs 23 airway generations have been observed but in mice only 12.

In humans, lung development begins after four weeks gestation. From the laryngo-tracheal groove, the ventral wall of the caudal primitive foregut starts to grow and forms a sac-like structure. During subsequent growth of the lung, the prospective trachea separates from the foregut by the formation of the so-called tracheo-esophageal septum. The most distal part of the tracheal tube divides into two buds, which will form the right and left primary bronchial buds. These primary buds are further ramified to form three secondary bronchial buds on the right and two secondary bronchial buds on the left side. These buds are the origin of the five lobes in the mature lung (Moore et al., 2002).

In mice, at embryonic day 8 (E8), signaling molecules from the cardiac mesoderm like growth factors FGF1 and FGF2 among others, specify the prospective lung field in the primitive foregut endoderm, which expresses the transcription factor *Nkx2.1* (or *Ttf1*). These NKX2.1-positive cells are the so-called pluripotent epithelial cells of the lung. At E9.5, similar to what has been observed in humans, the ventral foregut endoderm evaginates and elongates caudally, dividing into two buds that form the prospective trachea and the two main bronchi. The whole

process of lung development in humans and mice can be divided into four histologically distinguishable stages. The first stage is called pseudoglandular stage, followed by the canalicular stage and the saccular stage. Lung development finishes with the alveolar stage, which in humans starts prenatally but in mice postnatally (Figure 1). According to the developmental processes, lung development is split into the branching morphogenesis program from E9.5 until E16.5, followed by the alveolar epithelial differentiation program (Chang et al., 2013).

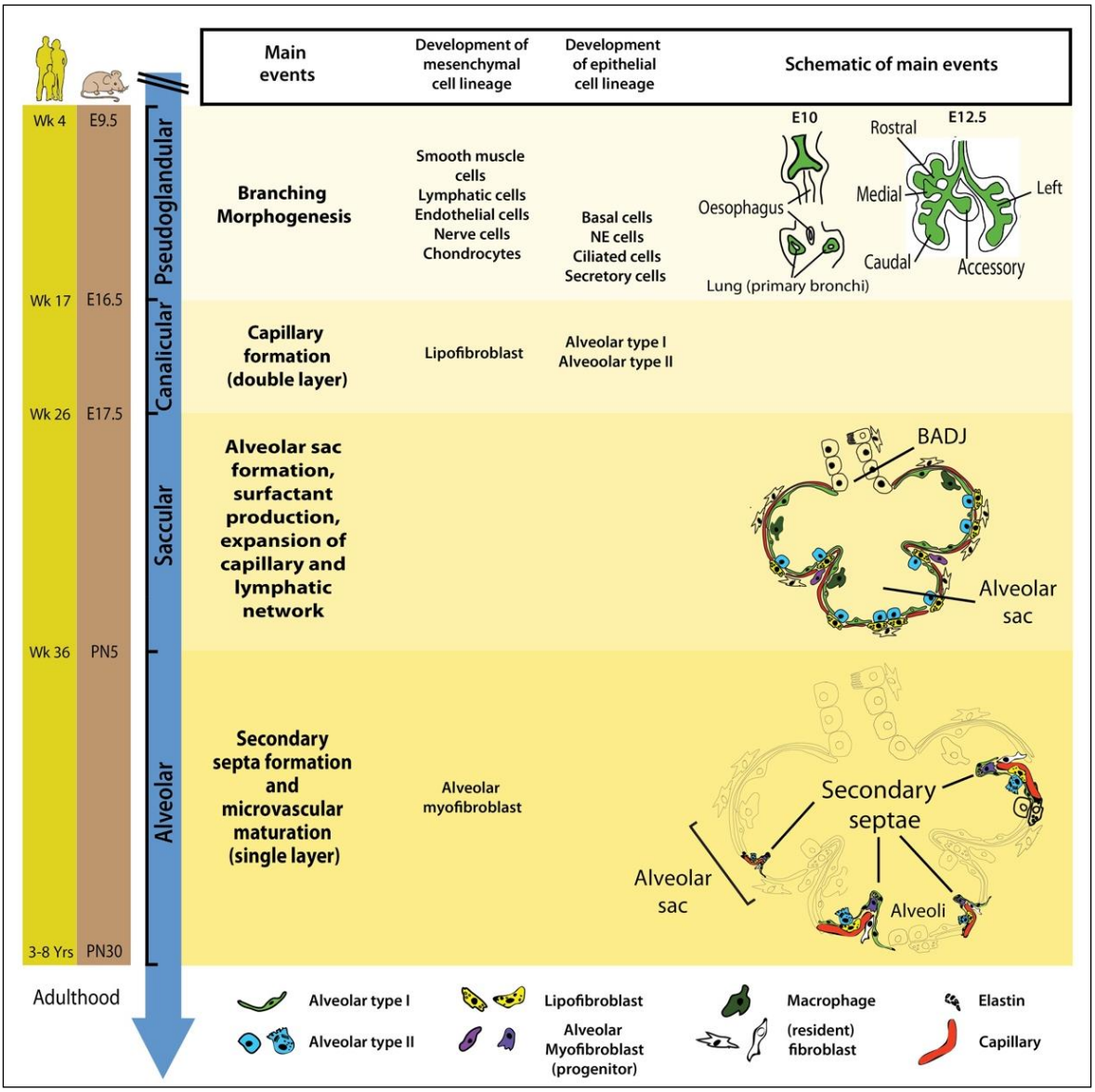

Figure 1. Timeline and stages of lung development in mice and humans.

Lung development starts with the specification of the lung domain in the foregut endoderm followed by the formation of primary lung buds. These buds will later give rise to the respiratory tree via the process of branching morphogenesis. The latter is a characteristic of the pseudoglandular stage of lung development. Most epithelial and mesenchymal cell types start to form during the pseudoglandular stage. The canalicular stage is characterized by blood capillary formation and the appearance of AECI/II. During the saccular stage, primitive alveoli (sac-like structures) start to form and this is accompanied by surfactant production and the expansion of capillary and lymphatic networks. The alveolar stage of lung development starts in utero in humans, whereas in mice, it starts postnatally (Chao et al., 2015).

Wk: week; E: embryonic; PN: postnatal; NE: neuroendocrine

The first stage is termed the pseudoglandular stage and takes place from embryonic week 4 until 17 in humans and from E9.5 until E16.5 in mice. During this stage the process of branching morphogenesis generates the basic tree-like structure of the lung including the conducting airways and the numerous terminal bronchioles surrounded by thick mesenchyme. At the same time, epithelial cell progenitors differentiate to basal, neuroendocrine, ciliated and secretory cells. The mesodermal lung compartment serves as progenitors for the smooth muscle, lymphatic, endothelial, nerve and chondrocytic cells. Importantly, most of the epithelial and mesenchymal cell types in the lung are formed during the late pseudoglandular stage (E13.5-E16.5). Accordingly, any injurious process present prenatally (e.g. inflammations due to chorioamnionitis) interfering with normal lung development at that time, could lead to disturbed formation of these two important compartments resulting in impaired pulmonary function postnatally.

In the next stage, called the canalicular stage (human: week 17-26; mouse: E16.5-E17.5), the respiratory bronchioles continue subdividing into smaller units, which consist of a primitive respiratory epithelium competent of gas exchange. This respiratory epithelium arises from differentiation of distal lung epithelial progenitors.

It has been shown that type I and type II alveolar epithelial cells (AEC I and II) emerge from a common alveolar bipotential progenitor (Treutlein et al., 2014). Concurrently, the mesenchyme surrounding the epithelium becomes thinner due to mesenchymal cell apoptosis (Kresch et al., 1998). Furthermore, another characteristic of this stage is the massive formation of a double-layer capillary network. In mice, interstitial fibroblasts containing cytoplasmic lipid droplets (so called lipofibroblast, LIF) emerge in the mesenchyme.

The saccular stage of lung development occurs approximately between 26 weeks and 36 weeks of gestation. In contrast, in mice this stage starts prenatally at E17.5 and ends postnatally at PN5. The main events during this stage are the formation of alveolar sacs, surfactant protein production and further thinning of the mesenchyme to facilitate gas exchange between the intraalveolar airspace and the capillaries located in the mesenchyme. Furthermore, expansion of the capillary and lymphatic networks continues.

The last stage of lung development is termed the alveolar stage (human: ~weeks 36 – 8 years; mouse: PN5-PN30). During this stage, the alveolar surface area increases massively at the expense of the mesenchyme through subdividing the alveolar sacs (also called primitive alveoli) into mature alveoli by secondary septa formation. This process is named alveolarization (or alveologenesis) and requires the interaction of many cell types located in the epithelium and the mesenchyme (Table 1).

Table 1. Overview of cells relevant for alveologenesis (Chao et al., 2016).

Name of cell	Name of progenitor cell	Localization of cell	Function of cell for alveologenesis	Interaction with other cells
Alveolar epithelial cell type I (AEC I)	Bipotent progenitor (SFTPC+, PDPN+) (Treutlein et al., 2014)	Epithelium	Providing the majority of alveolar surface area	AEC II (during regeneration) (Desai et al., 2014)
Alveolar epithelial cell type II (AEC II)	Bipotent progenitor (SFTPC+, PDPN+) (Treutlein et al., 2014)	Epithelium, close proximity to lipofibroblast	Surfactant production, transdifferentiation to AEC I after lung injury (Desai et al., 2014)	Formation and maintenance of Lipofibroblast via PTHRP (parathyroid hormone-related protein)/PPARγ (peroxisome proliferator-activated receptor gamma) signaling pathway (Schultz et al., 2002; Torday & Rehan, 2002)

Name of cell	**Name of progenitor cell**	**Localization of cell**	**Function of cell for alveologenesis**	**Interaction with other cells**
Alveolar myofibroblast	Alveolar myofibroblast progenitor; PDGFRα+ LIF (to be validated) (Perl & Gale, 2009)	Mesenchyme, tip of growing secondary septa	Deposition of Elastin in the apex of secondary septa and secondary septa formation (Noguchi et al., 1989; Vaccaro & Brody, 1978)	not known
Lipofibroblast	FGF10+ mesenchymal cell (El Agha et al., 2014; Al Alam et al., 2015a)	Mesenchyme, close proximity to AEC II	Secretion of triglycerides and leptin for AEC II (Torday & Rehan, 2002) postnatal niche for AEC II (Barkauskas et al., 2013)	AEC II (Schultz et al., 2002; Torday & Rehan, 2002), Epithelium (PDGFA) (Torday et al., 1995)
Endothelial cell	Endothelial progenitor cell (hemangioblasts)	Subepithelial mesenchyme (SEM)	Angio-/vasculogenesis important for alveologenesis (Thebaud et al., 2005)	Epithelium (Lazarus et al., 2011; Del Moral et al., 2006)

Secondary septa formation starts with the deposition of elastin in primary septa (wall of alveolar sacs) and subsequently secondary septa emerge at the place of elastin and elongate towards the alveolar sac airspace to subdivide it into the smallest respiratory units of the lung – the mature alveoli (Figure 2). Importantly, concomitant with this process, primary septa, still containing a double layer of capillaries, become thinner and a single capillary network emerges which allows more efficient gas exchange (microvascular maturation). In humans the bulk of alveolarization takes place during the first 6 months after birth (mouse: PN5- PN15) (Schittny et al., 2008). The alveolar myofibroblast, localized in the mesenchyme at the tip of the emerging secondary septa, is the cell responsible for secondary septa formation. While this stage starts prenatally in humans (approximately 36 weeks of gestation) it starts in mice at postnatal day 5 (PN5). For this reason, the mouse model of bronchopulmonary dysplasia (BPD), a model of hyperoxia-induced lung injury in the neonatal lung of mice, is a suitable animal model to mimic lung injury in the premature lung corresponding to those of preterm infants.

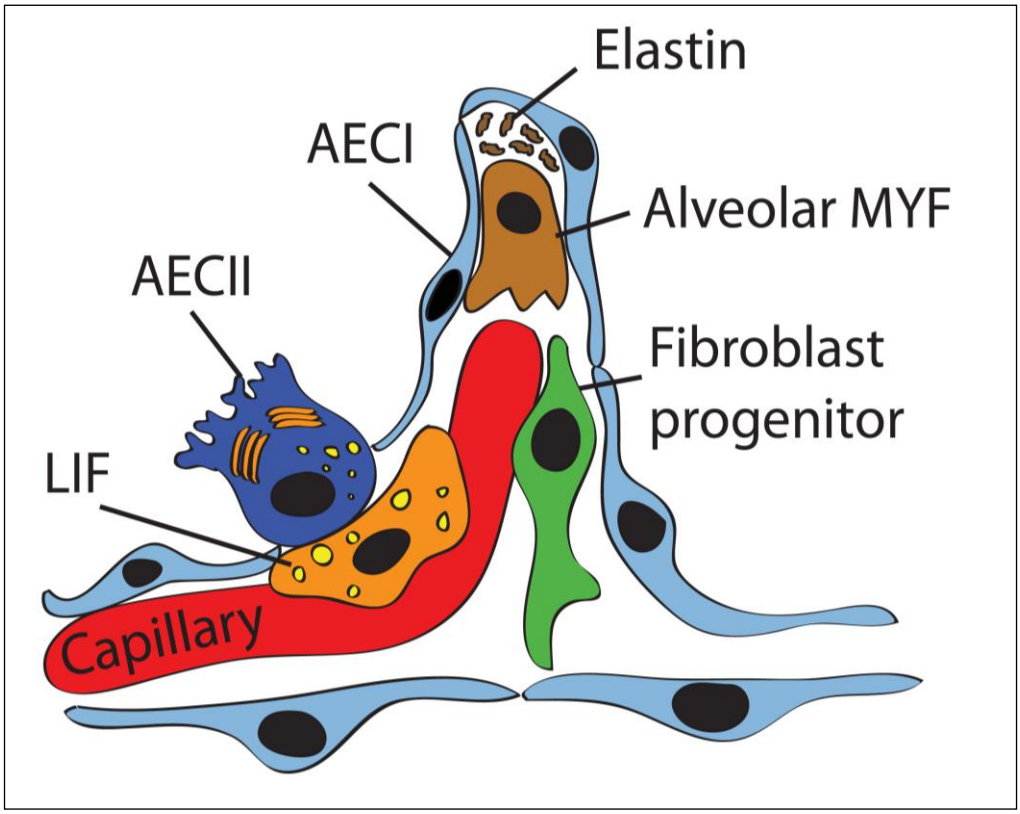

Figure 2. Schematic of the secondary septa during alveologenesis.

Most of the alveolar surface is occupied by AECI (gas exchange) whereas a minor surface is occupied by AECII (surfactant production). The alveolar wall consists of the blood capillary, lipofibroblast (LIF), resident fibroblast progenitor, alveolar myofibroblast (MYF) and extracellular matrix (ECM, mostly elastin). It has been proposed that alveolar MYF can originate from LIF but this concept needs further validation (Chao et al., 2015).

1.1.2. The epithelial-mesenchymal interaction during mouse embryonic lung development

In mice, during the late pseudoglandular stage (E13.5) the distal lung bud consists of three morphologically distinguishable layers. The outer layer is called mesothelium, the middle layer mesenchyme and the inner layer is termed epithelium. Further, the mesenchyme can be subdivided into the subepithelial mesenchyme (SEM) and submesothelial mesenchyme (SMM). By using lineage-tracing experiments it has been shown that the mesenchyme is populated by diverse progenitor cells which are positive for WNT2/GLI1/ISL1, RET, PDGFRα, VEGFR2, PROX1 and FGF10 (Peng et al., 2013; El Agha & Bellusci, 2014; El Agha et al., 2014). These progenitors further differentiate into airway smooth muscle cells (ASMC), vascular smooth muscle cells (VSMC), resident mesenchymal stem cells (MSC), lipofibroblasts (LIF), endothelial cells, chondrocytes, nerve cells, alveolar myofibroblasts, lymphatic cells and others. It has been demonstrated that mesenchymal progenitor cells are not only important in development but also in homeostasis and regeneration after injury (Volckaert et al., 2011)**.**

In contrast to the mesenchyme, the epithelium consists of a single layer of alveolar epithelial cells type I (AECI) and II (AECII). Recently, it has been demonstrated that they arise from the same bipotential progenitor cell population (Treutlein et al., 2014).

Much evidence gained by in-vitro and in-vivo experiments confirmed the important role of signaling molecules and proteins, which interact between epithelium and mesenchyme during lung development. For example, some of these signaling molecules that are important for the process of alveologenesis are listed in Table 2 (see also Table 1 for cellular interactions). This elaborate epithelial-mesenchymal crosstalk is essential for processes of lung specification, budding and branching. Key ligands like Fibroblast growth factors (FGF), WNT (wingless and int), Sonic hedgehog (SHH) and Bone morphogenetic proteins (BMP) are shown to initiate the pulmonary cell fate and specify the early lung domain at the ventral foregut endoderm (Hines & Sun, 2014). One of the most striking findings of the importance of epithelial-mesenchymal interactions during lung development was provided in recombination studies. Isolated distal lung mesenchyme, grafted on the tracheal epithelium, is able to induce ectopic budding accompanied by expression of surfactant protein C as a marker for AECII (Shannon, 1994; Shannon et al., 1998; Hyatt et al., 2004).

FGF10, one of the most important signaling molecule during embryonic lung development, is expressed in the mesenchyme and signals through the FGFR2b receptor located on the epithelium. The genetic deletion of *Fgf10* leads to lung and limb agenesis (Sekine et al., 1999). But induced ectopic FGFR2b signaling in the mesenchyme also causes disturbed development of epithelial branching (De Langhe et al., 2006). The authors proposed that mesenchymal FGF10 signaling suppresses the differentiation of alveolar myofibroblast progenitors. Furthermore, the blockade of FGFR2b ligands (e.g. FGF10) in the lung from E14.5 to E18.5 by overexpression of a soluble dominant negative receptor of *Fgfr2b* (*Sftpc-rtTA/+;tetOsolFgfr2b/+*), which blocks all FGFR2b ligands, also leads to arrest in secondary septa formation and alveolar simplification (Perl & Gale, 2009). This data suggests that FGFR2b ligands are also essential for the formation of alveolar myofibroblasts. Interestingly, treatment with retinoic acid, a biologically active derivative of vitamin A, induced re-alveolarization with increased PDGFRα-positive cells and decreased αSMA/ACTA2-positive cells. This alveolar regeneration can be abolished by concurrent induction of the dominant negative *Fgfr2b.* These data suggest that re-alveolarization is dependent on FGFR2b ligands.

Another important signaling molecule is WNT (e.g. WNT2, WNT2b among others),

which is expressed in the mesenchyme. By genetically deleting *Wnt2/2b* or *β-catenin* , lung agenesis due to loss of *Nkx2.1* has been observed (Goss et al., 2009; Harris-Johnson et al., 2009). These data suggest the importance of WNT ligands for the lung domain specification of the foregut endoderm at the beginning of embryonic lung development. Genetic deletion of *Wnt2* in mice also leads to abnormal formation of airway smooth muscle cells (ASMC) (Goss et al., 2011). The conditional deletion of *β-catenin* in the distal epithelium (*Spc-rtTA;tet(O)Cre*) in mice results in the inhibition of distal airway formation (Mucenski et al., 2003). This phenotype could be rescued by a gain of function approach for *β-catenin* (Mucenski et al., 2005).

BMP4 (Bone morphogenetic protein 4), SHH (Sonic hedgehog) and SPRY2 (Sprouty homolog 2) are inhibitors of FGF10. BMP4 is expressed in the endoderm, the mesenchyme and also in the distal epithelial buds. In vitro treatment with exogenous recombinant BMP4 leads to inhibition of FGF10-induced bud outgrowth. In comparison, SHH and SPRY2 are expressed in the epithelium of the distal buds. SHH, a secreted growth factor, signals in a paracrine fashion through the receptor Patched (PTC), which is located in the mesenchyme. In vitro experiments with lung explants demonstrated that SHH induce mesenchymal cell proliferation and differentiation (El Agha & Bellusci, 2014; Minowada et al., 1999). In contrast, SPRY2 inhibits the intracellular receptor tyrosine kinase signaling (Mailleux et al., 2001; Tefft et al., 2002; Bellusci et al., 1997a) and causes decreased epithelial branching.

Additional evidence for the importance of epithelial-mesenchymal interaction has been shown in AECII and lipofibroblast. The lipofibroblast (LIF) is a lipid-containing interstitial cell located in the mesenchyme in close proximity to AEC II (Figure 2). LIF are involved in the trafficking of lipids to the AECII for surfactant production (Torday et al., 1995; Tordet et al., 1981). Apart from triglycerides, LIF also secrete leptin and retinoic acid, both important for surfactant production and alveolar septation (Torday & Rehan, 2002; Simon & Mariani, 2007). On the other hand, AECII secrete parathyroid hormone-related protein (PTHRP) to signal through PTHRP receptors expressed on LIF, inducing expression of adipose differentiation-related protein (*Adrp*) via the peroxisome proliferator-activated receptor gamma (PPARγ) pathway (Figure 4). The current consensus is that this signaling pathway

is essential for the maintenance of the LIF phenotype as well as for regulation of surfactant production (Schultz et al., 2002; Torday & Rehan, 2002; Rehan & Torday, 2012; Rubin et al., 2004).

1.2. Bronchopulmonary dysplasia

Bronchopulmonary dysplasia (BPD) is a chronic lung disease of prematurely born infants and remains a leading cause of morbidity and mortality in newborns. The main histological characteristic is alveolar simplification. Until now there is no curative therapy for BPD. According to data from the Neonatal Research Network in the United States and the new severity-based definition of BPD 68% of premature infants born at the gestational age ≤ 28 weeks or at a birth weight lower than 1500g develop BPD (Stoll et al., 2010). The lower the gestational age and the birth weight, the higher is the risk to develop BPD (Bhandari & Bhandari, 2009). Long-term morbidity, such as susceptibility to pulmonary infection, asthma and neurodevelopmental impairment in child- and adulthood affect life quality and represent a considerable burden for the patients and health care systems.

The pathogenesis is known to be multifactorial (Figure 3), but the underlying molecular and cellular mechanisms are still poorly understood. In the following sections, more details regarding the pathogenesis, both from a clinical and from a basic scientific point of view, will be provided.

1.2.1. Pathogenesis of BPD from a clinical point of view

As mentioned above, the risk of BPD correlates inversely with the gestational age and the birth weight. This fact is associated with the need of mechanical ventilation and high oxygen delivery due to insufficient gas exchange in the immature lung postnatally. The barotrauma and oxygen toxicity associated with mechanical ventilation lead to inflammation contributing to damages of the lung structure. Apart from these major risk factors for BPD, pre- (e.g. chorioamnionitis) and postnatal infections (e.g. sepsis) are known to be further major factors, which cause lung injury (Figure 3) (Baraldi & Filippone, 2007). Pulmonary inflammatory responses due to bio- and barotrauma are characterized by an imbalance of pro-inflammatory cytokines and growth factors followed by the influx of inflammatory cells into the

lung (Shahzad et al., 2016). Using tracheal aspirates of mechanical ventilated preterm infants, several studies confirmed that high levels of pro-inflammatory cytokines like IL-1β, IL-6, IL-8 and TNF-α are associated with the later development of BPD (Todd et al., 1998; Speer, 2006). In the past two decades, advances in the treatment and management of preterm infants postnatally have been made. Among others, these advances include the prenatal use of corticosteroids (Roberts & Dalziel, 2006), the avoidance of invasive mechanical ventilation and the use of exogenous surfactant. Concurrent with these changes in treatment, the histological findings in autopsy specimens of infants who died from BPD have been changed. Main histological characteristics in the so-called “old” BPD (before the invention of exogenous surfactant) are interstitial fibrosis and squamous metaplasia of the airways. Lungs from “new” BPD during the post-surfactant era display mainly alveolar simplification and an immature microvasculature. According to these findings the “new” BPD is considered as a lung disease, which affects preterm infants born in the canalicular/saccular stage of lung development (e.g. 23 – 28 weeks of gestation), when lung development is interrupted by postnatal lung injury leading to the growth arrest of the lung with impaired secondary septation and decreased alveolar surface area. Using animal models, some of the major proteins that are involved in this process of alveologenesis and that are altered in patients with BPD have been described (Table 2). Further postnatal lung development in the alveolar stage is not able to catch up and to compensate this growth deficit leading to persistent limitations in lung function. This growth arrest also affects the development of the pulmonary vessels resulting in up to 25% of pulmonary hypertension – a severe clinical complication - in preterm infants with BPD (Rossor & Greenough, 2015). Finally, since not all of the preterm infants develop BPD, it has been proposed - based on results from genome-wide association studies - that polymorphisms (SNPs) in *MMP16* and *SPOCK2* might be associated with BPD (Hadchouel et al., 2011).

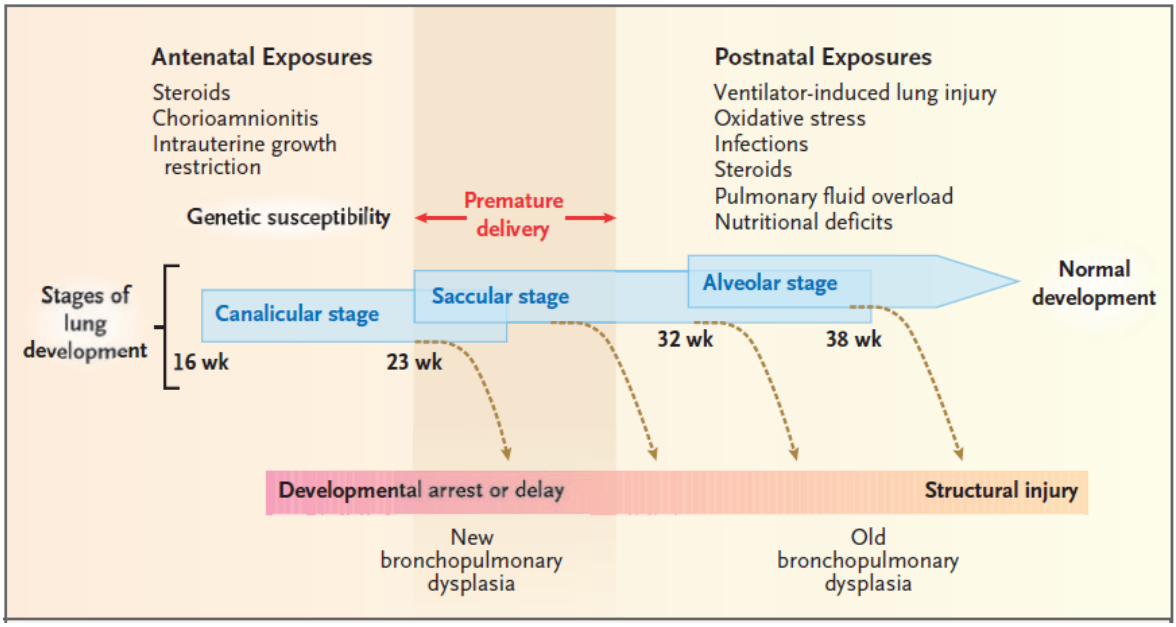

Figure 3. Schematic of the multifactorial pathogenesis of bronchopulmonary dysplasia (BPD).

Lungs of premature infants are often exposed to both pre- and/or postnatal injurious events (e.g. pre-/ postnatal infections, ventilator-induced lung injury, oxidative stress) leading to development of BPD. In the earlier time, the “old” BPD occured in premature infants born during the alveolar stage with respiratory distress syndrome who received aggressive mechanical ventilation and high concentrations of inspired oxygen. Nowadays, due to advances in prevention and treatment of respiratory distress syndrome (e.g. prenatal steroids, postnatal surfactant application, avoidance of invasive mechanical ventilation), BPD is considered as a developmental arrest or delay of the lung (“new” BPD) of premature infants, mainly born during the canalicular or saccular stages of lung development (adapted from Baraldi & Filippone, 2007).

1.2.2. Pathogenesis of BPD from a basic scientific point of view

As stated previously, the mechanisms responsible for alveolar simplification in BPD remain elusive. However, lung specimens from premature infants from pre- and post-surfactant era who died from BPD consistently showed abnormalities in the mesenchyme (interstitial fibrosis and dysmorphic microvasculature) with increased total collagen content (Husain et al., 1998; Thibeault et al., 2000; Thibeault et al.,

2003). Similar findings in plenty of animal models (rat, mice, baboon) mimicking the BPD conditions (oxygen delivery, mechanical ventilation, exogenous surfactant) support the hypothesis that the mesenchyme plays a pivotal role in disease pathogenesis (Warner et al., 1998; Dauger et al., 2003; Auten et al., 2009; Velten et al., 2010; Coalson et al., 1999) and reinforce the opinion that alveologenesis depends on a normally developed mesenchyme. Some of the most important proteins that are responsible for alveologenesis but that has been shown to be altered in humans with BPD will be described in the next section and listed in Table 2.

As described above, one of the major causes of BPD is believed to be inflammation. In line with what can be taken from studies with human samples (e.g. tracheal aspirates), increasing evidence gained in animal experiments support this hypothesis (Prince et al., 2005; Blackwell et al., 2011; Benjamin et al., 2010; Carver et al., 2013; Benjamin et al., 2007). For instance, it has been shown that lipopolysaccharides (LPS from Escherichia coli) inhibit branching morphogenesis in vitro (Prince et al., 2005). Blackwell and colleagues also observed the inhibition of airway branching in lung explants once incubated with activated resident macrophages. The proposed mechanism is that LPS activates nuclear factor kappa beta (NF-κB), which is then accompanied by increased activation of interleukin-1beta (IL-1β) and tumor necrosis factor-α (TNF-α) in resident macrophages (Blackwell et al., 2011). This effect caused by macrophage-mediated inflammation could be antagonized by depletion of macrophages in the lung. This inhibitory effect of inflammatory signals is linked with FGF10 – a key growth factor during lung development. In vitro experiments demonstrated that *Fgf10* expression is decreased in LPS-treated lung explants and primary fetal lung mesenchymal cells from saccular stage through activation of Toll-like receptors 2 and 4 (TLR2/4). Further, immunostaining showed a significantly lower quantity of FGF10-positive cells in lung tissues of premature infants who died from BPD (Benjamin et al., 2007). In line with this observation, a prospective study evaluating FGF10 levels in cord blood of 269 preterm infants found that low cord blood FGF10 levels may predict the subsequent development and severity of BPD (Mohamed & Aseeri, 2014).

Furthermore, it has been shown recently that mRNA and protein expression of PDGFRα and PDGFRβ in mesenchymal stromal cells (MSC) isolated from tracheal aspirates of premature neonates with BPD are decreased. Consistent with these findings, lungs of infants dying from BPD display less PDGFRα-positive cells in the alveolar septa. These data have been confirmed in animal studies using a BPD mouse model (75% oxygen for 14 days) (Popova et al., 2014). Most recently, using a novel three-dimensional human model of fibroblast activation associated with exposure to alternating hypoxia and hyperoxia, Sucre and colleagues identified the Notch pathway as a key driver of fibroblast activation and proliferation in response to changes in oxygen thereby contributing to BPD pathogenesis (Sucre et al., 2016).

As previously mentioned, the alveologenesis phase leads to a dramatic increase in alveolar surface, which is essential for gas exchange. The current consensus is that this process is interrupted by exogenous deleterious factors leading to simplification of alveoli in BPD. Many studies confirmed that the alveolar myofibroblast (MYF), located in the mesenchyme, is the unique cell type responsible for secondary septa formation. During alveologenesis, the alveolar myofibroblast is characterized by expression of alpha-smooth-muscle-actin (αSMA or ACTA2) compared to other mesenchymal fibroblast population. By deposition of elastin and collagen, the alveolar myofibroblast initiates the process of secondary septation (Noguchi et al., 1989; Vaccaro & Brody, 1978). Both elastin and alveolar myofibroblast have been shown to be critical for secondary septa formation (Vaccaro & Brody, 1978; Dickie et al., 2008). Expression of tropoelastin starts in the pseudoglandular stage of lung development and reaches the highest level during the alveolar stage (Mariani et al., 1997; Willet et al., 1999). The strongest evidence so far showing the importance of elastin for secondary septa formation came from the *elastin*-knock-out mice that reveal a complete failure of alveologenesis leading to an emphysematous-like phenotype (Wendel et al., 2000; Shifren et al., 2007). Interestingly, both hyperoxia and mechanical ventilation lead to increased expression of *elastin* (Bruce et al., 1993; Albertine et al., 1999; Nakamura et al., 2000). *Fgfr3* and *Fgfr4* have been shown to direct alveologenesis in the murine lung by controlling elastogenesis (Weinstein et al., 1998). By using mice homozygous for *Pdgfa*-null allele, Boström and colleagues demonstrated failed alveolar formation due to loss of alveolar myofibroblasts and consequent loss

of elastin fibers (Bostrom et al., 1996; Lindahl et al., 1997). Likewise, blocking antibody against PDGRα in newborn mice (PN1-PN7) led to aberrant elastin fiber deposition and impaired alveolar septation resulting in long-term failure in alveologenesis that lasted into adulthood. PDGFA is expressed in the epithelium and targets its receptor (PDGFRα) on mesenchymal cells such as alveolar myofibroblast and lipofibroblast. Given the many mesenchymal targets of PDGFA, it is not clear whether the impact of *Pdgfa* or *Pdgfrα* deletion on myofibroblast formation is due to a direct effect of PDGFA on alveolar myofibroblasts (and or alveolar myofibroblast progenitors) or whether it occurs indirectly via PDGFA action on other targets (ASMCs and LIF). Gain and loss of function for PDGFA/PDGFRα signaling using cell autonomous-based approaches in specific lineages should be carried out in the future to sort out these issues. During a pathological process, VEGFA has been found down-regulated in preterm infants with BPD (Bhatt et al., 2001; Lassus et al., 1999; Lassus et al., 2001). Furthermore, Thebaud and colleagues demonstrated that *Vegf* and *Vegfr2* are decreased in the hyperoxia model of BPD in newborn rats and that adenoviral administration of VEGF improved alveolar architecture and promoted capillary formation (Thebaud et al., 2005; Kunig et al., 2005). Although the trophic and angiogenic potential of VEGF on the lung vasculature is known, the aforementioned study and the studies from other groups suggest that vascular growth serves as a driving force for alveolar growth and maturation, leading to improvement of lung structure and promoting secondary septa formation. A recent report revealed the association of a *VEGF* polymorphism with BPD in Japanese preterm newborns (Fujioka et al., 2014).

Table 2. Overview of proteins that are known to be involved in alveologenesis (Chao et al., 2015).

Protein name	Origin	Localization/ Targets	Function in alveologenesis	Alterations in humans with BPD	Alterations in animal model of BPD	Effect of genetic modulation in the animal model
ELASTIN	Alveolar myofibroblast	Tip of growing secondary septa	secondary septa formation (tips)	Increased and disorganized in saccular walls (Thibeault et al., 2000; Thibeault et al., 2003)	Decreased in hyperoxia (Bruce et al., 1989)	KO: inhibited alveolarization (Wendel et al., 2000)
PDGFA	Epithelial cells, macrophages	*Pdgfr*α-expressing cells (ASMC, alv. MYF, LIF)	Chemotactic attractant for fibroblasts (Prodhan & Kinane, 2002)	Not known	Delayed in hyperoxia (Buch et al., 2000)	KO: inhibited alveolarization (Bostrom et al., 1996; Lindahl et al., 1997)

Protein name	**Origin**	**Localization/ Targets**	**Function in alveologenesis**	**Alterations in humans with BPD**	**Alterations in animal model of BPD**	**Effect of genetic modulation in the animal model**
FGF10	Mesenchymal cells located in SMM	Distal epithelial cells expressing FGFR2b	Under investigation	Decreased (Benjamin et al., 2007)	Decreased in LPS-model (Benjamin et al., 2010)	KO: lung agenesis Partial deficiency: delayed/ disturbed lung branching (Ramasamy et al., 2007)
TGF-β/ TGF-β1	Epithelial cells	Epithelial and mesenchymal cells	Modulation of cell survival, differentiation and ECM (elastin) deposition (McGowan & McNamer, 1990; McGowan et al., 1997)	Increased in tracheal aspirate (Kotecha et al., 1996)	Increased in hyperoxia (Nakanishi et al., 2007; Alejandre-Alcazar et al., 2007)	Overexpression: inhibition of branching morphogenesis and alveolarization (Gauldie et al., 2003) Inhibition: attenuated hyperoxia-induced hypoalveolarization (Nakanishi et al., 2007)

Protein name	**Origin**	**Localization/ Targets**	**Function in alveologenesis**	**Alterations in humans with BPD**	**Alterations in animal model of BPD**	**Effect of genetic modulation in the animal model**
VEGF	Epithelial (during embryonic development also in mesenchymal cells)	Endothelial cells (VEGFR1/2)	Stimulation of endothelial cells for angio-/ vasculogenesis (essential for alveolarization)	Decreased (Bhatt et al., 2001; Lassus et al., 2001)	Decreased in hyperoxia (DeLisser et al., 2006; Lassus et al., 1999)	Inhibition: hypoalveolarization (Le Cras et al., 2002; McGrath-Morrow et al., 2005)

Hyperoxia injury, one of the major risk factor in BPD pathogenesis, is thought to disrupt critical signaling pathways that direct lung development, including branching and septation (Warner et al., 1998). Many signaling pathways critical to these processes have been described (Roth-Kleiner & Post, 2005), notable among them, signaling by the fibroblast growth factor 10 (FGF10) and transforming growth factor (TGF)-β superfamily (Jankov & Keith Tanswell, 2004). Several studies have confirmed the role of TGF-β1 in inducing epithelial-mesenchymal transition (EMT) of alveolar epithelial cells (AEC) to myofibroblast-like cells. This process is accompanied by the deposition of extracellular matrix (ECM) leading to the formation of fibrotic areas in the lung and destruction of alveoli (Kim et al., 2006; Willis et al., 2005; Phan, 2002). Transforming growth factor (TGF)-β signaling can negatively regulate the branching (Roth-Kleiner & Post, 2005; Jankov & Keith Tanswell, 2004) and septation (Gauldie et al., 2003; Vicencio et al., 2004) phases of lung development. In case of the latter, adenoviral-mediated transfer of *Tgf-β1* to the neonatal rat lung or overexpression of *Tgf-β1* between postnatal days P7 and P14 in the mouse both induced histological changes analogous to those seen in BPD. Furthermore, *Smad3* knockout mice exhibited retarded alveolarization between days P7 and P28 (Chen et al., 2005), suggesting that *Tgf-β* also acts as a positive regulator of septation. This apparent paradox indicates that TGF-β signaling plays a critical and finely tuned role in alveolarization. Consistent with these data, *Smad3* deficiency in adult mice caused air space enlargement and centrilobar emphysema in late life (Bonniaud et al., 2004), suggesting a key role for TGF-β signaling in both the formation of alveoli and the maintenance of alveolar structure. However, despite a clear role in both normal and aberrant lung alveolarization (Morty et al., 2009), little is known about how TGF-β signaling regulates secondary septation and the generation of the alveolar gas exchange units. It has been hypothesized that the interplay between FGF signaling and TGF-β signaling plays a pivotal role in orchestrating the balance of amplification/differentiation of the epithelial alveolar lineage during embryonic lung development as well as homeostasis/regeneration in postnatal lung injury.

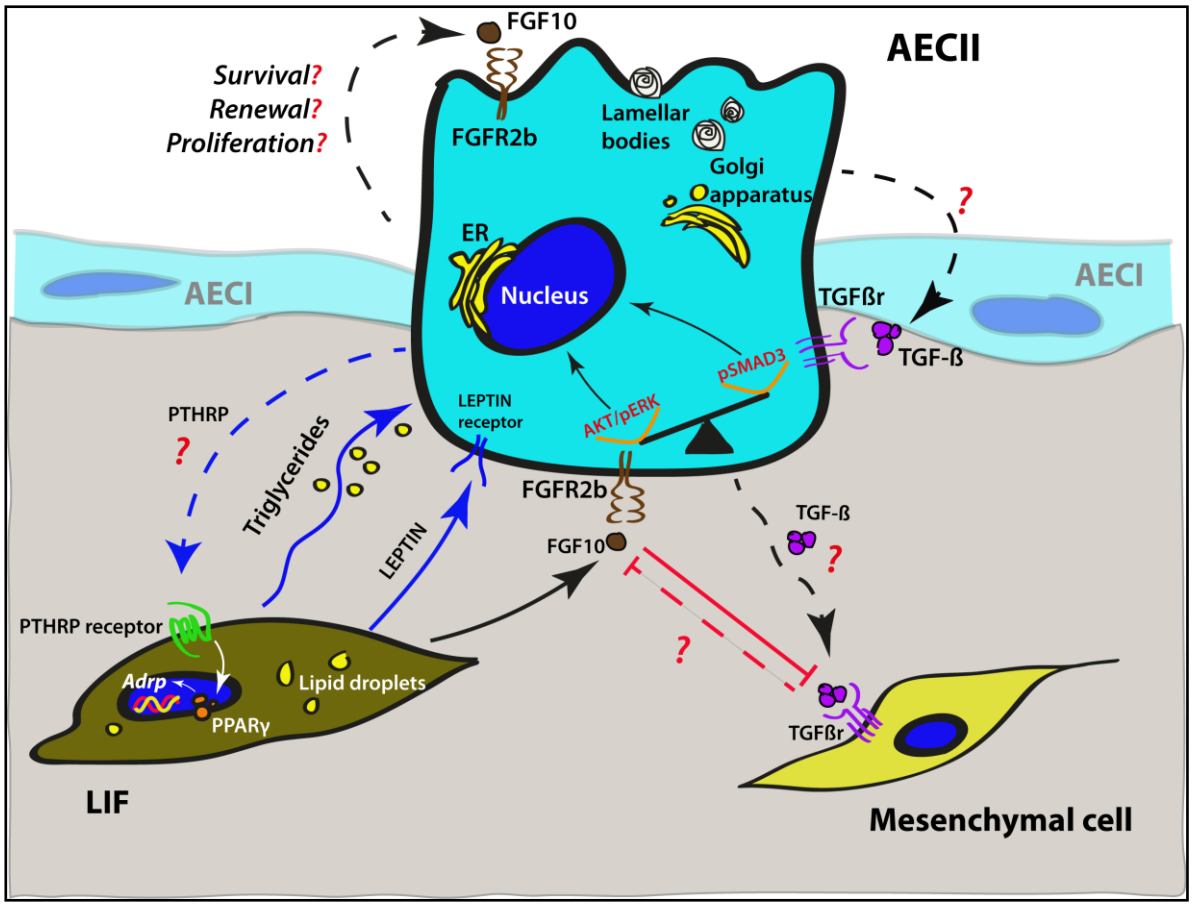

Figure 4. Model for the interplay of FGF10 and TGF-β signaling in epithelial (AECII) - mesenchymal (LIF/MSC) crosstalk during embryonic lung development and disease.

FGF10 secreted by lipofibroblasts (LIF) (among others) acting on AECII via FGFR2b signaling (AKT/pERK). TGF-β expressed by epithelial cells is acting either in an autocrine fashion to finely tune the balance with FGFR2b signaling or on the mesenchym. Further, LIF provides AECII with triglycerides (essential for surfactant production) and interact through leptin signaling molecules. In contrast, AECII signals via PTHRP towards LIF (still controversial). It remains to be proven whether FGF10 secreted by AECII acts in an autocrine manner to control survival, renewal and proliferation (Chao, unpublished).

1.3. FGF10 in lung development and disease

1.3.1. What do we know from experimental studies?

FGF10 is one of the most important signaling molecule during lung development. This has been shown by genetic deletion of *Fgf10* resulting in lung agenesis (Sekine et al., 1999; Bellusci et al., 1997a; Bellusci et al., 1997b). FGF10 belongs to a family of fibroblast growth factor which consists of 22 members subdivided in seven subfamilies (Itoh & Ornitz, 2011). Fibroblast growth factors act in an endocrine, paracrine or intracrine manner through seven receptors (FGFR 1b, 1c, 2b, 2c, 3b, 3c and 4). These receptors are encoded by four genes called *Fgfr1*, *Fgfr2*, *Fgfr3* and *Fgfr4*. Due to alternative splicing seven receptors with different ligand-binding specificity are expressed. Each receptor consists of three domains: an extracellular ligand-binding domain with three immunoglobulin-like loops (D I, D II, D III), a transmembrane domain and an intracellular tyrosine kinase domain.

At E12.5, during the early pseudoglandular stage of embryonic mouse lung development, FGF9 and FGF10 are essential for the branching morphogenesis as well as the differentiation of the epithelium and mesenchyme. FGF9 is expressed in the mesothelium and the epithelium and acts through FGFR2c and FGFR1c located on mesenchymal cells to maintain *Fgf10* expression as well as mesenchymal progenitor cells in a proliferative and undifferentiated status (del Moral et al., 2006). FGF10 is a diffusible key molecule controlling branching morphogenesis during early lung development in mice (Bellusci et al., 1997a; Bellusci et al., 1997b) but the exact mechanism of action remains unclear. Among other *Fgfs*, *Fgf10* is the only gene, which is expressed during the early pseudoglandular stage. FGF10 is secreted by mesenchymal cells located in close proximity to the mesothelium at the distal lung buds. FGF10 acts in a paracrine manner and binds mainly to fibroblast growth factor receptor 2-IIIb (FGFR2b) expressed on epithelial cells. Via chemotaxis FGF10 induces outgrowth of the distal epithelium. Several studies using transgenic mouse lines with a dysfunction in FGF10/FGFR2b signaling showed an abnormal branching morphogenesis, thereby confirming the importance of this pathway. Genetic deletion of *Fgf10* or *Fgfr2b* in mice led to a similar phenotype. The mutant pups die shortly after birth due to lung agenesis and multiple defects in other organs such as salivary gland, limb, inner ear, teeth, skin, pancreas, kidney, thyroid, pituitary gland, mammary

gland (Arman et al., 1999; De Moerlooze et al., 2000; Peters et al., 1994; Sekine et al., 1999; Mailleux et al., 2002).

Lu and colleagues treated mesenchyme-free epithelium with recombinant human FGF10 to identify epithelial-specific gene expressions during bud morphogenesis (Lu et al., 2005). Microarray analysis revealed a panel of transcriptional *Fgf10* targets, which are associated with cell rearrangement, migration, inflammatory processes, lipid metabolism, cell cycle and tumor invasion. Interestingly, the authors did not observe a remarkable induction of genes responsible for proliferation. *Fgf10* also controls the amplification of distal epithelial cell progenitors and the formation of multiple mesenchymal lineages during lung development. Hypomorphic *Fgf10*$^{lacZ/-}$ pups that have only approximately 20% *Fgf10* expression level compared to wild type (WT) display lung defects at birth with decreased branching, thickened primary septa and vascular abnormalities with intrapulmonary hemorrhages. They died within 24-48 hours after birth. Furthermore, *Fgf10* deficiency led to decrease in *Nkx2.1*- and *Sftpb*-expressing cells, which suggests that adequate *Fgf10* expression level is critical for the amplification of epithelial progenitors. Apart from the epithelium, a constitutive decrease in *Fgf10* expression affects not only the epithelium but also diminished PECAM and αSMA-positive cells in mesenchymal cell lineages (Ramasamy et al., 2007).

1.3.2. What is known in humans?

Humans with heterozygous mutations in the *FGF10* or *FGFR2B* gene are suffering from ALSG (aplasia of lacrimal and salivary glands) and LADD (lacrimo-auriculo-dento-digital) syndroms, respectively (Entesarian et al., 2005; Rohmann et al., 2006; Milunsky et al., 2006). Compared to infants with ALSG or LADD who do not show obvious lung defects, adult patients with haploinsufficiency of *FGF10* developed a significant decrease in lung function parameters (IVC, FEV1 and FEV1/IVC ratio) compared to non-carrier siblings which is similar in patients with chronic obstructive pulmonary disease (COPD) (Klar et al., 2011). Recently, it was shown in 220 COPD patients that polymorphisms in *FGF10* maybe be associated with susceptibility to COPD and severity of COPD (Ren et al., 2013). Based on our recent data gained from *Fgf10* heterozygous (*Fgf10*$^{+/-}$) mice we hypothesize that these patients acquired quantitative and qualitative congenital defects of the AECI and AECII cells due to *Fgf10* deficiency (Chao et al., 2017). As mentioned above,

FGF10-positive cells are diminished in lung autopsy tissues from infants died from BPD (Benjamin et al., 2007). The underlying mechanism is unclear.

Apart from *FGF10*, mutations of other *FGF* genes are also associated with diseases. For instance, homozygous mutation of *FGF3* leading to impaired secretion of FGF3 is described to cause deafness due to complete labyrinthine aplasia (Michel aplasia), microtia, and microdontia (LAMM syndrome) (Tekin et al., 2007). Mutations of *FGF23* lead to polypeptides less sensitive to protease cleavage compared to WT resulting in excessive loss of phosphate in the urine. This hereditary disease is called “autosomal dominant hypophosphatemic rickets” (ADHR) (White et al., 2001).

2. Objectives

Inflammation-induced Fibroblast growth factor 10 (FGF10) protein deficiency is associated with bronchopulmonary dysplasia (BPD) (Prince et al., 2005; Blackwell et al., 2011; Benjamin et al., 2010; Carver et al., 2013; Benjamin et al., 2007), a chronic lung disease of prematurely born infants characterized by arrested alveolar development. Until today, there is no experimental evidence for a direct role of FGF10 in BPD. For this reason, we used two mouse lines with constitutive *Fgf10* deficiency (*Fgf10*$^{+/-}$ and *Fgf10*$^{Lacz/-}$) to investigate the effect on lung development pre- and postnatally as well as in a BPD mouse model (hyperoxia-induced lung injury). Furthermore, we also used an inducible loss of function of FGF10/FGFR2b signaling (*Rosa26*$^{rtTA/+}$*;Tg(tet(o)sFgfr2b)/*+) to study the role of this signaling pathway pre- and postnatally in normoxia and during hyperoxia lung injury postnatally.

With the experiments performed in this study we aim to answer the following five main questions:

1) Does constitutive *Fgf10* deficiency affect embryonic lung development?

2) What is the impact of constitutive *Fgf10* deficiency on the cellular and molecular level of the developing lung?

3) What is the impact of constitutive *Fgf10* deficiency on hyperoxia lung injury in the newborn (BPD mouse model)?

4) Does blockade of FGF10/FGFR2b signaling affect embryonic and postnatal lung development?

5) Is FGF10/FGFR2b signaling relevant during postnatal hyperoxia lung injury?

3. Materials and Methods

3.1. Study approval

Animal experiments were approved by the Federal Authorities for Animal Research of the Regierungspräsidium Giessen, Hessen, Germany, protocol GI 20/10, no.105/2011. The experiments shown in Figures 14 and 15 were carried out under the protocol no. 31-08 at Children´s Hospital Los Angeles, in accordance with the National Institutes of Health Guidelines for the Use of Laboratory Animals.

3.2. Generation and genotyping of mice

3.2.1. Generation of *Fgf10*$^{+/-}$, *Fgf10*$^{Lacz/-}$ and *Rosa26*$^{rtTA/+}$*;Tg(tet(o)sFgfr2b)/+*

Fgf10$^{+/-}$ mice were generated by crossing *Fgf10*$^{flox/flox}$ mice (*Fgf10*$^{tm1.2Sms}$*/J*, Jackson Lab stock 023729) with *CMV-Cre* mice (*B6.C-Tg(CMV-cre)1Cgn/J*, Jackson Lab stock 006054). The resulting *Fgf10*$^{+/-}$ mice (*Fgf10*$^{tm1.1Sms}$*/J)* were crossed for at least five generations with C57BL/6 mice. *Fgf10*$^{+/-}$ and *Fgf10*$^{+/+}$ embryonic and postnatal mice were used (both males and females). The *Fgf10*$^{Lacz/-}$ embryos were previously generated (Danopoulos et al., 2013) by crossing the *Fgf10(Lacz/+)* (*Fgf10*$^{Tg(Myl3-lacZ)24Buck}$ obtained from Dr. Robert Kelly, Marseille, France and maintained on the C57BL/6 background for at least 5 generations) with the *Fgf10*$^{+/-}$ mice previously described. The *Rosa26*$^{rtTA/+}$*;Tg(tet(o)sFgfr2b)/+* mice (*Gt(ROSA)26Sor*$^{Tm1.1(rtTA,EGFP)Nagy}$ *Tg(tet0-sFgfr2b)1Jaw/CHC*) were generated by crossing *Rosa26rtTA/+* (*Gt(ROSA)26Sor*$^{Tm1.1(rtTA,EGFP)Nagy}$) with *Tg(tet(o)sFgfr2b)/+* mice (*Tg(tet0-sFgfr2b))1Jaw/CHC*, obtained from Dr. Jeffrey Whitsett, Cincinnatti, USA). The mice were kept on the CD1 background for at least 5 generations. Both male and female mice were used for the study. C57BL/6 males and females were used to generate wild type pups.

3.2.2. Genotyping of *Fgf10*$^{+/-}$, *Fgf10*$^{Lacz/-}$ and *Rosa26*$^{rtTA/+}$*;Tg(tet(o) sFgfr2b)/+*

Tissues from the distal tip of the tails were digested in 200ul Viagen including 1ul proteinase K in 55°C on a shaker overnight, then reaction was stopped in 85°C for 30min. Genotyping were done by PCR. For protocol and primer sequences please see Table 3. Genotyping were mainly done by a technician.

Table 3. Primer sequences and protocols for genotyping.

Mouse line	Primer sequence	PCR protocol		
		Step	**Temp. (°C)**	**Time**
Fgf10$^{+/-}$	1) GCA GAG ATT GCA AAG GAA GC 2) GTC TTT TTG ACT GAA ACC TCA C 3) ATC CTT GGG AGG CAG GAT AAC C	1	94	3min
		2	94	30sec
		3	60	30sec
		4 (repeat Step 2-4 39 times total)	72	1min
		5	72	10min
		6	4	hold
Fgf10$^{Lacz/-}$	1) LacZ: TTC ACT GGC CGT CGT TTT ACA ACG TCG TGA 2) LacZ: ATG TGA GCG AGT AAC AAC CCG TCG GAT TCT 3) Mlc1v: CGA GTG GAG CAT GTA CTT CCG TGT CCT GAA 4) Mlc1v: TCC CTA CCC AGT CAC AGT CAC AGC TGC ATA	1	94	1/2min
		2	94	30sec
		3	59	30sec
		4 (repeat Step 2-4 31 times total)	72	1min
		5	72	5min
		6	4	Hold

Mouse line	**Primer sequence**	**PCR protocol**		
		Step	**Temp. (°C)**	**Time**
Rosa26$^{rtTA/+}$	1) GAG TTC TCT GCT GCC TCC TG 2) CGA GGC GGA TAC AAG CAA TA 3) AAG ACC GCG AAG AGT TTG TC	1	94	3min
		2	63	1min
		3	72	1,5min
		4 (repeat Step 2-4 35 times total)	93	1min
		5	72	5min
		6	4	hold
Tg(tet(o)sFgfr 2b)/+	1) GAA GGA GAT CAC GGC TTC C 2) AGA CAG ATG ATA CTT CTG GGA CTG T	1	95	2min
		2	95	5sec
		3	65	5sec
		4 (repeat Step 2-4 35 times total)	72	20sec
		5	72	2min
		6	4	hold

3.2.3. Gel electrophoresis

PCR products were analyzed using a 1,5 % agarose gel containing TAE buffer with Sybrsafe (50 μl Sybrsafe + 500ml 1x TAE buffer). 10 μl of PCR samples were loaded with 2 μl loading dye (Biorad Nucleic Acid Sample loading buffer, 5x), then gel was run with 120V for 30-45 min. A molecular ladder (QX Size Marker, 100bp-2,5kb, Qiagen, Germany) was used to detect the expected band sizes (Table 4).

Table 4. Expected band size of genotyping products.

Mouse line	Expected band size for WT	Expected band size for mutant
Fgf10$^{+/-}$	174bp	500bp
Fgf10$^{Lacz/-}$	500bp	370bp
Rosa26$^{rtTA/+}$*;Tg(tet(o)sFgfr2b)/+*	*Rosa26rtTA:* 322bp	*Rosa26rtTA:* 215bp *solFgfr2b:* 110bp

3.3. Mice and doxycycline administration

In order to induce the expression of soluble *Fgfr2b* in *Rosa26*$^{rtTA/+}$*;Tg(tet(o)sFgfr2b)/+*, doxycycline food (625 mg doxycycline/kg) was given to pregnant females from E18.5 after plugging until postnatal day 3 of the pups. For the experiments shown in Figure 14 and Figure 15 one single intraperitoneal injection of doxycycline (0.0015 mg per gram body weight) was given to pregnant females. Then, doxycycline food (625 mg doxycycline/kg) was given to pregnant females until E18.5.

3.4. BPD mouse model: hyperoxia-induced lung injury

Newborn pups were subjected to HOX (85% O_2) injury from P0-P8 in a chamber (Proox Model 110, Biospherix, USA). To minimize oxygen toxicity and bias, nursing dams were rotated every 24 h between NOX and HOX. Pups and dams received food and water ad libitum.

3.5. Lung perfusion and isolation

After the mice were sacrificed the lung was flushed from the right ventricle to remove blood cells, then perfused through the trachea with a pressure of 20 cm H_2O with 5 ml 4% PFA. The trachea was tied off with a string, and the lung was removed and placed in 4% PFA for max. 24 h at 4°C. Lungs were then progressively dehydrated (30%, 50%, 70%, 99% ethanol, each 3 h), incubated in xylole, then in paraffine overnight and finally embedded with a Leica embedding machine (EG 1150C). Paraffin blocks were kept cold and 5 µm sections were cutted.

3.6. RNA extraction and quantitative real-time RT-PCR

The cranial lobes were removed, placed in QIAzol lysis reagent (Qiagen GmbH, Hilden, Germany), homogenized in GentleMACs and frozen in liquid nitrogen for RNA extraction. RNA was isolated using the RNeasy Mini Kit (Qiagen, Hilden, Germany) according to manufacturer´s instructions.

RNA was reverse-transcribed (QuantiTect Reverse Transcription Kit, Qiagen, Hilden, Germany). cDNA was diluted to a concentration of 5 ng/µL. Primers were designed using Roche Applied Sciences online Assay Design Tool. All primers were designed to span introns and blasted using NCBI software for specificity. Sybr Green Master Mix (invitrogen, Germany) was use for RT-PCR with a Roche LightCycler 480 machine. Samples were run in triplicates using *Hprt* as a reference gene. Mouse primers are listed below (Table 5).

Table 5. Primer sequences (forward/reverse) for qPCR.

Gene	Forward sequence (5'-3')	Reverse sequence (5'-3')
Fgf1	CCGAAGGGCTTTTATACGG	TCTTGGAGGTGTAAGTGTTATAATGG
Fgf3	GATTACTGCGGTGGAAGTGG	CCGTTCCACAAACTCACACTC
Fgf7	ACTATCTGCTTATAAAATGGCTGCT	GTGGGGCTTGATCATCTGAC
Fgf10	CGGGACCAAGAATGAAGACT	GCAACAACTCCGATTTCCAC
Hprt	CCTAAGATGAGCGCAAGTTGAA	CCACAGGACTAGAACACCTGCTAA

3.7. α-smooth muscle actin/ von-Willebrand-factor (vWF) double staining

3 µm paraffine sections were deparaffinized, endogenous peroxidase was removed by incubation with 3% H_2O_2-methanol solution for 20 min, then washed with aqua dest. and PBS each 2 x 5 min. For antigen retrieval, sections were trypsinized for 10 min at 37°C, then washed with PBS (4 x 5 min) and immersed in blocking buffer (10% BSA) for a further 20 min. After washing with PBS (4x 5 min), sections were blocked with Rodent Block M (Biocare Medical MM HRP-Polymer Kit, Cat. No. 1-800-799-9499) for 30 min, washed with PBS and incubated with primary antibody (alpha-actin 1:800 diluted, 30 min) and HRP polymer (20 min) before immersed in substrate solutions (Vip substrat Kit, vector, 30 sec – 4 min). Slides were monitored under the microscope for staining progression and washed with tap water for 5 min. Before staining for vWF, sections were immersed in blocking buffer (10% BSA) for 15 min, washed with PBS, blocked with serum (ImmPRESS Kit Anti-rabbit Ig), then sections were incubated with vWF antibody (1:1200 diluted) at 37°C for 30 min and washed again. After incubation with secondary antibody (Anti-rabbit Ig peroxidase, ImmPRESS reagent), sections were stained with DAB substrate Kit (SK-4100, vector) and staining progression was observed under the microscope. After washing with tap water, sections were counterstained with methyl green for nuclei on a heating plate (60°C), progressively dehydrated and coverslipped.

3.8. Vascular Morphometry

The degree of muscularization was determined from 3 µm mouse lung sections. Morphological assessment of lung vessel muscularization (outer diameter: 10-20 µm, 20-70 µm, 70-150 µm and >150µm) was performed via computer-assisted analysis (Leica Q Win Standard analyzing software) at 40x or 63x magnification under a microscope. The analytical software detected the vessels' endothelium that appeared in a brown color (vWF staining) and the muscle tissue surrounding the vessels that appeared in a violet color (α-SMA staining). The software distinguished between non-muscularized vessels (no smooth muscle cells detectable with α-SMA staining), partially muscularized (minimum one smooth muscle cell and maximum 75% of the vessel circumference with α-SMA staining), and fully muscularized (>75% of the vessel circumference with α-SMA staining).

The vascular morphometry was carried out by a technician.

3.9. Isolation of primary alveolar type II cells

AEC II cells were isolated according to a protocol published by Seimetz and colleagues (Seimetz et al., 2011). The whole lung was perfused with 1 ml PBS through the right ventricle to remove the intrapulmonal blood cells. Lungs were perfused with 1 ml Dispase through the trachea and the trachea was tied off with a string. Lungs were digested in 2 ml Dispase for 30 min at 37°C and minced. The suspension was sequentially filtered through 70, 40, and 10 µm nylon meshes and then centrifuged at 200 g for 10 min. The pellet was resuspended in Dulbecco's modified eagle medium (Invitrogen, Karlsruhe, Germany), and negative selection for lymphocytes/macrophages was performed by incubation on CD16/32- and CD45-coated Petri dishes for 45 min at 37°C. Negative selection for fibroblasts was performed by adherence for 45 min at 37°C on uncoated cell-culture dishes. Cell purity was analyzed in freshly isolated AECII cells directly after isolation by epithelial cell morphology and immunofluorescence analysis with Nile red. AECII cells used throughout this study demonstrated 95% ± 3% purity. The isolation was performed with the help of a technician since several samples needed to be taken care of at the same time.

3.10. Microarray experiments

RNA was purified using the RNeasy Mini Kit (Qiagen, Hilden, Germany) following the kit instructions. RNA quality was assessed by capillary electrophoresis using the Bioanalyzer 2100 (Agilent Technologies, Palo Alto, CA, USA). Purified total RNA was amplified and Cy5-labeled using the LIRAK kit (Agilent) according to the kit instructions. Per reaction, 200 ng of total RNA was used. The Cy-labeled aRNA was hybridized overnight to 8 x 60K 60mer oligonucleotide spotted microarray slides (Agilent Technologies, design ID 028005). Hybridization and subsequent washing and drying of the slides were performed following the Agilent hybridization protocol. The dried slides were scanned at 2 mm/pixel resolution using the InnoScan is900 (Innopsys, Carbonne, France). Image analysis was performed with Mapix 6.5.0 software, and calculated values for all spots were saved as GenePix results files. Stored data were evaluated using the R software and the limma package from BioConductor (Gentleman et al., 2004). Log mean spot signals were

taken for further analysis. Data was quantile-normalized before averaging. Genes were ranked for differential expression using a moderated t-statistic (Smyth, 2004). Pathway analyses were done using gene set tests on the ranks of the t-values. RNA samples were given to Dr. Jochen Wilhelm and microarray experiments were performed in his laboratory.

3.11. Western blotting

Loading buffer was added to protein samples from the lungs (5% SDS in bromophenol blue and β-mercaptoethanol), denatured for 8 min at 98°C and cooled on ice. 8 μg of protein sample was loaded on a 10% polyacrylamide gel and run at 35 mA per gel for approximately 1 h. Samples were then electrically transferred to a polyvinylidene fluoride (PVDF) membrane (Amersham) by semi-dry electro blotting (70 mA per Gel; gel size: 7 x 9 cm) for 90 min. The membrane was blocked with 5% milk in TBS-T blocking buffer at RT on a shaker for 1 h followed by incubation with primary antibody (Table 6) overnight at 4°C. After washing with 1x TBS-T four times for 15 min each, the membrane was incubated with the respective HRP-labeled secondary antibody (dilution 1:2000) at RT for 1 h followed by four times washing with 1x TBS-T buffer for 15 min each. The protein bands were detected by ECL (Enhanced Chemi-luminescence, Amersham, Germany) treatment, followed by exposure of the membrane.

Table 6. Antibodies for western blot.

Primary antibody (rabbit)	Company (Catalog number)	Dilution	Secondary antibody	Company (Catalog number)	Dilution
FGF10	Abcam (ab71794)	1:1000	Swine anti rabbit HRP	Dako (P0217)	1:2000
FGFR2	Santa Cruz (sc-122)	1:200	Swine anti rabbit HRP	Dako (P0217)	1:2000

Primary antibody (rabbit)	Company (Catalog number)	Dilution	Secondary antibody	Company (Catalog number)	Dilution
Mature SFTPC	Seven Hills (WRAB-76694)	1:3000	Swine anti rabbit HRP	Dako (P0217)	1:2000
Pro + Mature SFTPB	Abcam (ab 40876)	1:2000	Goat anti rabbit HRP	Abcam (ab 6721)	1:5000
B-ACTIN	Abcam (ab8227)	1:30.000	Swine anti rabbit HRP	Dako (P0217)	1:2000

3.12. Flow cytometry and Fluorescence Activated Cell Sorting analysis

Whole lungs were isolated in ice-cold Hank's balanced salt solution (HBSS). Then, lobes were chopped finely using sterile razor blades, digested in a 10 mL solution of 0.5% collagenase in HBSS on a heating plate (40°C) stirring 700 rpm for 60 min. Once the homogenate was dissociated, the cell suspension was successively passed through 20G, 24G, and 26G needles, then strained on 70 µm and 40 µm filters. One volume HBSS was added to dilute collagenase and cell suspensions were centrifuged at 1500 rpm for 5 min to remove the enzyme solution. Cells were then resuspended in 500 µL 10% FCS in DMEM and stained with fluorochrome-labeled anti-mouse antibodies for 20 min at 4°C (Table 7), followed by washing and flow cytometric analysis with LSR Fortessa equipped with FACSDiva™ software (BD Bioscience). Flow cytometry analysis with LSR Fortessa were done by Dr. Jennifer Quantius.

Table 7. Antibodies for flow cytometry/FACS.

Antibody	**Company (Catalog number)**	**Dilution**
Anti-Prosurfactant Protein C (proSP-C) Antibody	Millipore (AB3786)	1:500
T1alpha (Podoplanin) APC anti-mouse	Biolegend (127409)	1:20
EpCAM (CD326) APC/Cy7	Biolegend (118217)	1:50
Alexa Fluor 488 anti-mouse CD31 Antibody	Biolegend (102431)	1:50
BD Pharmingen FITC Rat Anti-Mouse CD45 (clone 30-F11)	BD Biosciences (553079)	1:50
PE anti-human/mouse CD49f Antibody	Biolegend (313611)	1:50
Pacific Blue anti-mouse Ly-6A/E (Sca-1) Antibody	Biolegend (108119)	1:50
PE/Cy7 anti-mouse CD24 Antibody	Biolegend (101821)	1:200
Rabbit serum	Sigma-Aldrich (R9133)	1:500
F(ab´)2-Goat anti-Rabbit IgG (H+L) Secondary Antibody, Alexa Fluor 555 conjugate	ThermoFisher Scientific (A-21430)	1:1000
Neg. control for T1alpha: APC Syrian Hamster IgG Isotype control	Biolegend (402012)	1:20

3.13. Alveolar morphometry

For alveolar morphometry, lungs were flushed subsequently with PBS and 4% paraformaldehyde in phosphate-buffered saline (pH 7.0) at a vascular pressure of 20 cm H_2O. Then PBS was infused via the trachea at a pressure of 20 cm H_2O and fixed with 4% paraformaldehyde in phosphate-buffered saline (pH 7.0) via the trachea at a pressure of 20 cm H_2O. Investigations were performed using 5 µm sections of paraffin-embedded left lobe of the lungs. The mean linear intercept, mean air space, and mean septal wall thickness were measured after staining with hematoxylin and eosin (HE). Total scans from the left lobe were analyzed using a Leica DM6000B microscope with an automated stage according to the procedure previously described (McGrath-Morrow et al., 2004; Woyda et al., 2009), which was implemented into the Qwin V3 software (Leica, Wetzlar, Germany). Horizontal lines (distance 40 µm) were placed across each lung section. The number of times the lines cross alveolar walls was calculated by multiplying the length of the horizontal lines and the number of lines per section then dividing by the number of intercepts. Bronchi and vessels above 50 µm in diameter were excluded prior to the computerized measurement. The air space was determined as the nonparenchymatous nonstained area. The septal wall thickness was measured as the length of the line perpendicularly crossing a septum. From the respective measurements, mean values were calculated.

3.14. Lung function measurement

The Mice were anaesthezised by intraperitoneal injection of a solution of 1.2 µl/g body weight of ketamin 10% and 0.6 µl/g body weight of Dormitor (1mg/ml). Deepness of anaesthesia was assessed by toe pinching. Then, incision of the skin was made at the level of larynx to access the trachea without opening the chest cavity. Horizontal tracheal incision was made to intubate the mouse and connect it to the flexivent fx1 (Scireq, Montreal, Canada) for lung function measurement (compliance, elastance and resistance). Each mouse, eight measurements of each 10 sec were performed and mean values were calculated.

3.15. Statistical analyses and figure assembly

Significance was determined by two-tailed Student´s t-test using GraphPad PRISM statistical analysis software. All data are presented as mean ± SEM. Values of $p<0.05$ were considered significant. Figures were assembled by using Adobe illustrator software.

4. Results

4.1. Validation of the BPD mouse model

First, we established and validated the BPD mouse model using hyperoxia-induced lung injury in neonatal mice leading to hypoalveologenesis. Wildtype pups were exposed to either normoxia or hyperoxia (85% oxygen) from P0 until P8 (Figure 5A). Lungs were analysed at P2, P5 and P8 by using H&E staining and alveolar morphometry. Compared to the normoxia group, lungs that were exposed to hyperoxia already revealed a macroscopically decrease in alveolar septation at P2 which became more obvious at P8 (Figure 5B). While, in the alveolar stage, the neonatal lung forms multiple alveoli in normoxia in a process called “secondary septa formation”, this process is significantly impaired in hyperoxia leading to dilated alveolar sacs, which lack secondary septa. This observation was confirmed by unbiased analysis using alveolar morphometry. Comparing hyperoxia group versus normoxia group the difference in mean linear intercept was constantly increasing during the time course of hyperoxia and became significant at P8 (Figure 5C). Accordingly, the airspace was higher in the hyperoxia group compared to the normoxia group but not significantly. The septal wall thickness did not show substantial differences in both groups.

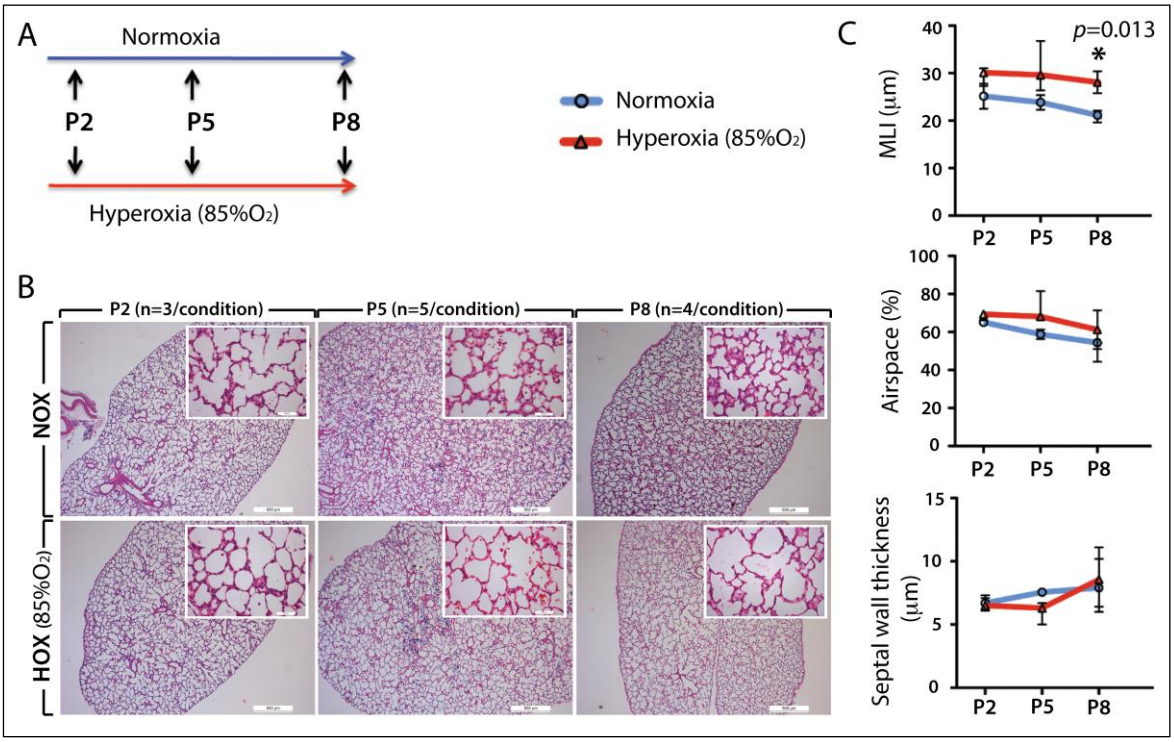

Figure 5. Validation of the HOX injury model to trigger hypoalveologenesis.

(A) Experimental approach. WT animals (C57BL/6) were subjected to HOX (85% O_2) or NOX (21% O_2) for up to 8 days. (**B**) Corresponding H&E staining at P2, P5 and P8 showing progressive defects in alveologenesis. (**C**) Morphometry for MLI, Airspace and Septal wall thickness showing significant increase in MLI at P8. Scale bars main images: 500 μm, insets in images: 50 μm.

4.2. Neonatal *Fgf10* expression in the wild type lung is low in normoxia and decrease significantly upon hyperoxia

Using qPCR, we first examined the expression level of *Fgf10* as well as associated *Fgf* genes of the same *Fgf* subfamily (*Fgf1, Fgf3 and Fgf 7*) in the lungs of C57BL/6 wild type (WT) pups at different time points during normal alveologenesis (between P0 and P35). These genes encode for FGF ligands acting via FGFR2b (Itoh & Ornitz, 2008). When normalized to their respective values for the first timepoint collected (P0), the results indicated a decrease in *Fgf10* expression over time, while the other FGFR2b ligands were maintained at stable levels (Figure 6Aa). Compared to *Fgf10* expression, *Fgf1* and *Fgf7* showed higher expressions while *Fgf3* was generally expressed at lower levels (Figure 6Ab). The examination of the expression (normalized to the first timepoint collected, P2) of these ligands in hyperoxia (HOX) (85% O_2 from P0 onwards) revealed *Fgf10* as the only FGFR2b ligand whose expression was significantly reduced at P5 and P8 compared to normoxia (NOX)-exposed WT lungs (Figure 6Ac).

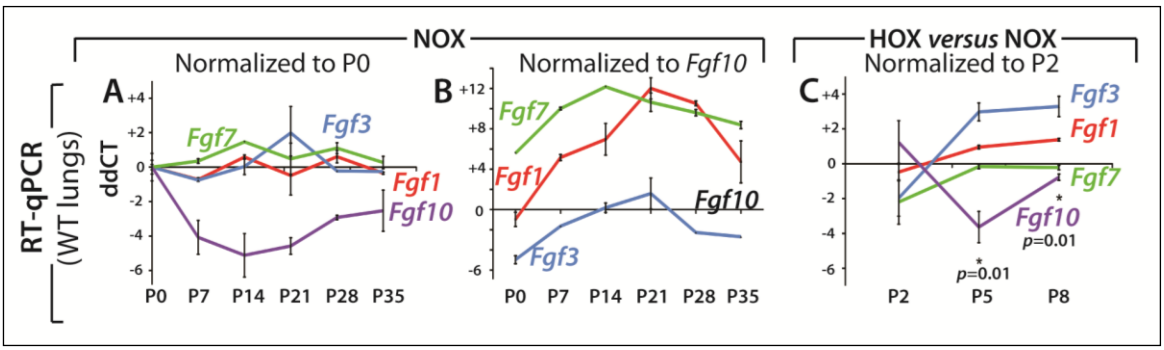

Figure 6. Postnatal *Fgf10* expression in normoxia and hyperoxia.

RT-qPCR for *Fgf1*, *3*, *7* and *10* in lungs at various postnatal stages in normoxia (NOX). (**A**) Normalization to P0 for each of the ligands indicates that *Fgf10* expression decreases postnatally compared to P0 and compared to the other ligands. (**B**) Normalization to *Fgf10* expression at each time point indicates that *Fgf1* and *Fgf7* are expressed at higher levels than *Fgf10*. (**C**) Comparison of FGFR2b ligands in hyperoxia (HOX) versus NOX indicates that *Fgf10* is the only gene, which decreases significantly upon HOX injury.

4.3. Effect of constitutive *Fgf10* deficiency on embryonic lung development at E12.5 and E18.5

4.3.1. *Fgf10*$^{+/-}$ mice show significant decrease in *Fgf10* expression, delayed branching morphogenesis due to decreased proliferation of the epithelium

Considering the previously reported decreased FGF10 protein in human patients with BPD, we investigated whether *Fgf10* deficiency in mice could be causative of the clinical complications observed in BPD. We therefore crossed *Fgf10*$^{+/-}$ males and WT females (both on the C57BL/6 background) to generate several litters of *Fgf10*$^{+/-}$ experimental and *Fgf10*$^{+/+}$ (WT) control embryonic and newborn littermate mice. We collected embryos at E12.5 (n=3 and n=4 for WT and *Fgf10*$^{+/-}$, respectively) and E18.5 (n=3 and n=7 for WT and *Fgf10*$^{+/-}$, respectively) and assessed levels of *Fgf10* mRNA expression in their lungs by qPCR. Our results indicate 23.7% and 57.9% reduction in *Fgf10* expression at E12.5 and E18.5 (p=0.04 and p=0.01, respectively) in *Fgf10*$^{+/-}$ versus WT lungs (Figure 7A).

Furthermore, embryonic lungs at E12.5 revealed a significant delay in branching morphogenesis in *Fgf10*$^{+/-}$ versus WT lungs, most likely due to decreased proliferation of the epithelium (Figure 7B-E). Flow cytometry analysis of the lung at E18.5 showed significant decreased number of AECII but an increase in AECI *Fgf10*$^{+/-}$ versus WT lungs (Figure 7F).

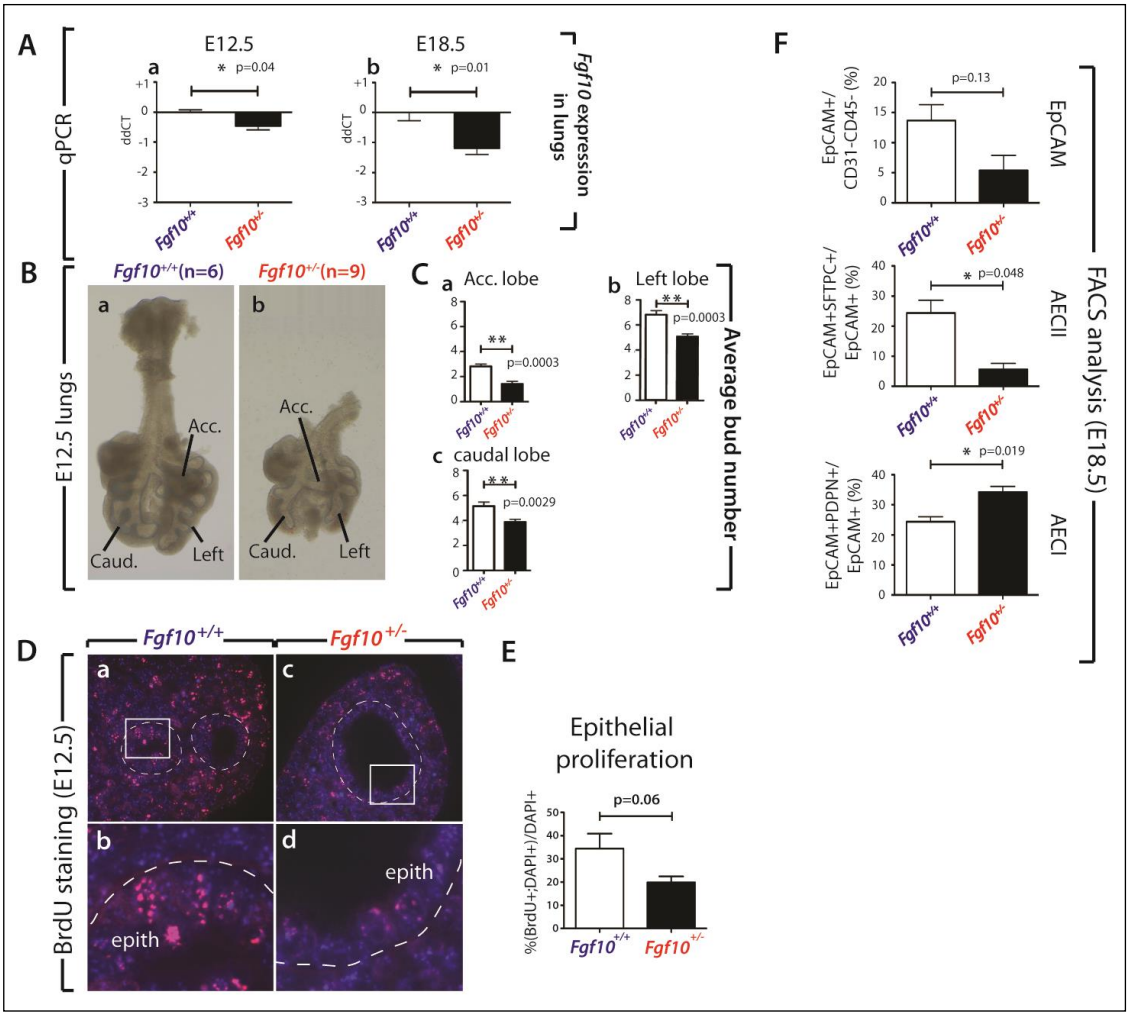

Figure 7. **Constitutive *Fgf10* deficiency leads to delayed branching due to defects of the epithelium.**

(A**)** *Fgf10* heterozygous lungs display decreased levels of *Fgf10* mRNA expression and **(**B**)** decreased epithelial branching at E12.5 (see **(**C**)** for quantification), associated with **(**D**)** decreased proliferation of the epithelium (see **(**E**)** for quantification). **(**F**)** At E18.5 *Fgf10*$^{+/-}$ lungs display decreased EPCAM-positive cells associated with a decrease in AECII and increase in AECI.

4.3.2. *Fgf10*$^{+/-}$ mice show impaired lung morphology and differential gene expression

We next examined the presence of potential lung defects in *Fgf10*$^{+/-}$ embryos at E18.5. We made use of previously described *Fgf10*$^{Lacz/-}$ hypomorphic mutants (Ramasamy et al., 2007b). These two lines exhibit 50% and 20% *Fgf10* expression compared to WT lungs, respectively. Figures 8Aa-c show the histology of the E18.5 WT (n=3), *Fgf10*$^{+/-}$ (n=7), and *Fgf10*$^{Lacz/-}$ hypomorphic (n=3) lungs. Quantification of the morphological defects (Figure 8B) indicated that *Fgf10*$^{+/-}$ lungs exhibited increased MLI and airspace with no change in septal wall thickness compared to WT. Interestingly, *Fgf10*$^{Lacz/-}$ hypomorphic lungs mostly showed increased septal wall thickness with moderate but significant increase in MLI. The reason for this difference is unclear.

In order to further characterize the nature of the lung morphological differences between the three conditions, we isolated RNA from WT (n=3), *Fgf10*$^{+/-}$ (n=7) and *Fgf10*$^{Lacz/-}$ hypomorphic (n=3) E18.5 lungs and carried out transcriptome analyses. Our approach using two distinct types of *Fgf10* mutants with different *Fgf10* levels allowed us to identify the top 70 genes (selected based on p-value), which were differentially regulated between *Fgf10*$^{Lacz/-}$ hypomorph and WT lungs and then to compare the expression of these selected genes between *Fgf10*$^{+/-}$ and WT lungs. The heat map in Figure 8Ca shows that these genes were indeed also similarly decreased or increased in *Fgf10*$^{+/-}$ versus WT lungs. The graph in Figure 8Cb summarizes the different cellular compartments and biological processes, which are potentially affected based on the known function of the identified genes. Interestingly, the expected epithelial defects of *Fgf10* deficiency could be caused partially by the dysregulated expression of a number of identified epithelium-specific genes, such as *lysophosphatidylcholine acyltransferase 1 (Lpcat1), phosphatidylisnositol-4-Phosphate 5-kinase, type I, alpha (Pip5k1a), G-protein-coupled receptor 30 (Gpr30), Calpain 6 (Capn6) and Pleiotrophin (Ptn)*. In particular, *Lpcat1* deficiency has been associated with neonatal death due to surfactant defects (Bridges et al., 2010), while *Ptn* promotes alveolar epithelial type II (AECII) cell proliferation and prevents their differentiation into AECI (Weng et al., 2009). In addition to those implicated in epithelial defects, we also identified changes in genes expressed in muscle, the immune system, nerves and the ECM

(Figure 8Cc). As a consequence of either direct or indirect effects of *Fgf10* on the different cellular compartments, these results highlight potential defects of *Fgf10*$^{+/-}$ lungs. Another project performed in our laboratory using qPCR to validate the changes in FGF signaling and the associated epithelial markers between *Fgf10*$^{+/-}$ and WT lungs at E18.5 showed significant decreased mRNA level of *Fgfr2b* and *Bmp4*, the latter a downstream target of FGF10 in the epithelium (data not shown). An overall trend of decreasing expression was also observed in other epithelial markers. *Epcam* expression was significantly reduced supporting alterations in the epithelial compartment, which is the main cellular target of FGF10 signaling. As FGF10 and TGF-β1 play opposite roles during lung development, we also investigated the expression of genes involved in TGF-β signaling and the associated ECM. We found significantly increased *Smad3*, *Smad7* and *IL-1β* expression, but no changes in *Tgf-β1* and *Tgf-β3*. Additionally, the expression of different forms of collagens (*Col1a1*, *Col1a2*, *Col3a1*, *Col5a2*) showed increasing trends (data not shown).

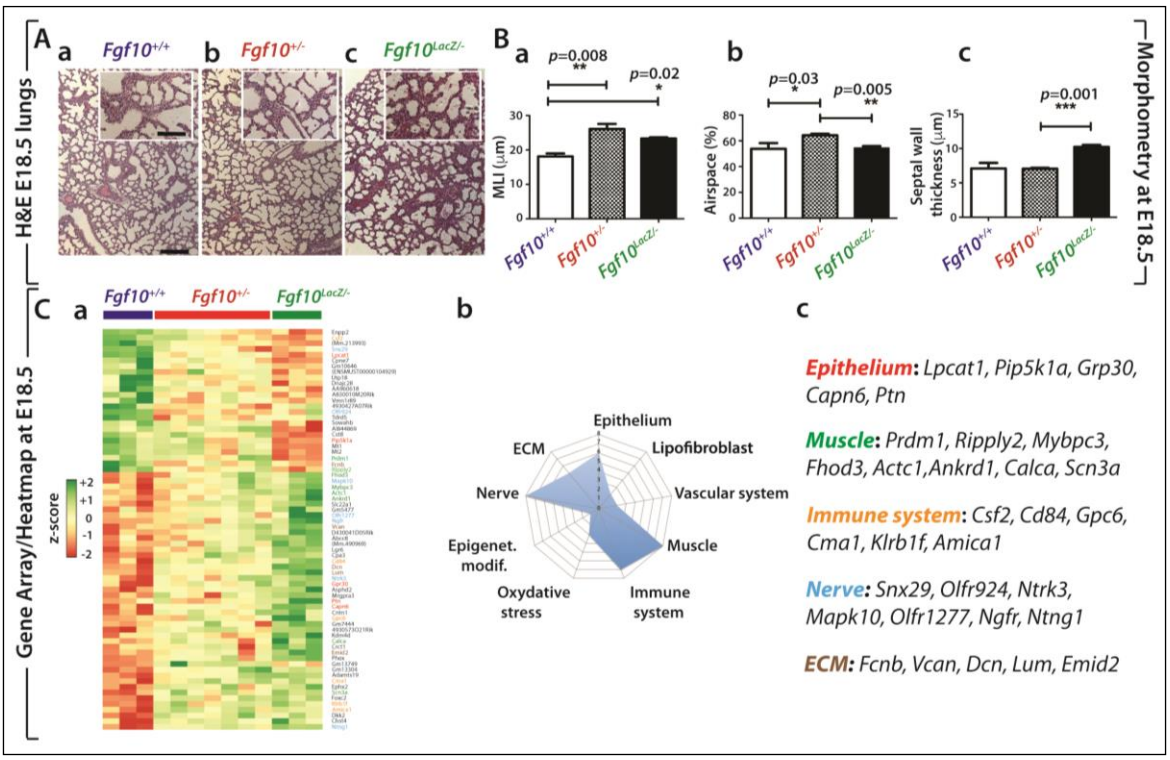

Figure 8. E18.5 *Fgf10*$^{+/-}$ lungs display perturbed morphometry and impaired gene expression.

(**A**) Haematoxylin/eosin staining of (**a**) *Fgf10*$^{+/+}$ (**b**) *Fgf10*$^{+/-}$ (**c**) and *Fgf10*$^{Lacz/-}$ lungs at E18.5. (**B**) Morphometry of the lungs shown in (**A**). Note the increase in (**a**) MLI, (**b**) airspace and no change in (b) septal wall thickness in *Fgf10*$^{+/-}$ lungs compared to *Fgf10*$^{+/+}$ (**C**) (**a**) Gene array-based/Heat map analysis of the whole lung of E18.5 *Fgf10*$^{+/+}$, *Fgf10*$^{+/-}$ and *Fgf10*$^{Lacz/-}$ lungs indicating that *Fgf10* deficient lungs display an impaired pattern of gene expression compared to *Fgf10*$^{+/+}$ lungs (see Figure S2 for greater magnification). (**b**) Symbolic representation of the genes affected grouped by cell types or processes. (**c**) Some of the relevant genes pertinent for the Epithelium, Muscle, Immune system, Nerve and ECM are listed. Scale bar Aa-c: 125 µm, inserts: 30 µm.

4.4. Effect of constitutive *Fgf10* deficiency on neonatal response to hyperoxia lung injury: Characterization of defects

4.4.1. *Fgf10*$^{+/-}$ mice reveal 100% lethality and significant defects in lung morphology upon neonatal hyperoxia lung injury

Before we tested the response of *Fgf10*$^{+/-}$ and the corresponding WT controls to HOX, we first analyzed *Fgf10*$^{+/-}$ (n=10) and WT (n=12) pups exposed to room air (normoxia) between P0 and P8 (Figure 9A). Newborn *Fgf10*$^{+/-}$ mice exposed to room air were completely viable. No macroscopic differences were observed between *Fgf10*$^{+/-}$ and WT littermates (data not shown). Morphometric analysis of P3 lungs (Figure 9Bb,d versus a,c, n=4 for each genotype) showed no significant differences between *Fgf10*$^{+/-}$ and WT for the mean linear intercept (MLI), airspace or septal wall thickness (Figure 9Ca-c). Our present results therefore show that at E18.5, morphometric analyzes reveal differences between the two genotypes. However, at P3, there is no obvious difference between *Fgf10*$^{+/-}$ and *Fgf10*$^{+/+}$ in NOX. The cellular and molecular mechanisms involved in this apparent recovery from E18.5 to P3 are still unknown.

To mimic the BPD phenotype, newborn pups were subjected to hyperoxia injury (85% oxygen) for up to 8 days (Figure 9D). In WT animals, this oxygen concentration is known to induce a BPD-like phenotype characterized by hypoalveolization (Berger & Bhandari, 2014) (see also Figure 5 for the validation of the model under our experimental conditions.). Two litters were generated and identical results were obtained. Figure 9E-G displays the results from one litter (14 pups). Survival analysis showed that 100% of the WT mice survived at day 8 while none of the *Fgf10*$^{+/-}$ experimental mice were alive at this time point. 50% lethality was observed already at P5, suggesting that damage to the lungs in *Fgf10*$^{+/-}$ neonates start earlier than P5 (Figure 9E). We therefore analyzed WT and *Fgf10*$^{+/-}$ lungs at postnatal day 3 (P3) during the course of HOX. At P3, hematoxylin-eosin staining of *Fgf10*$^{+/-}$ lungs (n=4) revealed an abnormal phenotype compared to WT lungs, with enlarged alveolar sacs and thinner interalveolar walls (Figure 9Fb,d versus a,c). Morphometric analysis demonstrated significant increase in MLI and airspace (both p=0.001) as well as decreased septal wall thickness (p=0.039) (Figure 9Ga-c). In conclusion, our results demonstrate that constitutive *Fgf10* deficiency leads to massive lethality of the pups upon HOX exposure. The

following experiments are designed to identify the onset, and the nature, of defects in *Fgf10*$^{+/-}$ lungs.

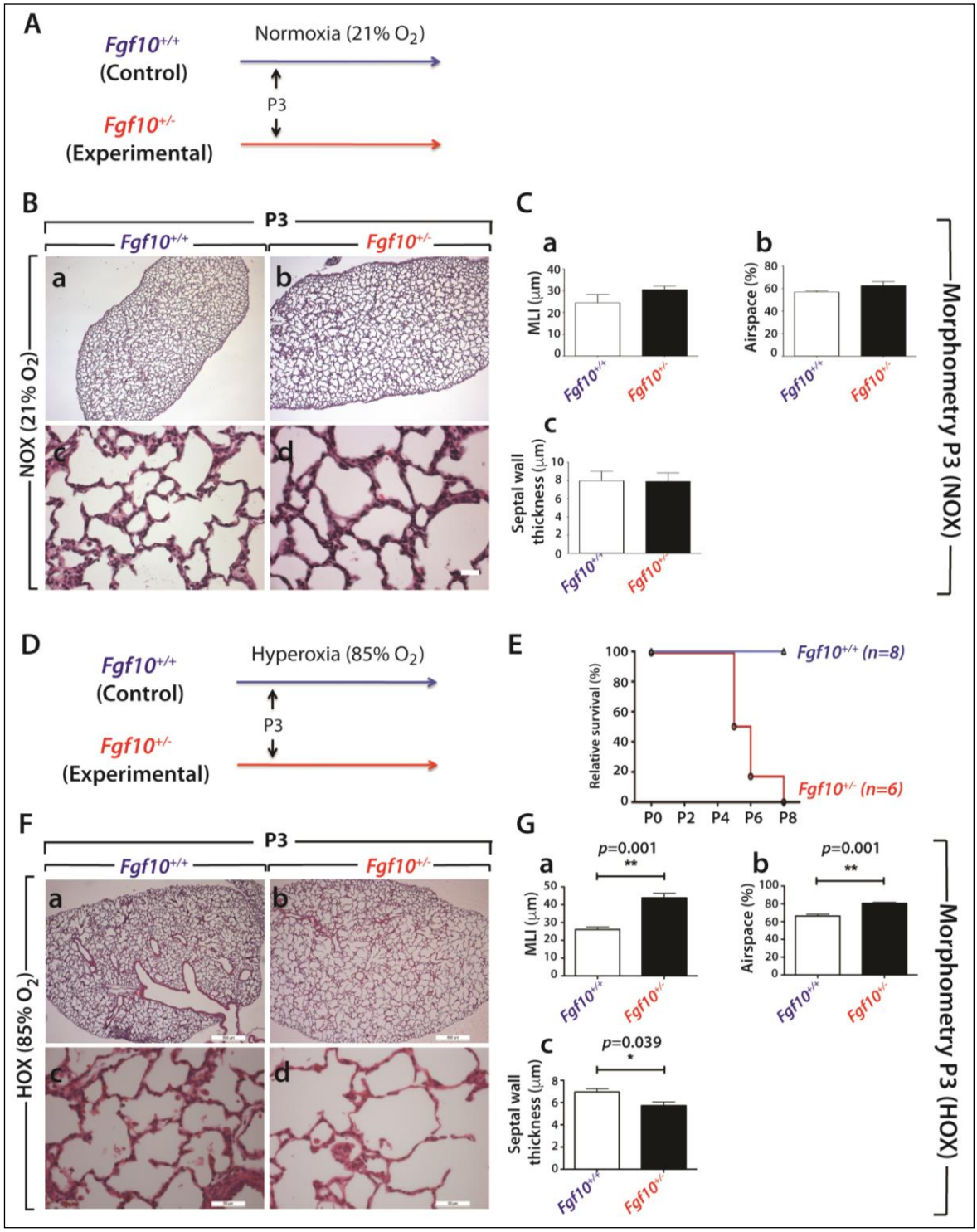

Figure 9. Constitutive *Fgf10* deficiency leads to neonatal death upon hyperoxia injury.

(**A**) Experimental set-up for NOX of *Fgf10*$^{+/-}$ (experimental group) and *Fgf10*$^{+/+}$ (control group) animals. (**B**) Haematoxylin/eosin staining of NOX exposed (**a,c**) control or (**b,d**) experimental lungs at P3. (**C**) Corresponding lung morphometric analysis. Note the absence of difference in (**a**) MLI, (**b**) airspace and (**c**) septal wall thickness. (**D**) Experimental set up for HOX of *Fgf10*$^{+/-}$ (experimental group) and *Fgf10*$^{+/+}$ (control group) animals. (**E**) Survival curve for HOX-exposed animals showing that all of the experimental animals died within 8 d, whereas all of the control animals survived. (**F**) Haematoxylin/eosin staining of HOX exposed (**a,c**) control or (**b,d**) experimental lungs at P3. (**G**) Corresponding lung morphometric analysis of HOX-exposed control and experimental animals. Note the increase in (**a**) MLI, (**b**) airspace and the decrease in (**c**) septal wall thickness. Scale bar for Ba,b: 500 µm, Bc,d: 50 µm, Fa,b: 500 µm and Fc,d: 50 µm

4.4.1.1. Adult *Fgf10*$^{+/-}$ mice in normoxia reveal impaired lung morphology and lung function at P70

Whereas there is no change in lung morphology at P3 in *Fgf10*$^{+/-}$ versus WT lungs (Figure 9B+C), the airspace is significantly decreased and the septal wall thickness is significantly increased in *Fgf10*$^{+/-}$ lungs at P70 (Figure 10A+B, WT n=4, *Fgf10*$^{+/-}$ n=3). Interestingly, this morphological change is associated with impaired lung function due to decrease in compliance and increase in elastance, while the resistance parameter does not change significantly (Figure 10C). Despite of the impaired lung function we did not observe any obvious reduction in activity or other changes in the appearance of the *Fgf10*$^{+/-}$ mice compared to WT mice. These data suggest a higher susceptibility of the lung tissue to the aging process in *Fgf10*$^{+/-}$ mice versus WT mice. A reduced regenerative capacity due to defects of stem/ progenitor cells could be a reason.

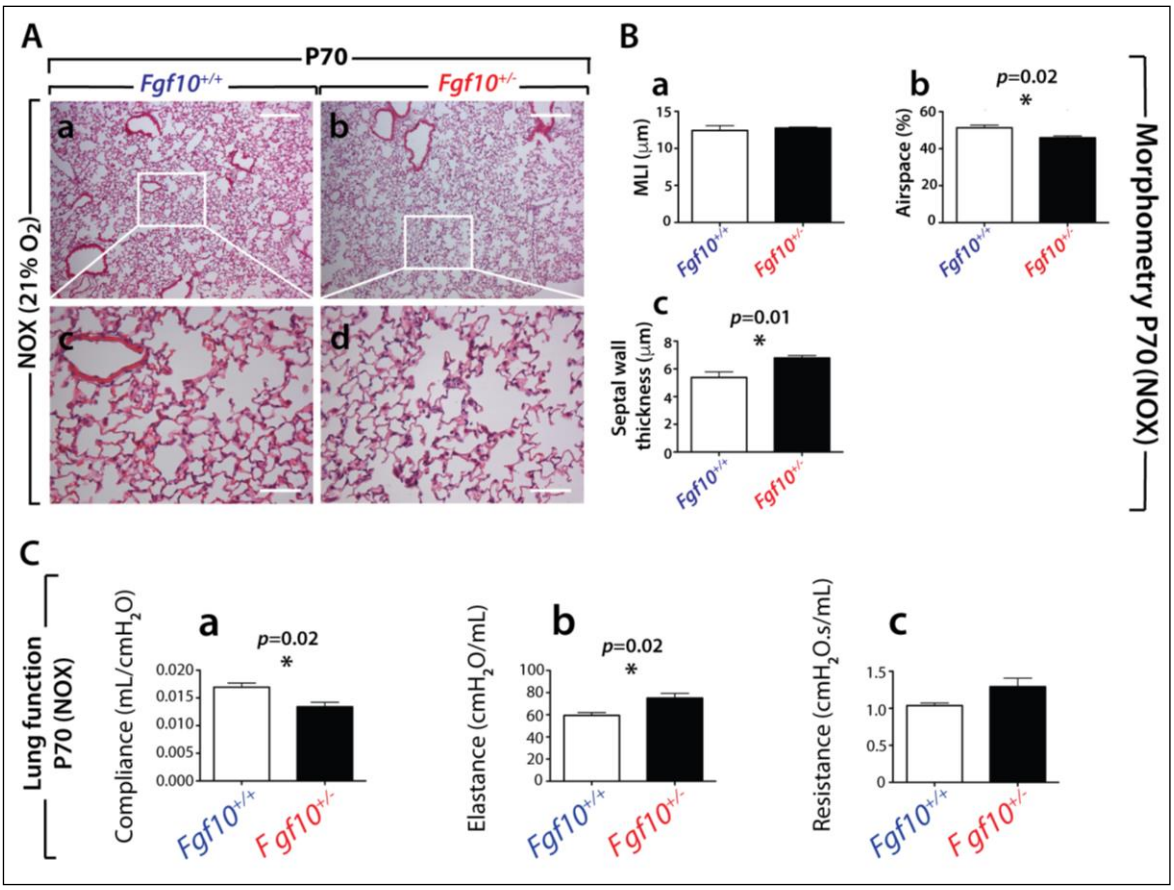

Figure 10. Constitutive *Fgf10* deficiency leads to impaired lung morphology and lung function at P70.

(**A**) Haematoxylin/eosin staining of NOX exposed (**a,c**) control or (**b,d**) experimental lungs at P70. (**B**) Corresponding lung morphometric analysis. Note the decreased (**b**) airspace and increased (**c**) septal wall thickness. (**C**) Lung function parameters at P70 reveals decreased (**a**) compliance, (**b**) increased elastance and no changes for (**c**) resistance. Scale bar for Aa,b: 500 µm, Ac,d: 50 µm.

4.4.2. Qualitative defects of AEC II cells

Our previous results suggested that *Fgf10*$^{+/-}$ lungs displayed epithelial abnormalities (Figure 7D). During lung development, the distal epithelium expressing FGFR2b responds to FGF10 secreted by the mesenchyme. It has been proposed that FGF10 signaling maintains the differentiation of the multipotent epithelial progenitors (positive for the transcription factors ID2, SOX9 and NKX2.1) (El Agha & Bellusci, 2014; Ramasamy et al., 2007; Volckaert et al., 2013). Interestingly, lineage tracing with the *Id2-CreERT2* driver line indicated that these multipotent progenitors give rise to AECI and AECII cells (Rawlins et al., 2009). Recently, single cell transcriptome analysis of the epithelium during lung development showed that AECI and AECII arise from a common bipotent epithelial progenitor pool, itself arising from the multipotent epithelial progenitor pool. In addition to the identification of a specific gene-set signature for AECI and AECII cells, which allows for a better characterization of these alveolar cells, this work showed that the bipotent progenitors expressed both gene-set signatures (Treutlein et al., 2014; Desai et al., 2014).

In order to define the contribution of AECII in the lethal phenotype observed in *Fgf10*$^{+/-}$ lungs, we isolated AECII from *Fgf10*$^{+/-}$ and WT P3 lungs in NOX and HOX conditions and compared their respective transcriptomes (see also supplementary material, Figure S1). In particular, we carried out an interaction "HOX x genotype" analysis. The volcano plot identified a set of genes that are either up- or down-regulated (Figure 11A). Interestingly, the majority of differences between the genotypes could be noted in the downregulated genes. The top 100 regulated

genes according to their *p*-values are represented in the corresponding heat maps (Figure 11Ba,b, see supplementary material, Figure S2 for greater magnification). We found a gene set (located in the lower part of the array) the expression of which was not drastically changed in HOX between the two genotypes (Figure 11Ba), but was differentially regulated in NOX conditions (Figure 11Bb). Furthermore, another gene set which was downregulated in HOX (located in the top part of the array) was upregulated in NOX conditions. KEGG analysis revealed that the altered processes were almost all linked to the immune system, and were downregulated in mutant AECII cells (Figure 11C). These processes were: systemic lupus erythematous, staphylococcus aureus infection, antigen presentation, graft versus host disease, and autoimmune thyroid disease, amongst others. In order to assess the differentiation status of the isolated AECII cells in *Fgf10*$^{+/-}$ versus WT lungs, we analysed the expression of the previously reported signatures for AECII and AECI (Treutlein et al., 2014) in the arrays generated from these cells in both NOX (Figure 11D) and HOX conditions (Figure 11E) (see supplementary material, Figure S3 for greater magnification.). In both conditions, we found a decrease in the AECII signature, with a corresponding increase in the AECI signature. Figure 11F, which shows a comparison of the differential expression between genotypes in HOX versus NOX confirms the differential clustering of the signatures for AECI and AECII.

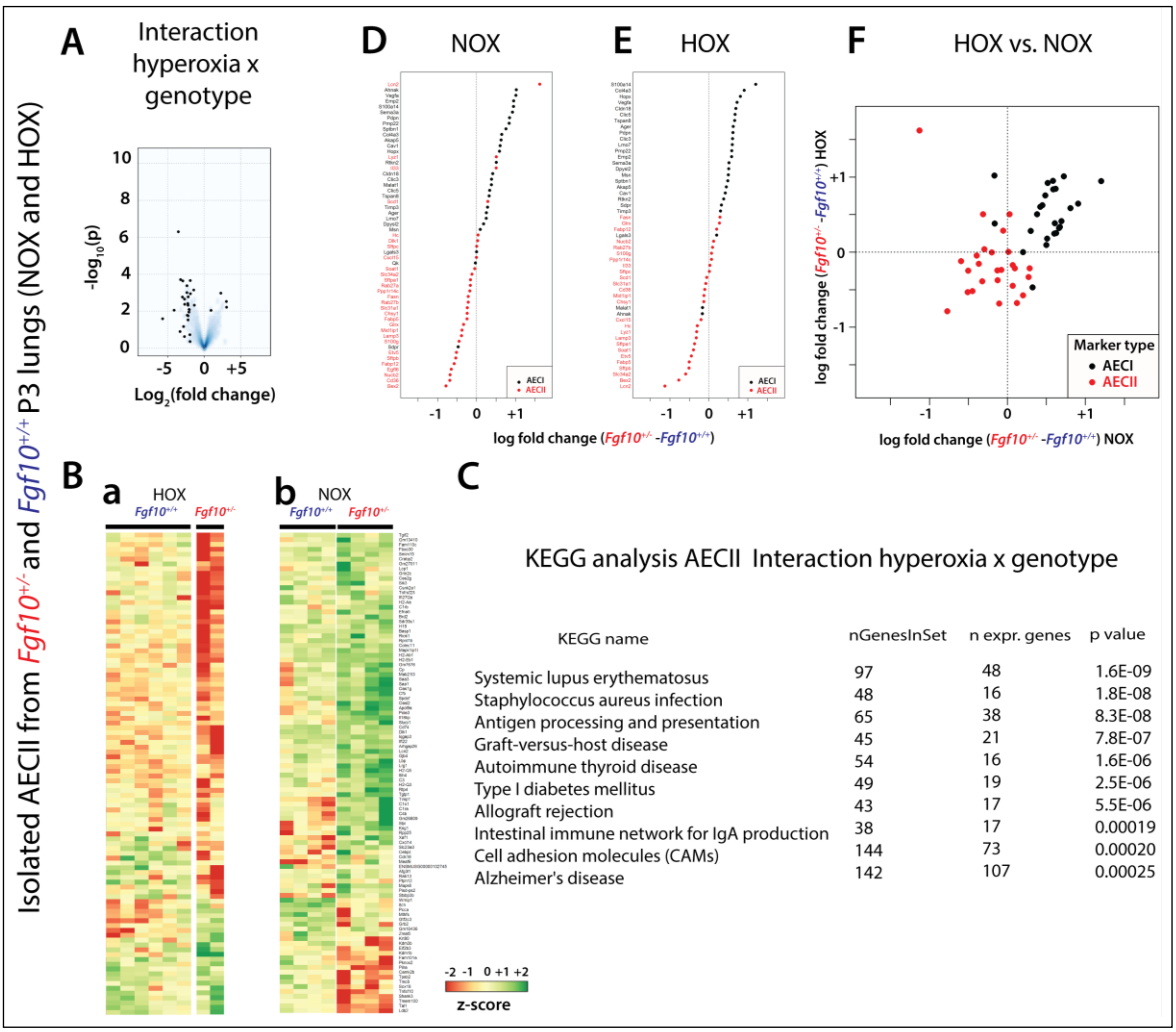

Figure 11. Interaction "hyperoxia x genotype" analysis to identify the significant genes/pathways differentially affected by HOX in isolated AECII cells from WT and *Fgf10*$^{+/-}$ lungs at P3.

(**A**) Volcano plot. (**B**) Top 100 regulated genes in (**a**) HOX versus (**b**) NOX in AECII cells isolated from *Fgf10*$^{+/-}$ and WT mice (see Figure S2 for greater magnification). (**C**) KEGG analysis of the interaction "hyperoxia x genotype". (**D**) AECI and AECII gene-set analysis comparing AECII cells isolated from *Fgf10*$^{+/-}$ and WT lungs in NOX (see Figure S3 for greater magnification). (**E**) AECI and AECII gene-set analysis comparing AECII cells isolated from *Fgf10*$^{+/-}$ and WT lungs in HOX. (see Figure S3 for greater magnification). (**F**) AECI and AECII gene-set analysis in AECII cells isolated from *Fgf10*$^{+/-}$ versus WT lungs in HOX or NOX.

4.4.3. *Fgf10*$^{+/-}$ lungs in the context of HOX exhibit decreased mature SFTPC expression associated with quantitative defects of AECII

Using western blotting (whole lung homogenates, n=4 for WT and n=3 for *Fgf10*$^{+/-}$ lungs at P3, Figure 12Aa,b) we quantified the protein expression of FGF10, FGFR2 (using an antibody which does not discriminate between the FGFR2b versus the FGFR2c isoform) and mature SFTPC and SFTPB. We noted a significantly reduced expression of all these markers in *Fgf10*$^{+/-}$ versus WT (Figure 12Ac-f).

Next, we investigated by FACS the number of total epithelial cells (using EpCAM as a general marker), AECI (T1α-positive), AECII (SFTPC-positive) and epithelial stem progenitor cells (EpiSPC, EpCAMhigh CD24low). In NOX, we observed a significant decrease in the ratio of EpCAM-positive cells over the total cell number in *Fgf10*$^{+/-}$ versus WT lungs (Figure 12Ba). Interestingly, rather than a global decrease in the ratio of AECI and AECII over the total number of cells in the *Fgf10*$^{+/-}$ versus WT lungs, we noted an increase in the ratio of AECI (Figure 12Bb) and an associated decrease in the ratio of AECII cells (Figure 12Bc) in the *Fgf10*$^{+/-}$ versus WT lungs. This observation has been confirmed in 10 weeks (P70) old *Fgf10*$^{+/-}$ versus WT lungs (Figure S4). This suggests that *Fgf10* deficiency leads to substantial differentiation of the previously identified bipotent progenitor cells along the AECI lineage at the expense of the AECII lineage. This defect is in addition to the previously described impaired differentiation of the AECII cells in *Fgf10*$^{+/-}$ versus WT P3 lungs (Figure 11D-F). Interestingly, no difference was observed in the ratio of EpiSPC cells over the EpCAM high population in *Fgf10*$^{+/-}$ versus WT lungs (Figure 12Bd). Following hyperoxia injury, the ratio of epithelial cells (EpCAM+) in *Fgf10*$^{+/-}$ versus WT was no longer significant, suggesting compensatory proliferative events in *Fgf10*$^{+/-}$ (Figure 12Be). However, the quantitative imbalance in AECI ratio in *Fgf10*$^{+/-}$ versus WT remained (Figure 12Bf), while the AECII (SFTPC-positive) ratio in *Fgf10*$^{+/-}$ versus WT was no longer significant (Figure 12Bg). This suggests that the AECII pool in *Fgf10*$^{+/-}$ is partially replenished upon HOX. As for NOX, no difference was observed in the ratio of EpiSPC cells in *Fgf10*$^{+/-}$ versus WT (Figure 12Bh). Investigating changes in the mesenchyme revealed significant increases in NOX, for the fraction of CD45-, CD31-, and EpCAM- over total cells in *Fgf10*$^{+/-}$ versus WT lungs (Figure S5Aa). This increase likely reflects the reduced number of epithelial cells. This difference

in the number of mesenchymal cells between the two genotypes was no longer detected in HOX (Figure S5Ab). Quantification of the ratio of hematopoietic and endothelial cells (defined as CD45-positive, CD31-positive, EpCAM-negative) by FACS showed no difference in NOX and HOX between *Fgf10*$^{+/-}$ and WT lungs at P3 (Figure S5B), suggesting no significant inflammation in *Fgf10*$^{+/-}$ versus WT at this stage.

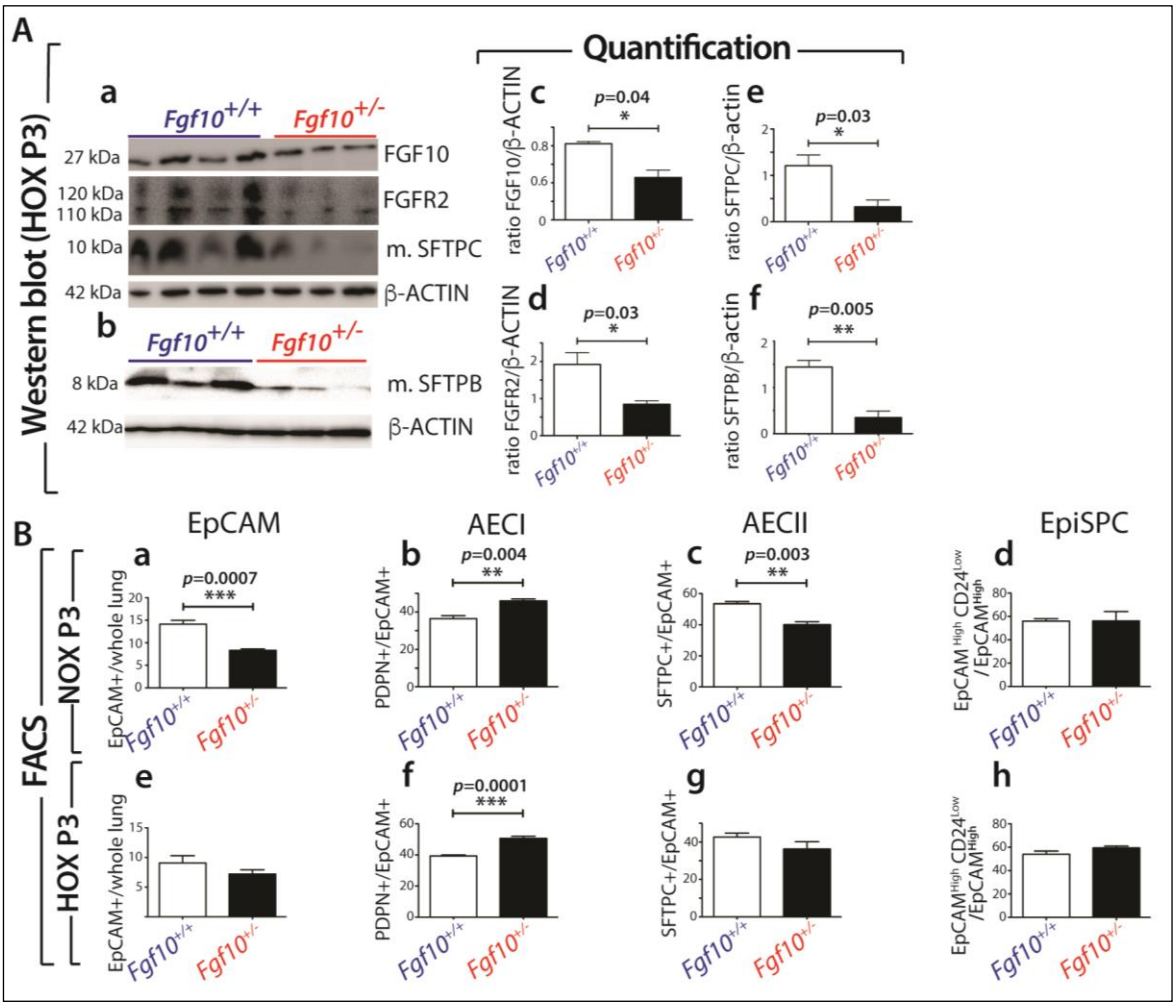

Figure 12. *Fgf10*$^{+/-}$ lungs in the context of HOX exhibit less mature-SFTPC and mature-SFTPB.

(**A**) Western blotting analysis (whole lung homogenates) for (**a**) FGF10, FGFR2, mature-SFTPC and α-ACTIN as well as (**b**) mature-SFTPB and α-ACTIN on *Fgf10*$^{+/+}$ and *Fgf10*$^{+/-}$ lungs exposed to HOX at P3. (**c-f**) Quantification of bands using ImageJ software. (**B**) Fluorescence Activated Cell Sorting in NOX (**a-d**) and HOX (**e-h**) of *Fgf10*$^{+/+}$ and *Fgf10*$^{+/-}$ P3 lungs for (**a,e**) epithelial cells (EpCAM+), (**b,f**) AECI, (**c,g**) AECII and (**d,h**) epithelial stem progenitor cells (EpiSPC).

4.4.4. Blood vessel numbers and their muscularization are indistinguishable between *Fgf10*$^{+/-}$ versus WT lungs in NOX

Vascular morphometry analysis at P3, to quantify the number of vessels and extent of muscularization of these vessels, was performed. Vessels were subdivided into four groups based on their diameters (10-20 µm, 20-70 µm, 70-150 µm and >150 µm). While no difference in total vessel count was noted, a substantial reduction was observed in the number of 70-150 µm vessels between *Fgf10*$^{+/-}$ versus WT in NOX ($p=0.049$) (Figure 13A). No difference in muscularization between *Fgf10*$^{+/-}$ and WT lungs was noted (Figure 13Ea-d).

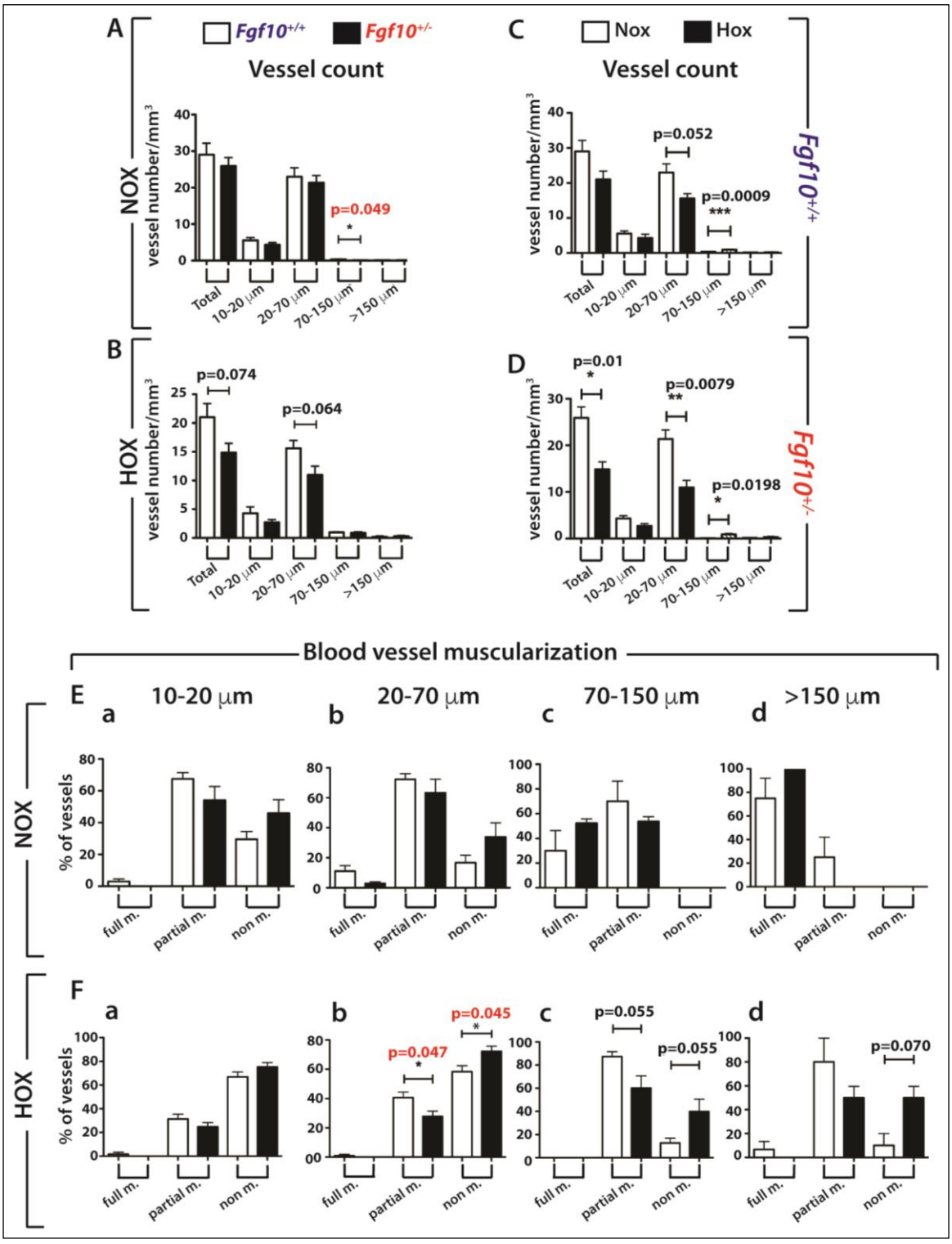
A
Fgf10+/+
Fgf10+/-
Vessel count
NOX
vessel number/mm3
p=0.049
Total
10-20 µm
20-70 µm
70-150 µm
>150 µm
C
Nox
Hox
Vessel count
p=0.052
p=0.0009
Fgf10+/+
B
HOX
p=0.074
p=0.064
D
p=0.01
p=0.0079
p=0.0198
Fgf10+/-
Blood vessel muscularization
E
a 10-20 µm
b 20-70 µm
c 70-150 µm
d >150 µm
% of vessels
full m.
partial m.
non m.
F
p=0.047
p=0.045
p=0.055
p=0.055
p=0.070

Figure 13: Analysis of the vascular defects in P3 *Fgf10*$^{+/-}$ versus *Fgf10*$^{+/+}$ (WT) in HOX indicates that *Fgf10*$^{+/-}$ vessels are more sensitive to HOX injury and exhibit a less muscularized phenotype.

(**A**) Total vessel count in NOX between P3 *Fgf10*$^{+/+}$ and *Fgf10*$^{+/-}$ lungs. No significant difference is observed. (**B**) Total vessel count in HOX between P3 *Fgf10*$^{+/+}$ and *Fgf10*$^{+/-}$ lungs. There is a decreasing trend in the total number of blood vessels in *Fgf10*$^{+/-}$ lungs as well as for the group of blood vessel with 20-70 µm diameter. (**C+D**) Total vessel count between NOX and HOX in (**C**) *Fgf10*$^{+/+}$ and (**D**) *Fgf10*$^{+/-}$ lungs. Note the decrease in the number of blood vessels displaying a 20-70 µm and 70-150 µm diameter upon HOX for both *Fgf10*$^{+/+}$ and *Fgf10*$^{+/-}$ lungs. Note also the significant decrease in the total number of blood vessels of all diameters included in (**D**) *Fgf10*$^{+/-}$ lungs, suggesting that the blood vessels in *Fgf10*$^{+/-}$ lungs are more sensitive to HOX. (**E**) Blood vessel muscularization in normoxia between *Fgf10*$^{+/+}$ and *Fgf10*$^{+/-}$ lungs for blood vessels at (**a**) 10-20 µm, (**b**) 20-70 µm, (**c**) 70-150 µm and (**d**)>150 µm. No significant difference is observed. (**F**) Blood vessel muscularization in hyperoxia between *Fgf10*$^{+/+}$ and *Fgf10*$^{+/-}$ lungs for blood vessels at (**a**) 10-20 µm, (**b**) 20-70 µm, (**c**) 70-150 µm and (**d**)>150 µm. Note that for the 20-70 µm and 70-150 µm, there is a decrease in the partially muscularized vessels and an increase in the number of non-muscularized vessels between the *Fgf10*$^{+/-}$ and *Fgf10*$^{+/+}$ lungs indicating a less muscularized, more immature vascular phenotype in *Fgf10*$^{+/-}$ lungs.

4.4.5. A trend towards decreased number of blood vessels and decreased muscularization is observed in *Fgf10*$^{+/-}$ versus WT lungs exposed to HOX

We first compared the number of blood vessels in *Fgf10*$^{+/-}$ versus WT lungs in HOX (Figure 13B). We observed a trend towards a decrease in total blood vessel count in *Fgf10*$^{+/-}$ with the 20-70 µm blood vessels being the most affected. Next, we compared the number of blood vessels in WT and *Fgf10*$^{+/-}$ in HOX versus NOX (Figure 13C). In WT lungs, we observed a trend towards a drop in total blood vessel count upon HOX injury, the 20-70 µm blood vessels being the most affected (Figure 13C). Interestingly, in WT lungs, HOX significantly increased the number of 70-150 µm blood vessels ($p=0.0009$). In *Fgf10*$^{+/-}$ lungs, HOX significantly reduced

the total blood vessel count (p=0.01) (Figure 13D). As for the WT, we observed a decrease in the number of 20-70 µm blood vessels (p=0.0079) and an increase in the number of 70-150 µm blood vessels (p=0.0198). Finally, we analyzed blood vessel muscularization (Figure 13Fa-d). A major loss of muscularization was seen for the group of blood vessel with 20-70 µm diameter (Figure 13Fb) and a trend towards reduction was observed for the blood vessels with 70-150 µm diameter. In spite of these defects, we failed to see any evidence of lung hemorrhage in *Fgf10*$^{+/-}$ lungs in HOX (either at P3, P5, or P8, data not shown), which suggests that the contribution of the vascular system to the lethal phenotype is likely minor in our experimental conditions.

4.5. Effect of blockade of FGFR2b ligands in normoxia and hyperoxia

4.5.1. Attenuation of FGFR2b ligands during the pseudoglandular (E14.5) and saccular (E16.5) stage of embryonic lung development affects alveolar lineage formation

In order to confirm what we observed in the constitutive *Fgf10* deficient mice, we tested functionally the role of FGF signaling during embryonic alveolar lineage formation. We used a previously reported dominant negative soluble *Fgfr2b* expression approach (*Rosa26rtTA/+;Tg(tet(O)sFgfr2b)/+* mice) to trap, in an ubiquitous and doxycycline-based inducible manner, all the FGFR2b ligands, thereby turning off FGFR2b signaling mediated by FGF1, 3, 7 and 10 (see Figure 6) (Al Alam et al., 2015; Volckaert et al., 2011; Danopoulos et al., 2013; MacKenzie et al., 2015; Parsa et al., 2010; Parsa et al., 2008). In this first functional in vivo experiment, we attenuated FGFR2b signaling from E14.5 to E18.5 (Figure 14A). The examination of the experimental (n=3) and control lungs (n=4) revealed abnormal lung development with delayed growth as well as quantitatively decreased and dilated epithelial end buds (Figure 14B). The epithelial (EpCAM-positive), AECI (T1α-positive) and AECII (SFTPC-positive) cell populations were validated by FACS (Figure 14C). In spite of a total reduction of EpCAM-positive cells by 300% in experimental versus control lungs (data not shown), the EpCAM-positive/whole lung homogenate ratio did not change between experimental and control lung but a clear reduction of the ratio of AECI and AECII (to the total

number of EpCAM+ cells) was observed indicating aborted alveolar lineage formation.

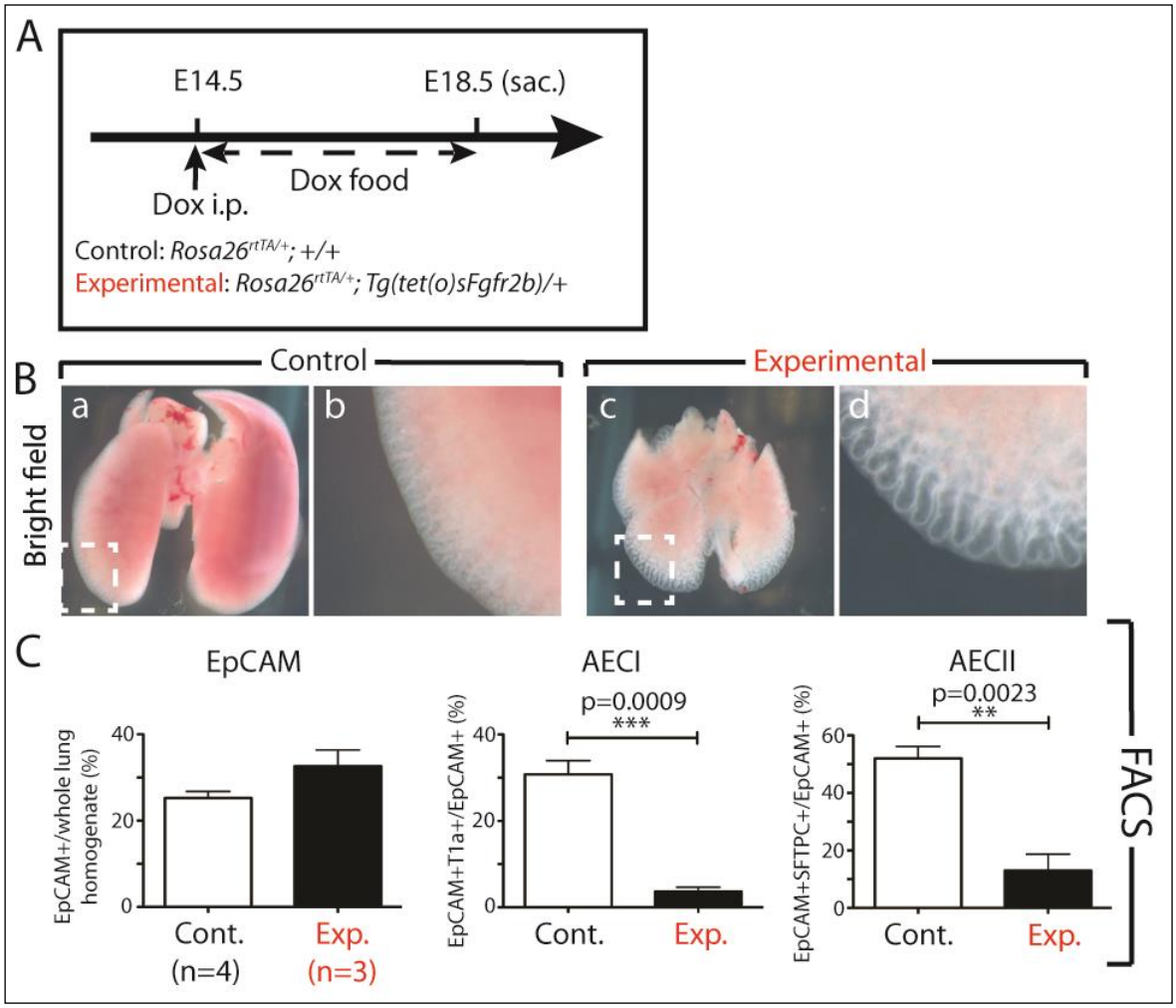

Figure 14. Inhibition of FGFR2b signaling from E14.5 to E18.5 leads to impaired AECI and AECII formation.

(**A**) Experimental approach. Pregnant females carrying control and experimental embryos were given doxycycline intraperitoneally and via food from E14.5 to E18.5. (**B**) Appearance of the control and experimental lungs at E18.5. Note the reduced size and dilated branches at the tip in the experimental versus control lung. (**C**) FACS for EpCAM+, T1α+ and SFTPC+ cells in control and experimental lungs at E18.5. Note that the epithelial-mesenchymal ratio of experimental and control lungs are similar in spite of reduced size for the mutant. The number of SFTPC+ and T1α+ cells (over EpCAM+ cells) in experimental versus control lungs is significantly reduced.

Next, we attenuated FGFR2b signaling from E16.5 to E18.5 (Figure 15A). At E18.5 the experimental (n=5) and control (n=3) lungs were macroscopically undistinguishable (Figure 15B). The proportions of EpCAM-positive, T1α-positive and SFTPC-positive cells were quantified by FACS. No changes were observed for the EpCAM ratio between experimental and control lungs (as well as for the total number of EpCAM-positive cells - data not shown). Interestingly, we found a reduction in the ratio of AECII cells associated with an increase in the ratio of AECI cells which suggests that FGF signaling controls the differentiation balance between AECI and AECII in favor of AECII cells (Figure 15C).

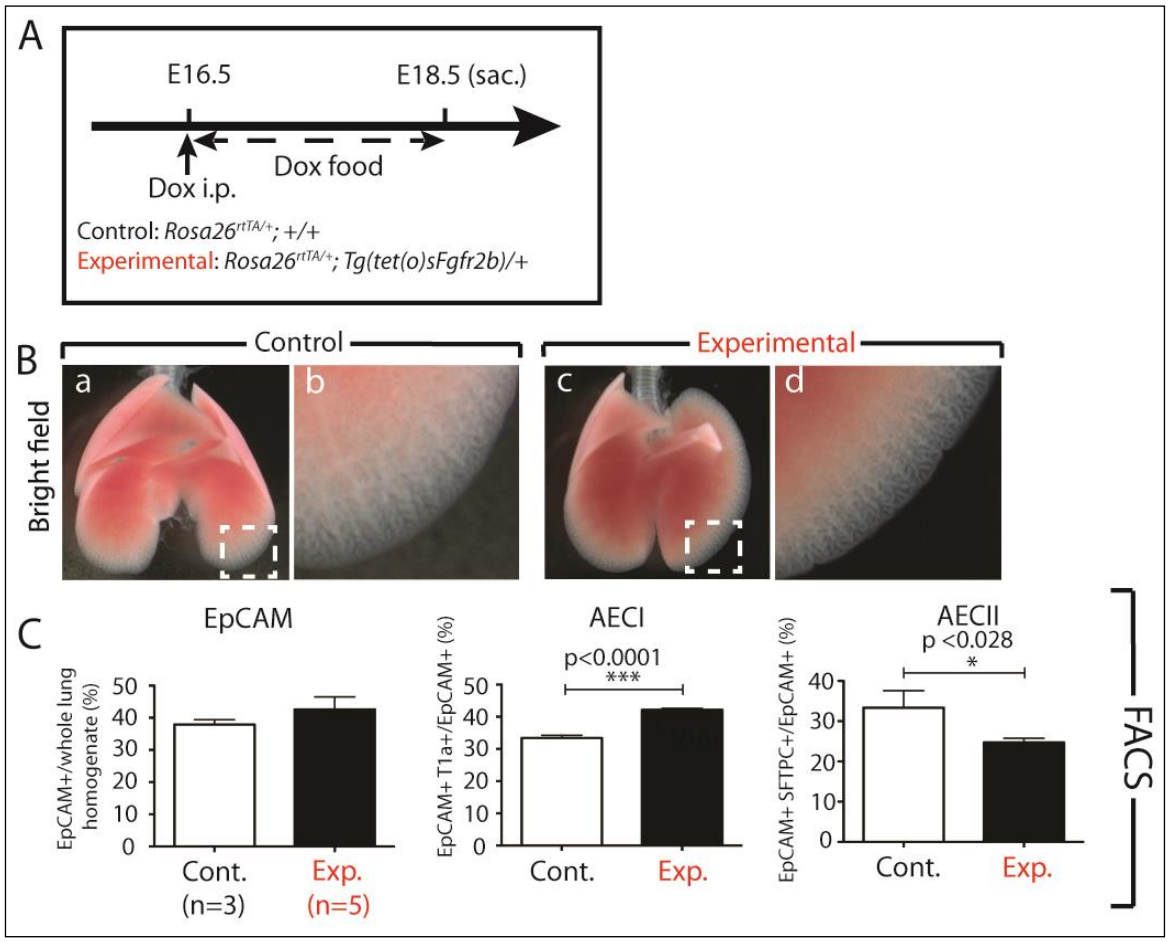

Figure 15: Transient FGFR2b signaling inhibition from E16.5 to E18.5 leads to increased T1α+ and reduced SFTPC+ cells (over EpCAM+ cells).

(**A**) Experimental approach. Pregnant females carrying control and experimental embryos were given doxycycline intraperitoneally and via food from E16.5 to E18.5. (**B**) Appearance of the control and experimental lungs at E18.5. Macroscopically there was no difference between the experimental versus control lung. (**C**) FACS for EpCAM+, T1α+ and SFTPC+ in control and experimental lungs at E18.5. Note the reduction in the fraction of AECII cells (SFTPC+) while the fraction of AECI (T1α+) cells increases.

4.5.2. Postnatal attenuation of FGFR2b ligands in NOX, during the saccular/alveolar stage of lung development, does not cause lung structural defects or lethality

As no congenital mutation in the *FGF10* gene in patients with BPD has been reported so far, it is reasonable to assume that *FGF10* deficiency in BPD patients occurs after the premature birth of these babies. It is therefore likely that in BPD babies, the initial stages of lung development occur in the presence of normal levels of *FGF10*. To mimic this situation in a mouse model, we again used the previously mentioned *Rosa26rtTA/+;Tg(tet(O)sFgfr2b)/+* mice. Using this approach, we silenced FGFR2b signaling in the postnatal lung during the saccular and the beginning of the alveolar stages, between P0 and P8 (Figure 16A-D). In NOX, we observed no lethality (Figure 16B) and no structural defects (Figure 16C,D) between double transgenic experimental lungs (DTG) and single transgenic control lungs (STG). Similar results were observed upon exposure to doxycycline for a longer time period, from P0 to P105 (Figure S6).

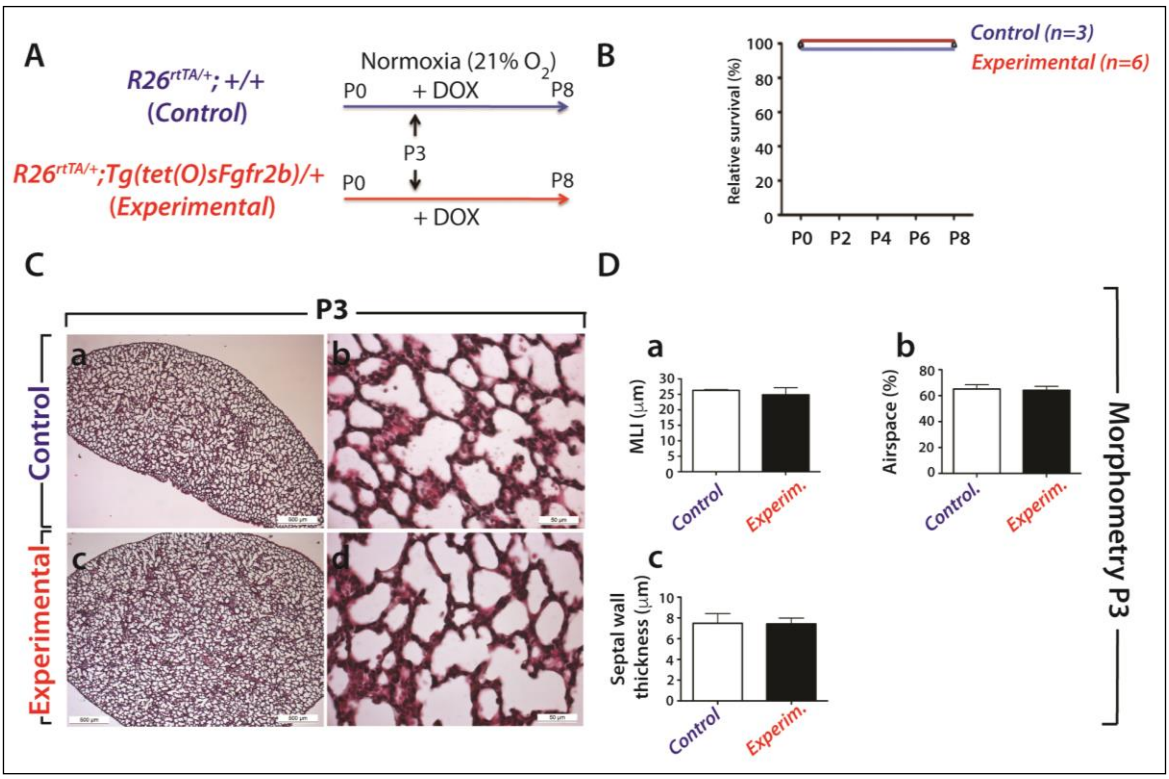

Figure 16. Attenuation of FGFR2b ligands postnatally in the context of NOX does not affect lung morphology.

(**A**) Experimental set-up for NOX of *R26rtTA/+;Tg(tet(O)sFgfr2b)/+* (experimental group) and *R26rtTA/+; +/+* (control group) animals. Animals are fed with doxycycline-containing food to induce the dominant negative soluble *Fgfr2b* in the experimental group. (**B**) Survival curve for NOX exposed animals indicating that all experimental and control animals survive in NOX. (**C**) Haematoxylin/eosin staining of NOX exposed (**a,b**) control or (**c,d**) experimental lungs at P3. (**D**) Corresponding lung morphometric analysis. Note the absence of differences in (**a**) MLI, (**b**) airspace and (**c**) septal wall thickness. Scale bar for Ca,c: 500 µm and Cb,d: 50 µm.

4.5.3. Postnatal attenuation of FGFR2b ligands in HOX, during the saccular/alveolar stage of lung development, leads to significant lethality due to decreased SFTPC expression

In contrast to NOX, the exposure to HOX induced 50% lethality in the *Rosa26rtTA/+;Tg(tet(O)sFgfr2b)/+* DTG experimental group, beginning at P6

(Figure 17A,B). Compared to *Fgf10*$^{+/-}$ neonatal mice, this lethality started one day later (see Figure 8E) and the lethality rate at P8 was lower (100% versus 50% death in *Fgf10*$^{+/-}$ versus DTG, respectively). Morphometry at P3 (Figure 17C,Da) showed increased MLI (+19.3%, p=0.029) between DTG experimental and STG control groups. This value, compared to the *Fgf10*$^{+/-}$ versus WT in HOX (Figure 8Ga) (+68.2%, p=0.001), supports our conclusion that, in HOX, DTG lungs exhibit a less severe phenotype than *Fgf10*$^{+/-}$ lungs. Overall, we conclude that in HOX a complete attenuation of FGFR2b ligands postnatally leads to lethality. However, the constitutive decrease in *Fgf10* expression throughout the different phases of lung development adds further complications, making the phenotype more severe.

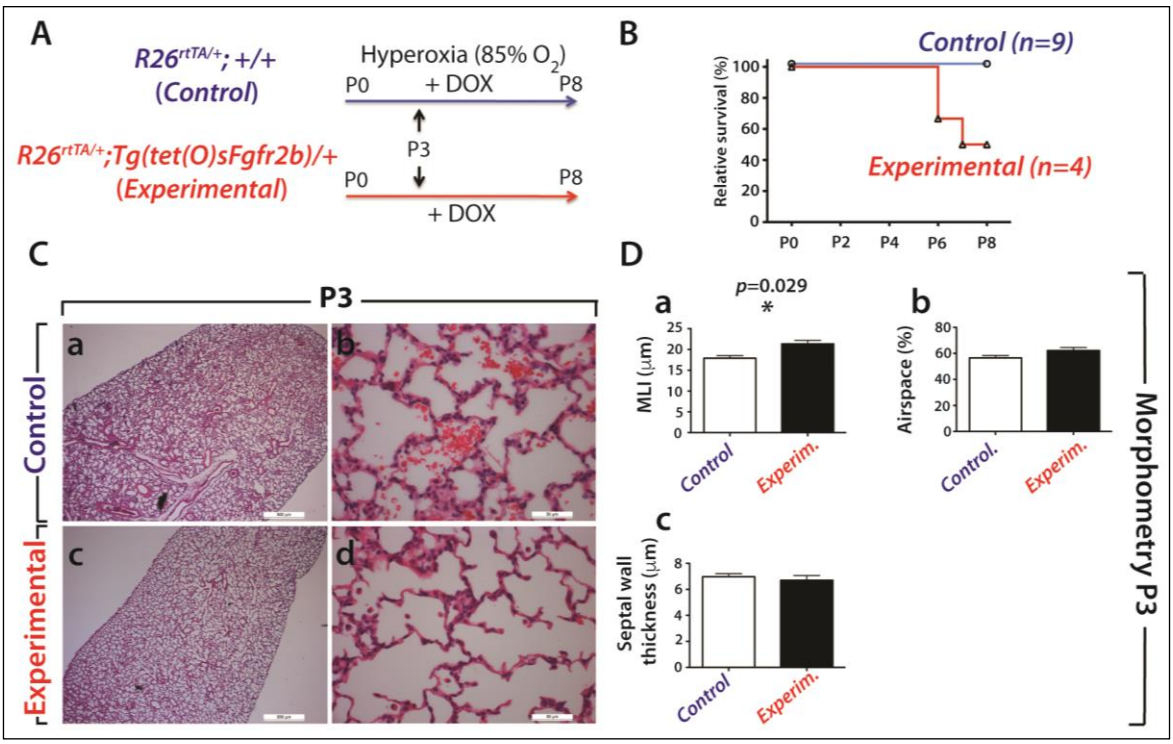

Figure 17. Attenuation of FGFR2b ligands postnatally in the context of HOX exposed pups leads to significant lethality.

(**A**) Experimental set-up for HOX of *R26rtTA/+;Tg(tet(O)sFgfr2b)/+* (experimental group) and *R26rtTA/+; +/+* (control group) animals. (**B**) Survival curve for HOX exposed animals indicating that 50% of the experimental animals die within 8 days while all the control animals survive. (**C**) Haematoxylin/eosin staining of HOX exposed (**a,b**) control or (**c,d**) experimental lungs at P3. (**D**) Corresponding lung morphometric analysis of HOX exposed control and experimental animals. Note the increase in (**a**) MLI while (**b**) airspace and (**c**) septal wall thickness are not affected. Scale bar for Ca,c: 500 µm and Cb,d: 50 µm.

As the *Fgf10*$^{+/-}$ versus WT lungs at P3 in HOX presented quantitative defects (increased AECI, decreased AECII) as well as impaired AECII differentiation (reduced AECII signature, increased AECI signature) associated with reduced SFTPC expression, we also carried out western blot for SFTPC and FACS analysis to quantify the number of total epithelial cells (using EpCAM as a general marker), AECI (T1α-positive) and AECII (SFTPC-positive) in DTG and STG P3 lungs in NOX and HOX (Figure 18). In NOX, we did not find any significant difference between DTG and STG lungs (Figure 18A,B). By contrast, in HOX we observed a reduction in SFTPC expression (Figure 18C), suggesting defective AECII cells (western blots were done by Negah Ahmadvand). However, FACS analysis failed to show quantitative differences between DTG experimental and STG control groups for epithelial, AECI and AECII cell numbers (Figure 18D).

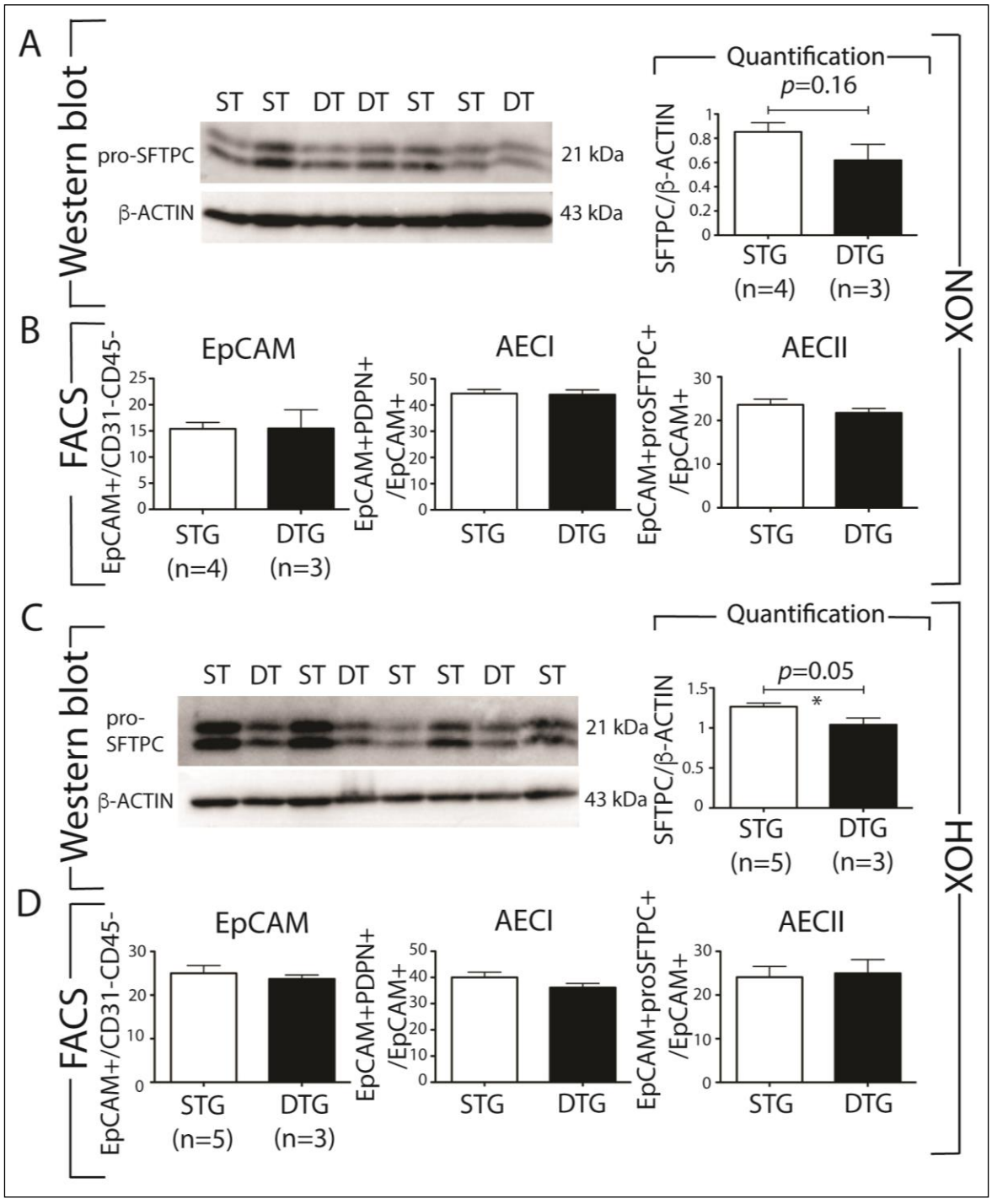
A
Western blot
ST ST DT DT ST ST DT
pro-SFTPC
β-ACTIN
21 kDa
43 kDa
Quantification
p=0.16
SFTPC/β-ACTIN
STG (n=4)
DTG (n=3)
XON
B
FACS
EpCAM+/CD31-CD45-
EpCAM
AECI
AECII
EpCAM+PDPN+ /EpCAM+
EpCAM+proSFTPC+ /EpCAM+
STG (n=4)
DTG (n=3)
C
Western blot
ST DT ST DT ST ST DT ST
pro-SFTPC
β-ACTIN
21 kDa
43 kDa
Quantification
p=0.05
*
SFTPC/β-ACTIN
STG (n=5)
DTG (n=3)
XOH
D
FACS
EpCAM+/CD31-CD45-
EpCAM
AECI
AECII
EpCAM+PDPN+ /EpCAM+
EpCAM+proSFTPC+ /EpCAM+
STG (n=5)
DTG (n=3)

Figure 18. *Rosa26rtTA/+;Tg(tet(o)sFgfr2b)/+* (DTG) lungs in the context of HOX exhibit decreased SFTPC expression without quantitative change in the prevalence of epithelial (EpCAM+), AECI and AECII cells.

(A) Western blot analysis for pro-SFTPC and β-ACTIN of STG and DTG P3 lungs exposed to NOX. Quantification of the western blot results shows no difference between STG and DTG mice. (**B**) Fluorescence Activated Cell Sorting of cells from STG and DTG P3 lungs in NOX for Epcam, AECI and AECII cells. No quantitative changes are observed in NOX. (**C**) Western blot analysis for pro-SFTPC and β-ACTIN on STG and DTG P3 lungs exposed to HOX. Quantification of the western blot results shows a significant decrease in SFTPC expression in DTG versus STG mice. (**D**) Fluorescence Activated Cell Sorting of cells of STG and DTG P3 lungs in HOX for epithelial (EpCAM+), AECI and AECII cells. No quantitative changes are observed in HOX.

4.6. Summary of results

In summary, the questions asked at the beginning of this study (see section 2. Objectives) could be answered as follow:

1) Does constitutive *Fgf10* deficiency affect embryonic lung development?

   Yes, constitutive *Fgf10* deficiency leads to delayed branching of the embryonic lung due to decreased proliferation of the epithelium at E12.5. Furthermore, at E18.5 the lung morphology and gene expression are changed.

2) What is the impact of constitutive *Fgf10* deficiency on the cellular and molecular level of the lung?

   On the cellular level constitutive *Fgf10* deficiency leads to increase of the AECI population on the expense of the AECII population in normoxia and hyperoxia. Genes for FGF10 signaling was downregulated and genes for TGF-β signaling was upregulated at E18.5. Most important, in isolated AECII cells the gene signatures for AECII is decreased. Instead, the AECII

cells acquire the gene signatures of AECI cells.

3) What is the impact of constitutive *Fgf10* deficiency on hyperoxia lung injury in the newborn (BPD mouse model)?

   Constitutive *Fgf10* deficiency leads to quantitative and qualitative defects of the AECII cells resulting in susceptibility of the lung towards oxygen toxicity (BPD mouse model). As a consequence of this susceptibility the lung epithelium reveals a higher degree of damage and significant decrease in surfactant protein B and C production upon hyperoxia lung injury, which leads to death.

4) Does blockade of FGF10/FGFR2b signaling affect embryonic and postnatal lung development?

   Yes, blockade of FGF10/FGFR2b signaling starting at late pseudoglandular stage (E14.5) leads to decrease of AECI and AECII. In comparison, blockade of FGF10/FGFR2b signaling starting at saccular stage (E16.5) reveals a quantitative increase of AECI on the expenses of AECII. In contrast, postnatal blockade of FGF10/FGFR2b signaling from P0-P105 does not affect lung structure.

5) Is FGF10/FGFR2b signaling relevant during postnatal hyperoxia lung injury?

   FGF10/FGFR2b signaling during postnatal hyperoxia lung injury is relevant since a blockade leads to lethality due to increased damage of the lung tissue and decreased production of surfactant protein C.

5. Discussion

Our study provides, for the first time, experimental evidence in mice that *Fgf10*-mRNA levels are critical for proper alveolar lineage formation. *Fgf10* is essential for the proper differentiation of the AECII cells and for the formation of the appropriate number and ratio of AECII versus AECI cells. In the presence of reduced *Fgf10* expression, the differentiation of AECII cells is impaired, as evidenced by the reduced expression of AECII markers and the concomitant increased expression of AECI markers. Furthermore, FACS analysis indicates that, compared to their WT littermates, the ratio of AECI cells to the total number of EpCAM-positive cells is increased, while that of AECII cells ratio is decreased. In the context of HOX injury, these quantitative and qualitative defects in the alveolar lineage are associated with 100% lethality, which most likely results from the observed defective surfactant production. This supports our conclusion that defective AECII cells are causative for this lethal phenotype. Interestingly, decrease in FGF10 expression has also been reported in the lungs of BPD patients. Premature babies at risk of developing BPD are generally born between 24 and 28 weeks, which corresponds to the end of the canalicular/mid-saccular stages of lung development. This is the time when the bipotent epithelial progenitors in the alveolar lineage differentiate into AECI and AECII. Supporting the observation of AECII defects in BPD patients, a collaborative project provided evidence for decreased SFTPC expression in lungs of patients with BPD by using immunostaining (data not shown). We also have demonstrated that the attenuation of FGFR2b signaling during the saccular stage, in the context of HOX injury, leads to lethality due to abnormal surfactant production. Altogether, our results demonstrate a critical role for *Fgf10* in alveolar lineage formation and suggest that quantitative and qualitative differences in AECII could be causative for lethality in BPD patients.

5.1. Take home message on the transcriptional approach

An unbiased transcriptional approach was carried out with isolated AECII cells from *Fgf10*$^{+/-}$ and WT P3 lungs in HOX and NOX. Overall, at this time point, focusing on a specific cellular target of FGF10 signaling, our approach failed to find major differences between the two genotypes that could explain the lethal phenotype. Most of the differences identified in the analysis "hyperoxia x genotype" revealed changes in KEGG pathways dealing with the immune response, such as

staphylococcus aureus infection, antigen processing and presentation, and graft versus host disease. Since the lung epithelium is the first line of defense to bacterial or viral infections, in the future it will be important to define how *Fgf10* controls inflammation via its action on AECII cells. Interestingly, inflammation has been shown to inhibit *Fgf10* expression (Benjamin et al., 2010). FGF10 also prevents LPS-induced acute lung injury in rats (Tong et al., 2014). A first hint that the AECII cells in *Fgf10*$^{+/-}$ versus WT were defective was obtained by the analysis of AECII differentiation using the previously described AECII and AECI signatures (Treutlein et al., 2014). This is the first time, to our knowledge, that these specific alveolar epithelial signatures have been validated in disease lung models and it underscores the importance of a better definition, at the molecular level, of the AECII cells.

5.2. *Fgf10* controls the differentiation of the epithelium along the alveolar/AECII lineage

Fgf10 has been previously described to maintain the undifferentiated status of the SOX9/ID2 positive cells in the distal epithelium (Volckaert et al., 2013; Nyeng et al., 2008). These are considered to be mutipotent epithelial progenitor cells in the developing lung. Lineage tracing using *Id2-CreERT2* showed that they give rise to both bronchiolar and alveolar progenitors. Based on single cell transcriptome studies of the developing epithelium, the alveolar progenitors have been proposed to represent a population of “bipotent progenitor cells”. These bipotent cells can differentiate into either AECI or AECII cells. However, what controls their differentiation remains unknown. A gene signature characteristic of each cell type has been described. The bipotent progenitor cells exhibit both signatures. Our results suggest that *Fgf10* may play a key role in directing the differentiation of the bipotent progenitor cells towards the AECII lineage (Figure 19). This conclusion is based on the observation that while the total number of epithelial cells is decreased in *Fgf10*$^{+/-}$ lungs, the ratio of AECII cells (to the total number of EpCAM-positive cells) is also decreased, while that of AECI cells is increased. Interestingly, *Fgf10* hypomorphic lungs, exhibiting around 20% of the WT *Fgf10* mRNA level, also show a pronounced defect in AECII cells (Ramasamy et al., 2007), supporting a role for *Fgf10* in the ontogeny of the AECII lineage. In the future, lineage-tracing studies of the bipotent progenitor cells in the context of *Fgf10* deficiency should be

performed to test this hypothesis. If this is a consequence of direct FGF10 signaling to the epithelium via FGFR2b, then the specific deletion of *Fgfr2b* in these bipotent progenitor cells should only allow the formation of AECI cells. The role of the other FGFR2b ligands in this differentiation process, which are abundantly expressed in the lung (mainly FGF1 and FGF7), is unclear and will also need to be addressed. The observation that surfactant production, which is AECII's primary function, is compromised in *Fgf10*$^{+/-}$ in HOX supports our conclusion that AECII cells from *Fgf10*$^{+/-}$ lungs are deficient. Interestingly, AECII cells in *Fgf10*$^{+/-}$ lungs are still capable of producing adequate surfactant to allow normal lung function in room air. However, following HOX, it seems that these cells are prematurely lost due to built in developmental (differentiation) defects that remain to be defined. These defects assumably lead to either more susceptibility of AECII to HOX injury or decrease in regenerative capacity of AECII stem cells (Barkauskas et al., 2013) or other still unidentified sources. In WT mice, AECII cells are also affected by HOX. Figure 12Bc,g indicates a 19% drop in HOX versus NOX. Interestingly, the AECII cells in *Fgf10*$^{+/-}$ drop less (8% decrease in HOX versus NOX), indicating that AECII cells in *Fgf10*$^{+/-}$ lungs attempt to replenish the failing AECII pool. In this regard, another project in our laboratory found an increase in epithelial proliferation by using immunostaining. Confirming the FACS results, the western blot analysis clearly shows a significant decrease in SFTPC production, which is likely a major contributor to the lethal phenotype upon injury. Interestingly, the genome-wide association study failed to associate single-nucleotide polymorphisms in the *FGF10* gene with BPD. Constitutive mutations in *FGF10* therefore appear to be rare, or non-existent, in BPD patients. However, the reduction in FGF10, which is linked to inflammation, is likely directly associated with the clinical manifestations. It is noteworthy that BPD occurs in the context of lung immaturity superimposed by iatrogenic injury. The more immature the infant's lung is, the higher is the risk for developmental defects that may interfere with normal repair of injuries. Our results are also of concern regarding ALSG or LADD patients (exhibiting *FGF10* or *FGFR2b* mutations). While these patients initially appear to have normal function, they develop chronic obstructive pulmonary disease (Klar et al., 2011). This is likely associated with deficient repair of the epithelium upon injury. It still remains to be investigated whether this is due to developmental defects in the epithelial progenitors and/or insufficient postnatal *Fgf10* levels that compromise epithelial maintenance. One aspect is clear; these

patients will likely be more prone to lung disease than the normal population. At a minimum, preventive measures should be considered for these “at risk” patients.

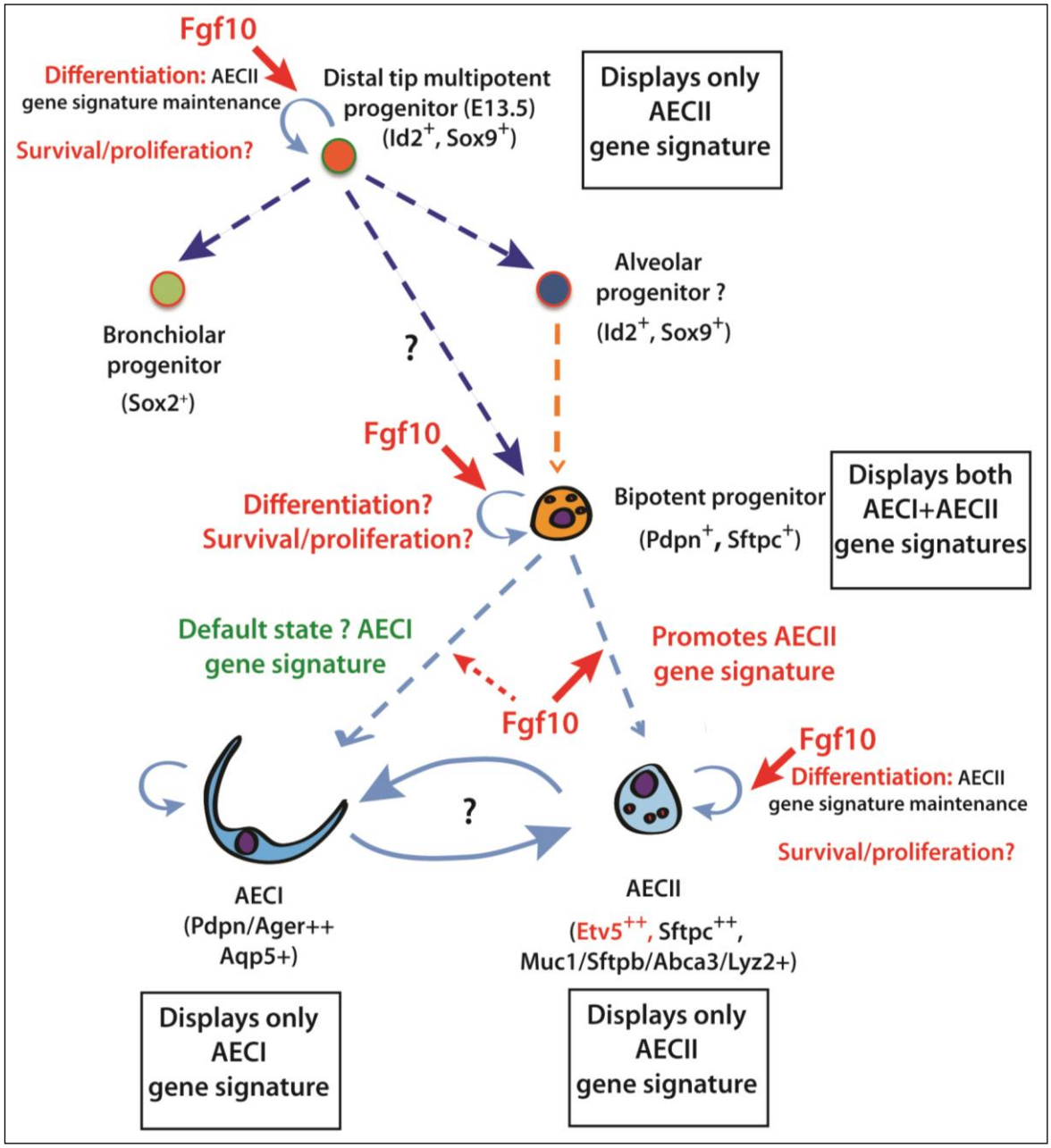

Figure 19. Model for the role of *Fgf10* in alveolar lineage formation during embryonic lung development.

We hypothesize that *Fgf10*, among others, is controlling the differentiation of the multipotent progenitor cells (ID2+, SOX9+) located at the distal tip of the branches towards the alveolar progenitor cells (ID2+, SOX9+) during the pseudoglandular stage of embryonic lung development. In turn, the alveolar progenitor cells will give rise to the bipotent progenitor cells during the saccular stage which display both AECI and AECII gene signatures. Whether the bipotent progenitor cells could arise directly from the multipotent progenitor cells needs to be proven. Our data suggest that *Fgf10* might orchestrate the differentiation as well as the survival/proliferation of this progenitor cell population. Finally, our data give evidence that *Fgf10* promotes the differentiation of the bipotent progenitor cell towards the AECII cell (modified from El Agha et al., 2014).

5.3. Impact of *Fgf10* deficiency on the vascular system

We have previously reported a clear link between *Fgf10* deficiency and vascular defects in *Fgf10*$^{Lacz/-}$ hypomorphic lungs (Ramasamy et al., 2007). We showed that *Vegfa* is a target of FGF10 in the developing lung epithelium and that decreased *Fgf10* levels eventually translate into decreased *Vegfa* and associated vascular defects. Another project from our group dealing with the effect of *Fgf10* deficiency on the development of the pulmonary vasculature found that *Vegfa* shows a trend towards reduction in E18.5 *Fgf10*$^{+/-}$ lungs. In the *Fgf10*$^{Lacz/-}$ hypomorphic lungs, the vascular tree is severely underdeveloped (Ramasamy et al., 2007). Such defects were not observed in P3 *Fgf10*$^{+/-}$ lungs in NOX, but emerge after HOX exposure, and are characterized by a significant drop in the number of blood vessels and by more immature (smooth muscle actin-negative) blood vessels (Figure 13). However, these defects did not seem to lead to lung hemorrhages, either at P3 or at later time points analyzed, suggesting that the observed lethality is not due to a failing vascular system. Interestingly, vascular defects, primarily pulmonary hypertension (PH), have been proposed as the main causes of lethality in infants with BPD (Kool et al., 2014). The PH phenotype was not observed in our experimental model, which suggests that additional pathways affecting the vascular system are implicated in BPD. However, the presence of more immature

(smooth muscle actin-negative) blood vessels in our experimental model raises the possibility that FGF10 signaling contributes to the formation of vascular smooth muscle cells via its action on PDGFB (Ramasamy et al., 2007), or via a more direct action on smooth muscle cell progenitors. Interestingly, FGF10 has been shown to act directly on mesenchymal-derived cells such as cardiomyocytes (Rochais et al., 2014), adipocyte stem cells (Sakaue et al., 2002), and lipofibroblasts (Al Alam et al., 2015), supporting the idea that in the lung FGF10 does not only act on the epithelium. In addition to its role on the epithelium and mesenchyme, it was also recently reported that FGF signaling to the endothelial cells is required for injury response, but not for vascular homeostasis (Oladipupo et al., 2014). FGF10 has also been shown to directly support the proliferation of endothelial cells (Sugimoto et al., 2014). It is therefore tempting to subdivide the effects of decreased *Fgf10* expression on the vasculature into two classes: one class linked to developmental defects where the blood vessels are more sensitive and immature, and one class linked to the role of FGF10 in repair as a proliferative factor for the endothelium, thereby limiting the vascular damages triggered by HOX. In *Fgf10*$^{+/-}$ mice, the normal function of the vasculature is likely affected by both developmental defects and insufficient repair upon injury.

5.4. Role of FGF10 signaling in secondary septa formation during alveologenesis

Alveologenesis is critical to the formation of the alveoli from lung saccules. Alveoli represent the minimal respiratory unit of the lung. Their formation is initiated by emergence of the secondary septa, a transient elongated structure emerging from the saccular walls. Secondary septa are composed of alveolar myofibroblasts, which deposit elastin at their apex. Both elastin and alveolar myofibroblasts are critical for the formation of the secondary septa as demonstrated by the *elastin* Ko mice (Wendel et al., 2000) and *Pdgfa* ko mice (Bostrom et al., 1996) in both of which alveologenesis is significantly reduced or blocked. The origin of the alveolar myofibroblasts is still controversial. However, it appears that FGFR2b ligands are critical for their formation. *Fgf10*$^{Lacz/-}$ hypomorphic lungs (expressing only 20% of WT) display enlarged respiratory airways at birth, characterized by the absence of smooth muscle actin myofibroblasts (Ramasamy et al., 2007).

Consistent with a role for FGF10 signaling in the formation of the alveolar

myofibroblasts, the inhibition of FGFR2b ligands using the soluble *Fgfr2b* approach from E16.5 to E18.5 leads to impaired postnatal alveologenesis (Hokuto et al., 2003). In this context, defective secondary septa formation can be corrected by retinoic acid. However, re-expression of the dominant negative soluble *Fgfr2b* also blocks the regeneration process, indicating that FGFR2b ligands expressed in the postnatal lung are also critical for the formation of the secondary septa (Perl & Gale, 2009). Secondary septa formation can also be induced following left lung pneumonectomy in mice. The formation of the new secondary septa is inhibited by the expression of the dominant negative soluble *Fgfr2b* (Chen et al., 2012). These data indicate that one or several FGFR2b ligands, in particular FGF10, are directly responsible for the formation of the alveolar myofibroblasts. However, it is still unclear if this is a direct effect of FGF10 on the alveolar myofibroblast progenitors or an indirect effect via FGF10 action on AECII cells, which are also a major component of the forming alveoli. Use of specific driver lines to target the alveolar myofibroblast progenitors will be instrumental to follow their fates in the context of lung injury or regeneration.

5.5. Future perspectives

In view of the numerous lung diseases characterized by lack and/or destruction of alveoli (e.g. BPD, COPD), the fundamental understanding of the alveologenesis process with its coordinated cellular interactions and intricate signaling network which exists between epithelial, mesenchymal and endothelial is essential. For this purpose, developmental biologists have been working extensively to unravel the molecular and cellular bases of mouse lung development, both pre- and postnatally. In this context, *Fgf10* has been shown to be a major player for the processes in development and repair after lung injury. In the future, the pneumonectomy mouse model combined with genetically modified mouse lines, lineage tracing approaches and single cell transcriptomic analyses will be powerful tools to shed new lights on the regenerative aspects associated with de novo alveologenesis. Last, but not least, the knowledge about progenitor / stem cells located in niches of the postnatal lung will be a valuable source of information that would be useful in triggering lung regeneration subsequent to injury. Such knowledge is critical to develop innovative therapies to treat lung diseases.

6. Summary

The evidence confirming the key role of *Fgf10* in embryonic lung development is strong. Inflammation-induced FGF10 deficiency has been shown in preterm infants who suffer from bronchopulmonary dysplasia (BPD) but only little is known about the underlying mechanism. Thus, information regarding the role of this major signaling pathway may open new therapeutic avenues to protect or regenerate the alveolar structure in particular. To demonstrate the effect of *Fgf10* deficiency for prenatal and postnatal lung development in normoxic conditions, we used a constitutive heterozygous *Fgf10*$^{+/-}$ mouse line. Lung morphometry and gene array were performed to identify changes in lung structure and global gene expression in *Fgf10*$^{+/-}$ versus *Fgf10*$^{+/+}$ (WT) littermate lungs at E18.5. As oxygen toxicity is one of the major risk factors contributing to BPD we used the hyperoxia-induced BPD mouse model (85% oxygen from P0 – P8) to investigate the impact of *Fgf10* deficiency. Surprisingly, 100% of *Fgf10*$^{+/-}$ pups died within 8 days of hyperoxia injury. We therefore chose P3, a time point at which there was no observable lethality, to collect pups for further analysis involving lung morphometry, gene array, fluorescence activated cell sorting (FACS), immunofluorescence (IF), reverse transcriptase-quantitative polymerase chain reaction (RT-qPCR), and western blot. In summary, constitutive decrease in *Fgf10* mRNA levels leads to lung congenital defects, which are compatible with postnatal survival, but which compromise the ability of the lungs to cope with sub-lethal hyperoxia injury. The results provide evidence that *Fgf10* deficiency during embryonic lung development affects the formation of AECII quantitatively and qualitatively. Considering that the vascular compartment of the lung plays a pivotal role in the control of lung epithelial growth (Thebaud, 2007; Thebaud & Abman, 2007), we also used vascular morphometry (vessel count and vessel muscularization) to determine potential pathological changes. Furthermore, we used a previously described double transgenic system in mice to attenuate all FGFR2b ligands pre- and post-natally in the context of hyperoxia injury (Danopoulos et al., 2013; MacKenzie et al., 2015; Parsa et al., 2010; Parsa et al., 2008; Al Alam et al., 2015).

Summary of results:

During lung development, our findings demonstrate that:

1. Neonatal *Fgf10* expression in the wild type lung is low in normoxia and decrease significantly upon hyperoxia.
2. *Fgf10*$^{+/-}$ mice at E12.5 show significant decrease in *Fgf10* expression and delayed branching morphogenesis due to decreased proliferation of the epithelium.
3. *Fgf10*$^{+/-}$ mice show impaired lung morphology and differential gene expression at E18.5.
4. *Fgf10*$^{+/-}$ mice at P70 reveal impaired lung morphology and lung function.
5. Blood vessel numbers and their muscularization are indistinguishable between *Fgf10*$^{+/-}$ versus WT lungs.

In the context of neonatal hyperoxia lung injury our results show that:

1. *Fgf10*$^{+/-}$ mice reveal 100% lethality and significant defects in lung morphology.
2. *Fgf10*$^{+/-}$ mice show quantitative and qualitative defects of AEC II cells.
3. *Fgf10*$^{+/-}$ mice show decreased number of blood vessels and decreased muscularization.

In the context of attenuation of FGFR2b ligands we observed that:

1. Prenatal attenuation affects the formation of the AECI and AECII quantitatively.
2. In normoxia postnatal attenuation during the saccular/alveolar stage of lung development does not cause lung structural defects or lethality.
3. In hyperoxia postnatal attenuation during the saccular/alveolar stage of lung development leads to significant lethality due to decreased surfactant protein C (SFTPC) expression.

We report for the first time the precise and detailed analysis of the consequence of *Fgf10* deficiency in mice on normal lung development and during hyperoxia injury. Our results indicate that FGF10 deficiency in neonates with BPD could be linked to

defective alveolar epithelial lineage formation. In turn, deficient AECII cells could be causative for some of the observed lung defects. This knowledge may be critical in designing therapies to prevent lung injury in neonates at risk for BPD and in lung disorders characterized by *Fgf10* deficiency.

7. Zusammenfassung

Die Schlüsselrolle von *Fgf10* für die embryonale Lungenentwicklung ist hinreichend belegt. Bei Frühgeborenen mit Bronchopulmonale Dysplasie (BPD) konnte eine durch Inflammation induzierte verminderte Expression von FGF10 gezeigt werden. Der zugrundeliegende Mechanismus ist jedoch kaum bekannt. Daher würde das tiefere Verständnis hinsichtlich der Rolle dieses essentiellen Signalweges in der Protektion und Regeneration der Alveolen möglicherweise neue therapeutische Wege eröffnen. Um den Effekt von *Fgf10* Defizienz auf die prä- und postnatale Lungenentwicklung zu untersuchen, griffen wir auf eine *Fgf10*$^{+/-}$ Mauslinie zurück, die heterozygot für *Fgf10* ist. Mit Hilfe der Lungenmorphometrie und Gene Array Analysen wurden Veränderungen in der Lungenstruktur und der globalen Genexpression an E18.5 bei *Fgf10*$^{+/-}$ versus *Fgf10*$^{+/+}$ (Wildtyp) Geschwistertieren erfasst. Da die Sauerstofftoxizität eine der Hauptfaktoren in der Pathogenese der BPD ist, wurden die Auswirkungen der *Fgf10* Defizienz in einem durch Hyperoxie induzierten BPD Mausmodell (85% O_2 von P0-P8) untersucht. Es konnte festgestellt werden, dass 100% der *Fgf10*$^{+/-}$ Mäuse während der Hyperoxiephase versterben, während alle WT Mäuse überlebten. Weitergehende Untersuchungen wurden an P3 mit Hilfe von Lungenmorphometrie, Gene Array, FACS, Immunhistochemie/ Immunfluoreszenz, RT-qPCR und Western blot durchgeführt. Zusammenfassend kann konstatiert werden, dass eine konstitutive *Fgf10* Defizienz zu kongenitalen Lungendefekten führt, die zwar postnatal mit dem Überleben vereinbar sind, jedoch bei Auftreten einer Hyperoxie-induzierten Lungenschädigung zu einer erhöhten Vulnerabilität der Lunge führen. Die erzielten Resultate weisen auf quantitative und qualitative Defekte der Alveolarepithelzellen Typ II (AECII) hin, welche auf die *Fgf10* Defizienz zurückzuführen sind. Da das Gefäßkompartiment ebenfalls mit dem Wachstum des Lungenepithels in Zusammenhang steht (Thebaud, 2007; Thebaud & Abman, 2007), wurden mittels Gefäßmorphometrie (Anzahl der Gefäße und ihre Muskularisierung) potenzielle Veränderungen analysiert. Schließlich wurden mit Hilfe einer induzierbaren Mauslinie in vivo FGFR2B Liganden prä- und postnatal während der Hyperoxiephase blockiert und die Effekte untersucht (Danopoulos et al., 2013; MacKenzie et al., 2015; Parsa et al., 2010; Parsa et al., 2008; Al Alam et al., 2015).

Zusammenfassung der Resultate:

Während der Lungenentwicklung lässt sich folgendes feststellen:

1. In Normoxie ist die neonatale *Fgf10* Expression bei Wildtyp Mäusen niedrig, während sie in Hyperoxie signifikant abnimmt.
2. *Fgf10*$^{+/-}$ Mäuse zeigen an E12.5 eine erniedrigte *Fgf10* Expression und eine verzögerte Verästelung der Lunge aufgrund einer verminderten Proliferation des Epithels.
3. *Fgf10*$^{+/-}$ Mäuse zeigen an E18.5 eine veränderte Lungenmorphologie und veränderte Genexpression.
4. *Fgf10*$^{+/-}$ Mäuse zeigen an P70 eine veränderte Lungenmorphologie und verminderte Lungenfunktion.
5. *Fgf10*$^{+/-}$ Mäuse zeigen an P3 keine Veränderungen der Gefäße (Anzahl und Muskularisierung).

Im Kontext der neonatalen Hyperoxie-induzierten Lungenschädigung ergaben die Resultate folgendes:

1. *Fgf10*$^{+/-}$ Mäuse zeigen eine 100%-ige Letalität mit einer signifikant schwerwiegenderen Lungenschädigung.
2. *Fgf10*$^{+/-}$ Mäuse zeigen an P3 quantitative und qualitative Defekte der AECII.
3. *Fgf10*$^{+/-}$ Mäuse zeigen an P3 eine verminderte Anzahl und Muskularisierung der Gefäße.

Im Zusammenhang mit der Blockade von FGFR2b Liganden beobachteten wir folgendes:

1. Eine pränatale Blockade von FGFR2b Liganden führt zur quantitativen Fehldifferenzierung der AECI und AECII.
2. In Normoxie führt eine postnatale Blockade von FGFR2b Liganden im sakkulären/alveolären Stadium der Lungenentwicklung zu keinen Defekten der Lungenstruktur und keiner Letalität.

3. In Hyperoxie führt eine postnatale Blockade von FGFR2b Liganden im sakkulären/alveolären Stadium der Lungenentwicklung zu einer erhöhten Letalität assoziiert mit einer verminderten Surfactant protein C (SFTPC) Expression.

Zusammenfasssend berichten wir erstmalig präzise und detailliert über die Effekte einer *Fgf10* Defizienz auf die normale Lungenentwicklung und die Hyperoxie-induzierte Lungenschädigung (BPD Mausmodell). Unsere Resultate zeigen, dass *Fgf10* Defizienz bei Neugeborenen mit BPD mit einer gestörten Bildung der Alveolarepithelzellen assoziiert sein könnte. Andererseits könnten defiziente AECII ursächlich zu der Pathogenese der BPD beitragen. Die Resultate der vorliegenden Arbeit können für zukünftige Therapieansätze zur Behandlung von Patienten mit BPD oder Lungenerkrankungen mit *Fgf10* Defizienz von Nutzen sein.

8. References

Albertine, K. H., G. P. Jones, B. C. Starcher, J. F. Bohnsack, P. L. Davis, S. C. Cho, D. P. Carlton and R. D. Bland (1999). “Chronic lung injury in preterm lambs. Disordered respiratory tract development.” Am J Respir Crit Care Med **159**(3), 945-958.

Alejandre-Alcazar, M. A., G. Kwapiszewska, I. Reiss, O. V. Amarie, L. M. Marsh, J. Sevilla-Perez, M. Wygrecka, B. Eul, S. Köbrich, M. Hesse, R. T. Schermuly, W. Seeger, O. Eickelberg and R. E. Morty (2007). “Hyperoxia modulates TGF-beta/BMP signaling in a mouse model of bronchopulmonary dysplasia.” Am J Physiol Lung Cell Mol Physiol **292**(2), L537-549.

Al Alam, D., E. El Agha, R. Sakurai, V. Kheirollahi, A. Moiseenko, S. Danopoulos, A. Shrestha, C. Schmoldt, J. Quantius, S. Herold, C. M. Chao, C. Tiozzo, S. De Langhe, M. V. Plikus, M. Thornton, B. Grubbs, P. Minoo, V. K. Rehan and S. Bellusci (2015). "Evidence for the involvement of fibroblast growth factor 10 in lipofibroblast formation during embryonic lung development." Development **142**(23): 4139-4150.

Arman, E., R. Haffner-Krausz, M. Gorivodsky and P. Lonai (1999). "Fgfr2 is required for limb outgrowth and lung-branching morphogenesis." Proc Natl Acad Sci U S A **96**(21): 11895-11899.

Auten, R. L., S. N. Mason, K. M. Auten and M. Brahmajothi (2009). "Hyperoxia impairs postnatal alveolar epithelial development via NADPH oxidase in newborn mice." Am J Physiol Lung Cell Mol Physiol **297**(1): L134-142.

Baraldi, E. and M. Filippone (2007). "Chronic lung disease after premature birth." N Engl J Med. 357(19):1946-55.

Barkauskas, C. E., M. J. Cronce, C. R. Rackley, E. J. Bowie, D. R. Keene, B. R. Stripp, S. H. Randell, P. W. Noble and B. L. Hogan (2013). "Type 2 alveolar cells are stem cells in adult lung." J Clin Invest **123**(7): 3025-3036.

Bellusci, S., Y. Furuta, M. G. Rush, R. Henderson, G. Winnier and B. L. Hogan (1997). "Involvement of Sonic hedgehog (Shh) in mouse embryonic lung growth and morphogenesis." Development **124**(1): 53-63.

Bellusci, S., J. Grindley, H. Emoto, N. Itoh and B. L. Hogan (1997). "Fibroblast growth factor 10 (FGF10) and branching morphogenesis in the embryonic mouse lung." Development **124**(23): 4867-4878.

Benjamin, J. T., B. J. Carver, E. J. Plosa, Y. Yamamoto, J. D. Miller, J. H. Liu, R. van der Meer, T. S. Blackwell and L. S. Prince (2010). "NF-kappaB activation limits airway branching through inhibition of Sp1-mediated fibroblast growth factor-10 expression." J Immunol **185**(8): 4896-4903.

Benjamin, J. T., R. J. Smith, B. A. Halloran, T. J. Day, D. R. Kelly and L. S. Prince (2007). "FGF-10 is decreased in bronchopulmonary dysplasia and suppressed by Toll-like receptor activation." Am J Physiol Lung Cell Mol Physiol **292**(2): L550-558.

Berger, J. and V. Bhandari (2014). "Animal models of bronchopulmonary dysplasia. The term mouse models." Am J Physiol Lung Cell Mol Physiol **307**(12): L936-947.

Bhandari, A. and V. Bhandari (2009). "Pitfalls, problems, and progress in bronchopulmonary dysplasia." Pediatrics **123**(6): 1562-1573.

Bhatt, A. J., G. S. Pryhuber, H. Huyck, R. H. Watkins, L. A. Metlay and W. M. Maniscalco (2001). "Disrupted pulmonary vasculature and decreased vascular endothelial growth factor, Flt-1, and TIE-2 in human infants dying with bronchopulmonary dysplasia." Am J Respir Crit Care Med **164**(10 Pt 1), 1971-1980.

Blackwell, T. S., A. N. Hipps, Y. Yamamoto, W. Han, W. J. Barham, M. C. Ostrowski, F. E. Yull and L. S. Prince (2011). "NF-kappaB signaling in fetal lung macrophages disrupts airway morphogenesis." J Immunol **187**(5): 2740-2747.

Bonniaud P., M. Kolb, T. Galt, J. Robertson, C. Robbins, M. Stampfli, C. Lavery, P. J. Margetts, A. B. Roberts and J. Gauldie (2004). Smad3 null mice develop airspace enlargement and are resistant to TGF-beta-mediated pulmonary fibrosis. J Immunol **173**(3):2099-108.

Bostrom, H., K. Willetts, M. Pekny, P. Leveen, P. Lindahl, H. Hedstrand, M. Pekna, M. Hellstrom, S. Gebre-Medhin, M. Schalling, M. Nilsson, S. Kurland, J. Tornell, J. K. Heath and C. Betsholtz (1996). "PDGF-A signaling is a critical event in lung alveolar myofibroblast development and alveogenesis." Cell **85**(6): 863-873.

Bridges, J. P., M. Ikegami, L. L. Brilli, X. Chen, R. J. Mason and J. M. Shannon (2010). "LPCAT1 regulates surfactant phospholipid synthesis and is required for transitioning to air breathing in mice." J Clin Invest **120**(5): 1736-1748.

Bruce, M. C., E. N. Bruce, K. Janiga and A. Chetty (1993). "Hyperoxic exposure of developing rat lung decreases tropoelastin mRNA levels that rebound postexposure." The American journal of physiology **265**(3 Pt 1), L293-300.

Bruce, M. C., R. Pawlowski and J. F. Jr. Tomashefski (1989). "Changes in lung elastic fiber structure and concentration associated with hyperoxic exposure in the developing rat lung." Am Rev Respir Dis **140**(4), 1067-1074.

Buch, S., R. N. Han, J. Cabacungan, J. Wang, S. Yuan, R. Belcastro, J. Deimling, R. Jankov, X. Luo, S. J. Lye, M. Post and A. K. Tanswell (2000). "Changes in expression of platelet-derived growth factor and its receptors in the lungs of newborn rats exposed to air or 60% O(2)." Pediatr Res **48**(4), 423-433.

Carver, B. J., E. J. Plosa, A. M. Stinnett, T. S. Blackwell and L. S. Prince (2013). "Interactions between NF-kappaB and SP3 connect inflammatory signaling with reduced FGF-10 expression." J Biol Chem **288**(21): 15318-15325.

Chang, D. R., D. Martinez Alanis, R. K. Miller, H. Ji, H. Akiyama, P. D. McCrea and J. Chen (2013). "Lung epithelial branching program antagonizes alveolar differentiation." Proc Natl Acad Sci U S A **110**(45): 18042-18051.

Chao C. M., E. El Agha, C. Tiozzo, P. Minoo and S. Bellusci (2015). "A breath of fresh air on the mesenchyme: impact of impaired mesenchymal development on the pathogenesis of bronchopulmonary dysplasia." Front Med (Lausanne). 2:27. doi: 10.3389/fmed.2015.00027. Review.

Chao C. M., A. Moiseenko, K. P. Zimmer and S. Bellusci (2016). "Alveologenesis: key cellular players and fibroblast growth factor 10 signaling." Mol Cell Pediatr. **3**(1):17. doi: 10.1186/s40348-016-0045-7. Review.

Chao, C. M., F. Yahya, A. Moiseenko, C. Tiozzo, A. Shrestha, N. Ahmadvand, E. El Agha, J. Quantius, S. Dilai, V. Kheirollahi, M. Jones, J. Wilhem, G. Carraro, H. Ehrhardt, K. P. Zimmer, G. Barreto, K. Ahlbrecht, R. E. Morty, S. Herold, R. G. Abellar, W. Seeger, R. Schermuly, J. S. Zhang, P. Minoo and S. Bellusci (2017). "Fgf10 deficiency is causative for lethality in a mouse model of bronchopulmonary dysplasia." J Pathol **241**(1): 91-103.

Chen H., J. Sun, S. Buckley, C. Chen, D. Warburton, X. F. Wang, W. Shi (2005). "Abnormal mouse lung alveolarization caused by Smad3 deficiency is a developmental antecedent of centrilobular emphysema." Am J Physiol Lung Cell Mol Physiol **288**(4):L683-91.

Chen, L., T. Acciani, T. Le Cras, C. Lutzko and A. K. Perl (2012). "Dynamic regulation of platelet-derived growth factor receptor alpha expression in alveolar fibroblasts during realveolarization." Am J Respir Cell Mol Biol **47**(4): 517-527.

Coalson, J. J., V. T. Winter, T. Siler-Khodr and B. A. Yoder (1999). "Neonatal chronic lung disease in extremely immature baboons." American journal of respiratory and critical care medicine **160**(4): 1333-1346.

Danopoulos, S., S. Parsa, D. Al Alam, R. Tabatabai, S. Baptista, C. Tiozzo, G. Carraro, M. Wheeler, G. Barreto, T. Braun, X. Li, M. K. Hajihosseini and S. Bellusci (2013). "Transient Inhibition of FGFR2b-ligands signaling leads to irreversible loss of cellular beta-catenin organization and signaling in AER during mouse limb development." PLoS One **8**(10): e76248.

Dauger, S., L. Ferkdadji, G. Saumon, G. Vardon, M. Peuchmaur, C. Gaultier and J. Gallego (2003). "Neonatal exposure to 65% oxygen durably impairs lung architecture and breathing pattern in adult mice." Chest **123**(2): 530-538.

De Langhe, S. P., G. Carraro, D. Warburton, M. K. Hajihosseini and S. Bellusci (2006). "Levels of mesenchymal FGFR2 signaling modulate smooth muscle progenitor cell commitment in the lung." Developmental biology **299**(1): 52-62.

DeLisser, H. M., B. P. Helmke, G. Cao, P. M. Egan, D. Taichman, M. Fehrenbach, A. Zaman, Z. Cui, G. S. Mohan, H. S. Baldwin, P. F. Davies and R. C. Savani (2006). "Loss of PECAM-1 function impairs alveolarization." J Biol Chem **281**(13), 8724-8731.

De Moerlooze, L., B. Spencer-Dene, J. M. Revest, M. Hajihosseini, I. Rosewell and C. Dickson (2000). "An important role for the IIIb isoform of fibroblast growth factor receptor 2 (FGFR2) in mesenchymal-epithelial signalling during mouse organogenesis." Development **127**(3): 483-492.

del Moral, P. M., S. P. De Langhe, F. G. Sala, J. M. Veltmaat, D. Tefft, K. Wang, D. Warburton and S. Bellusci (2006). "Differential role of FGF9 on epithelium and mesenchyme in mouse embryonic lung." Dev Biol **293**(1): 77-89.

Desai, T. J., D. G. Brownfield and M. A. Krasnow (2014). "Alveolar progenitor and stem cells in lung development, renewal and cancer." Nature **507**(7491): 190-194.

Dickie, R., Y. T. Wang, J. P. Butler, H. Schulz and A. Tsuda (2008). "Distribution and quantity of contractile tissue in postnatal development of rat alveolar interstitium." Anat Rec (Hoboken) **291**(1), 83-93.

El Agha, E. and S. Bellusci (2014). "Walking along the Fibroblast Growth Factor 10 Route: A Key Pathway to Understand the Control and Regulation of Epithelial and Mesenchymal Cell-Lineage Formation during Lung Development and Repair after Injury." Scientifica (Cairo) **2014**: 538379.

El Agha, E., S. Herold, D. Al Alam, J. Quantius, B. MacKenzie, G. Carraro, A. Moiseenko, C. M. Chao, P. Minoo, W. Seeger and S. Bellusci (2014). "Fgf10-positive cells represent a progenitor cell population during lung development and postnatally." Development **141**(2): 296-306.

Entesarian, M., H. Matsson, J. Klar, B. Bergendal, L. Olson, R. Arakaki, Y. Hayashi, H. Ohuchi, B. Falahat, A. I. Bolstad, R. Jonsson, M. Wahren-Herlenius and N. Dahl (2005). "Mutations in the gene encoding fibroblast growth factor 10 are associated with aplasia of lacrimal and salivary glands." Nat Genet **37**(2): 125-127.

Fujioka, K., A. Shibata, T. Yokota, T. Koda, M. Nagasaka, M. Yagi, Y. Takeshima, H. Yamada, K. Iijima and I Morioka (2014). "Association of a vascular endothelial growth factor polymorphism with the development of bronchopulmonary dysplasia in Japanese premature newborns." Sci Rep 4:4459.

Gauldie, J., T. Galt, P. Bonniaud, C. Robbins, M. Kelly and D. Warburton (2003). "Transfer of the active form of transforming growth factor-beta 1 gene to newborn rat lung induces changes consistent with bronchopulmonary dysplasia." Am J Pathol **163**(6), 2575-2584.

Gentleman, R. C., V. J. Carey, D. M. Bates, B. Bolstad, M. Dettling, S. Dudoit, B. Ellis, L. Gautier, Y. Ge, J. Gentry, K. Hornik, T. Hothorn, W. Huber, S. Iacus, R. Irizarry, F. Leisch, C. Li, M. Maechler, A. J. Rossini, G. Sawitzki, C. Smith, G. Smyth, L. Tierney, J. Y. Yang and J. Zhang (2004). "Bioconductor: open software development for computational biology and bioinformatics." Genome Biol **5**(10): R80.

Goss, A. M., Y. Tian, L. Cheng, J. Yang, D. Zhou, E. D. Cohen and E. E. Morrisey (2011). "Wnt2 signaling is necessary and sufficient to activate the airway smooth muscle program in the lung by regulating myocardin/Mrtf-B and Fgf10 expression." Dev Biol **356**(2): 541-552.

Goss, A. M., Y. Tian, T. Tsukiyama, E. D. Cohen, D. Zhou, M. M. Lu, T. P. Yamaguchi and E. E. Morrisey (2009). "Wnt2/2b and beta-catenin signaling are necessary and sufficient to specify lung progenitors in the foregut." Dev Cell **17**(2): 290-298.

Hadchouel, A., X. Durrmeyer, E. Bouzigon, R. Incitti, J. Huusko, P. H. Jarreau, R. Lenclen, F. Demenais, M. L. Franco-Montoya, I. Layouni, J. Patkai, J. Bourbon, M. Hallman, C. Danan and C. Delacourt (2011). "Identification of SPOCK2 as a susceptibility gene for bronchopulmonary dysplasia." American journal of respiratory and critical care medicine **184**(10): 1164-1170.

Harris-Johnson, K. S., E. T. Domyan, C. M. Vezina and X. Sun (2009). "beta-Catenin promotes respiratory progenitor identity in mouse foregut." Proceedings of the National Academy of Sciences of the United States of America **106**(38): 16287-16292.

Hines, E. A. and X. Sun (2014). "Tissue crosstalk in lung development." J Cell Biochem **115**(9): 1469-1477.

Hokuto, I., A. K. Perl and J. A. Whitsett (2003). "Prenatal, but not postnatal, inhibition of fibroblast growth factor receptor signaling causes emphysema." J Biol Chem **278**(1): 415-421.

Husain, A. N., N. H. Siddiqui and J. T. Stocker (1998). "Pathology of arrested acinar development in postsurfactant bronchopulmonary dysplasia." Human pathology **29**(7): 710-717.

Hyatt, B. A., X. Shangguan and J. M. Shannon (2004). "FGF-10 induces SP-C and Bmp4 and regulates proximal-distal patterning in embryonic tracheal epithelium." American journal of physiology. Lung cellular and molecular physiology **287**(6): L1116-1126.

Itoh, N. and D. M. Ornitz (2008). "Functional evolutionary history of the mouse Fgf gene family." Dev Dyn **237**(1): 18-27.

Itoh, N. and D. M. Ornitz (2011). "Fibroblast growth factors: from molecular evolution to roles in development, metabolism and disease." J Biochem **149**(2): 121-130.

Jankov R. P. and A. Keith Tanswell (2004). "Growth factors, postnatal lung growth and bronchopulmonary dysplasia." Paediatr Respir Rev 5 Suppl A:S265-75.

Kim, K. K., M. C. Kugler, P. J. Wolters, L. Robillard, M. G. Galvez, A. N. Brumwell, D. Sheppard and H. A. Chapman (2006). "Alveolar epithelial cell mesenchymal transition develops in vivo during pulmonary fibrosis and is regulated by the extracellular matrix." Proceedings of the National Academy of Sciences of the United States of America **103**(35): 13180-13185.

Klar, J., P. Blomstrand, C. Brunmark, J. Badhai, H. F. Hakansson, C. S. Brange, B. Bergendal and N. Dahl (2011). "Fibroblast growth factor 10 haploinsufficiency causes chronic obstructive pulmonary disease." J Med Genet **48**(10): 705-709.

Kool, H., D. Mous, D. Tibboel, A. de Klein and R. J. Rottier (2014). "Pulmonary vascular development goes awry in congenital lung abnormalities." Birth Defects Res C Embryo Today **102**(4): 343-358.

Kotecha, S., A. Wangoo, M. Silverman and R. J. Shaw (1996). "Increase in the concentration of transforming growth factor beta-1 in bronchoalveolar lavage fluid before development of chronic lung disease of prematurity." J Pediatr **128**(4), 464-469.

Kresch, M. J., C. Christian, F. Wu and N. Hussain (1998). "Ontogeny of apoptosis during lung development." Pediatr Res **43**(3):426-431.

Kunig, A. M., V. Balasubramaniam, N. E. Markham, D. Morgan, G. Montgomery, T. R. Grover and S. H. Abman (2005). "Recombinant human VEGF treatment enhances alveolarization after hyperoxic lung injury in neonatal rats." Am J Physiol Lung Cell Mol Physiol. **289**(4), L529-535.

Lassus, P., A. Ristimaki, O. Ylikorkala, L. Viinikka and S. Andersson (1999). "Vascular endothelial growth factor in human preterm lung." Am J Respir Crit Care Med **159**(5 Pt 1), 1429-1433.

Lassus, P., M. Turanlahti, P. Heikkila, L. C. Andersson, I. Nupponen, A. Sarnesto, and S. Andersson (2001). "Pulmonary vascular endothelial growth factor and Flt-1 in fetuses, in acute and chronic lung disease, and in persistent pulmonary hypertension of the newborn." Am J Respir Crit Care Med **164**(10 Pt 1), 1981-1987.

Lazarus, A., P. M. Del-Moral, O. Ilovich, E. Mishani, D. Warburton and E. Keshet (2011). "A perfusion-independent role of blood vessels in determining branching stereotypy of lung airways." Development **138**(11), 2359-2368.

Le Cras, T. D., N. E. Markham, R. M. Tuder, N. F. Voelkel and S. H. Abman (2002). "Treatment of newborn rats with a VEGF receptor inhibitor causes pulmonary hypertension and abnormal lung structure." Am J Physiol Lung Cell Mol Physiol **283**(3), L555-562.

Lindahl, P., L. Karlsson, M. Hellstrom, S. Gebre-Medhin, K. Willetts, J. K. Heath and C. Betsholtz (1997). "Alveogenesis failure in PDGF-A-deficient mice is coupled to lack of distal spreading of alveolar smooth muscle cell progenitors during lung development." Development **124**(20), 3943-3953.

Lu, J., K. I. Izvolsky, J. Qian and W. V. Cardoso (2005). "Identification of FGF10 targets in the embryonic lung epithelium during bud morphogenesis." J Biol Chem **280**(6): 4834-4841.

MacKenzie, B., I. Henneke, S. Hezel, D. Al Alam, E. El Agha, C. M. Chao, J. Quantius, J. Wilhelm, M. Jones, K. Goth, X. Li, W. Seeger, M. Konigshoff, S. Herold, A. A. Rizvanov, A. Gunther and S. Bellusci (2015). "Attenuating endogenous Fgfr2b ligands during bleomycin-induced lung fibrosis does not compromise murine lung repair." Am J Physiol Lung Cell Mol Physiol **308**(10): L1014-1024.

Mailleux, A. A., B. Spencer-Dene, C. Dillon, D. Ndiaye, C. Savona-Baron, N. Itoh, S. Kato, C. Dickson, J. P. Thiery and S. Bellusci (2002). "Role of FGF10/FGFR2b signaling during mammary gland development in the mouse embryo." Development **129**(1): 53-60.

Mailleux, A. A., D. Tefft, D. Ndiaye, N. Itoh, J. P. Thiery, D. Warburton and S. Bellusci (2001). "Evidence that SPROUTY2 functions as an inhibitor of mouse embryonic lung growth and morphogenesis." Mech Dev **102**(1-2): 81-94.

Mariani, T. J., S. Sandefur and R. A. Pierce (1997). "Elastin in lung development." Exp Lung Res **23**(2), 131-145.

Mcgowan, S. E. and R. Mcnamer (1990). "Transforming growth factor-beta increases elastin production by neonatal rat lung fibroblasts." Am J Respir Cell Mol Biol **3**(4), 369-376.

Mcgowan, S. E., S. K. Jackson, P. J. Olson, T. Parekh and L. I. Gold (1997). "Exogenous and endogenous transforming growth factors-beta influence elastin gene expression in cultured lung fibroblasts." Am J Respir Cell Mol Biol **17**(1), 25-35.

McGrath-Morrow, S. A., C. Cho, S. Soutiere, W. Mitzner and R. Tuder (2004). "The effect of neonatal hyperoxia on the lung of p21Waf1/Cip1/Sdi1-deficient mice." Am J Respir Cell Mol Biol **30**(5): 635-640.

Mcgrath-Morrow, S. A., C. Cho, L. Zhen, D. J. Hicklin and R. M. Tuder (2005). "Vascular endothelial growth factor receptor 2 blockade disrupts postnatal lung development." Am J Respir Cell Mol Biol **32**(5), 420-427.

Milunsky, J. M., G. Zhao, T. A. Maher, R. Colby and D. B. Everman (2006). "LADD syndrome is caused by FGF10 mutations." Clin Genet **69**(4): 349-354.

Minowada, G., L. A. Jarvis, C. L. Chi, A. Neubuser, X. Sun, N. Hacohen, M. A. Krasnow and G. R. Martin (1999). "Vertebrate Sprouty genes are induced by FGF signaling and can cause chondrodysplasia when overexpressed." Development **126**(20): 4465-4475.

Mohamed, W. A. and M. A. Aseeri (2014). "Cord blood fibroblast growth factor-10 as a possible predictor of bronchopulmonary dysplasia in preterm infants." J Neonatal Perinatal Med **7**(2): 101-105.

Moore, K. L. P., TVN (2002). The Developing Human: Clinically Oriented Embryology. Philadelphia, W.B. Saunders Co.

Morty R. E , M. Königshoff, O. Eickelberg (2009). "Transforming growth factor-beta signaling across ages: from distorted lung development to chronic obstructive pulmonary disease." Proc Am Thorac Soc **6**(7):607-13.

Mucenski, M. L., J. M. Nation, A. R. Thitoff, V. Besnard, Y. Xu, S. E. Wert, N. Harada, M. M. Taketo, M. T. Stahlman and J. A. Whitsett (2005). "Beta-catenin regulates differentiation of respiratory epithelial cells in vivo." Am J Physiol Lung Cell Mol Physiol **289**(6): L971-979.

Mucenski, M. L., S. E. Wert, J. M. Nation, D. E. Loudy, J. Huelsken, W. Birchmeier, E. E. Morrisey and J. A. Whitsett (2003). "beta-Catenin is required for specification of proximal/distal cell fate during lung morphogenesis." J Biol Chem **278**(41): 40231-40238.

Nakamura, T., M. Liu, E. Mourgeon, A. Slutsky and M. Post (2000). "Mechanical strain and dexamethasone selectively increase surfactant protein C and tropoelastin gene expression." Am J Physiol Lung Cell Mol Physiol **278**(5), L974-980.

Nakanishi, H., T. Sugiura, J. B. Streisand, S. M. Lonning and J. D. Jr. Roberts (2007). "TGF-beta-neutralizing antibodies improve pulmonary alveologenesis and vasculogenesis in the injured newborn lung." Am J Physiol Lung Cell Mol Physiol **293**(1), L151-161.

Noguchi, A., R. Reddy, J. D. Kursar, W. C. Parks and R. P. Mecham (1989). "Smooth muscle isoactin and elastin in fetal bovine lung." Experimental lung research **15**(4), 537-552.

Nyeng, P., G. A. Norgaard, S. Kobberup and J. Jensen (2008). "FGF10 maintains distal lung bud epithelium and excessive signaling leads to progenitor state arrest, distalization, and goblet cell metaplasia." BMC Dev Biol **8**: 2.

Oladipupo, S. S., C. Smith, A. Santeford, C. Park, A. Sene, L. A. Wiley, P. Osei-Owusu, J. Hsu, N. Zapata, F. Liu, R. Nakamura, K. J. Lavine, K. J. Blumer, K. Choi, R. S. Apte and D. M. Ornitz (2014). "Endothelial cell FGF signaling is required for injury response but not for vascular homeostasis." Proc Natl Acad Sci U S A **111**(37): 13379-13384.

Parsa, S., K. Kuremoto, K. Seidel, R. Tabatabai, B. Mackenzie, T. Yamaza, K. Akiyama, J. Branch, C. J. Koh, D. Al Alam, O. D. Klein and S. Bellusci (2010). "Signaling by FGFR2b controls the regenerative capacity of adult mouse incisors." Development **137**(22): 3743-3752.

Parsa, S., S. K. Ramasamy, S. De Langhe, V. V. Gupte, J. J. Haigh, D. Medina and S. Bellusci (2008). "Terminal end bud maintenance in mammary gland is dependent upon FGFR2b signaling." Dev Biol **317**(1): 121-131.

Peng, T., Y. Tian, C. J. Boogerd, M. M. Lu, R. S. Kadzik, K. M. Stewart, S. M. Evans and E. E. Morrisey (2013). "Coordination of heart and lung co-development by a multipotent cardiopulmonary progenitor." Nature **500**(7464): 589-592.

Perl, A. K. and E. Gale (2009). "FGF signaling is required for myofibroblast differentiation during alveolar regeneration." American journal of physiology. Lung cellular and molecular physiology **297**(2): L299-308.

Peters, K., S. Werner, X. Liao, S. Wert, J. Whitsett and L. Williams (1994). "Targeted expression of a dominant negative FGF receptor blocks branching morphogenesis and epithelial differentiation of the mouse lung." EMBO J **13**(14): 3296-3301.

Phan, S. H. (2002). "The myofibroblast in pulmonary fibrosis." Chest **122**(6 Suppl): 286S-289S.

Popova, A. P., J. K. Bentley, T. X. Cui, M. N. Richardson, M. J. Linn, J. Lei, Q. Chen, A. M. Goldsmith, G. S. Pryhuber and M. B. Hershenson (2014). "Reduced platelet-derived growth factor receptor expression is a primary feature of human bronchopulmonary dysplasia." American journal of physiology. Lung cellular and molecular physiology **307**(3): L231-239.

Prince, L. S., H. I. Dieperink, V. O. Okoh, G. A. Fierro-Perez and R. L. Lallone (2005). "Toll-like receptor signaling inhibits structural development of the distal fetal mouse lung." Developmental dynamics : an official publication of the American Association of Anatomists **233**(2): 553-561.

Prodhan, P. and T. B. Kinane (2002). "Developmental paradigms in terminal lung development." Bioessays **24**(11), 1052-1059.

Ramasamy, S. K., A. A. Mailleux, V. V. Gupte, F. Mata, F. G. Sala, J. M. Veltmaat, P. M. Del Moral, S. De Langhe, S. Parsa, L. K. Kelly, R. Kelly, W. Shia, E. Keshet, P. Minoo, D. Warburton and S. Bellusci (2007). "Fgf10 dosage is critical for the amplification of epithelial cell progenitors and for the formation of multiple mesenchymal lineages during lung development." Dev Biol **307**(2): 237-247.

Rawlins, E. L., C. P. Clark, Y. Xue and B. L. Hogan (2009). "The Id2+ distal tip lung epithelium contains individual multipotent embryonic progenitor cells." Development **136**(22): 3741-3745.

Rehan, V. K. and J. S. Torday (2012). "PPARgamma Signaling Mediates the Evolution, Development, Homeostasis, and Repair of the Lung." PPAR research **2012**: 289867.

Ren, J. T., K. Feng, P. Wang, W. H. Peng, Y. H. Jia, K. Liu, H. J. Lu (2013). "Relationship between the gene polymorphism in fibroblast growth factor-10 and susceptibility to chronic obstructive pulmonary disease: 220 cases." Zhonghua Jie He He Hu Xi Za Zhi. 2013 Dec;36(12):935-9.

Roberts, D. and S. Dalziel (2006). "Antenatal corticosteroids for accelerating fetal lung maturation for women at risk of preterm birth." The Cochrane database of systematic reviews, CD004454.

Rochais, F., R. Sturny, C. M. Chao, K. Mesbah, M. Bennett, T. J. Mohun, S. Bellusci and R. G. Kelly (2014). "FGF10 promotes regional foetal cardiomyocyte proliferation and adult cardiomyocyte cell-cycle re-entry." Cardiovasc Res **104**(3): 432-442.

Rohmann, E., H. G. Brunner, H. Kayserili, O. Uyguner, G. Nurnberg, E. D. Lew, A. Dobbie, V. P. Eswarakumar, A. Uzumcu, M. Ulubil-Emeroglu, J. G. Leroy, Y. Li, C. Becker, K. Lehnerdt, C. W. Cremers, M. Yuksel-Apak, P. Nurnberg, C. Kubisch, J. Schlessinger, H. van Bokhoven and B. Wollnik (2006). "Mutations in different components of FGF signaling in LADD syndrome." Nat Genet **38**(4): 414-417.

Rossor, T. and A. Greenough (2015). "Advances in paediatric pulmonary vascular disease associated with bronchopulmonary dysplasia." Expert Rev Respir Med **9**(1): 35-43.

Roth-Kleiner M and M. Post (2005). "Similarities and dissimilarities of branching and septation during lung development." Pediatr Pulmonol **40**(2):113-34.

Rubin, L. P., C. S. Kovacs, M. E. De Paepe, S. W. Tsai, J. S. Torday and H. M. Kronenberg (2004). "Arrested pulmonary alveolar cytodifferentiation and defective surfactant synthesis in mice missing the gene for parathyroid hormone-related protein." Developmental dynamics : an official publication of the American Association of Anatomists **230**(2): 278-289.

Sakaue, H., M. Konishi, W. Ogawa, T. Asaki, T. Mori, M. Yamasaki, M. Takata, H. Ueno, S. Kato, M. Kasuga and N. Itoh (2002). "Requirement of fibroblast growth factor 10 in development of white adipose tissue." Genes Dev **16**(8): 908-912.

Schittny, J. C., S. I. Mund and M. Stampanoni (2008). "Evidence and structural mechanism for late lung alveolarization." American journal of physiology. Lung cellular and molecular physiology **294**(2): L246-254.

Schultz, C. J., E. Torres, C. Londos and J. S. Torday (2002). "Role of adipocyte differentiation-related protein in surfactant phospholipid synthesis by type II cells." American journal of physiology. Lung cellular and molecular physiology **283**(2): L288-296.

Seimetz, M., N. Parajuli, A. Pichl, F. Veit, G. Kwapiszewska, F. C. Weisel, K. Milger, B. Egemnazarov, A. Turowska, B. Fuchs, S. Nikam, M. Roth, A. Sydykov, T. Medebach, W. Klepetko, P. Jaksch, R. Dumitrascu, H. Garn, R. Voswinckel, S. Kostin, W. Seeger, R. T. Schermuly, F. Grimminger, H. A. Ghofrani and N. Weissmann (2011). "Inducible NOS inhibition reverses tobacco-smoke-induced emphysema and pulmonary hypertension in mice." Cell **147**(2): 293-305.

Sekine, K., H. Ohuchi, M. Fujiwara, M. Yamasaki, T. Yoshizawa, T. Sato, N. Yagishita, D. Matsui, Y. Koga, N. Itoh and S. Kato (1999). "Fgf10 is essential for limb and lung formation." Nat Genet **21**(1): 138-141.

Shahzad, T., S. Radajewski, C. M. Chao, S. Bellusci and H. Ehrhardt (2016). "Pathogenesis of bronchopulmonary dysplasia: when inflammation meets organ development." Mol Cell Pediatr **3**(1): 23.

Shannon, J. M. (1994). "Induction of alveolar type II cell differentiation in fetal tracheal epithelium by grafted distal lung mesenchyme." Developmental biology **166**(2): 600-614.

Shannon, J. M., L. D. Nielsen, S. A. Gebb and S. H. Randell (1998). "Mesenchyme specifies epithelial differentiation in reciprocal recombinants of embryonic lung and trachea." Developmental dynamics : an official publication of the American Association of Anatomists **212**(4): 482-494.

Shifren, A., A. G. Durmowicz, R. H. Knutsen, E. Hirano and R. P. Mecham (2007). "Elastin protein levels are a vital modifier affecting normal lung development

and susceptibility to emphysema." Am J Physiol Lung Cell Mol Physiol **292**(3), L778-787.

Simon, D. M. and T. J. Mariani (2007). "Role of PPARs and Retinoid X Receptors in the Regulation of Lung Maturation and Development." PPAR research **2007**: 91240.

Smyth, G. K. (2004). "Linear models and empirical bayes methods for assessing differential expression in microarray experiments." Stat Appl Genet Mol Biol **3**: Article3.

Speer, C. P. (2006). "Pulmonary inflammation and bronchopulmonary dysplasia." J Perinatol **26 Suppl 1**: S57-62; discussion S63-54.

Stoll, B. J., N. I. Hansen, E. F. Bell, S. Shankaran, A. R. Laptook, M. C. Walsh, E. C. Hale, N. S. Newman, K. Schibler, W. A. Carlo, K. A. Kennedy, B. B. Poindexter, N. N. Finer, R. A. Ehrenkranz, S. Duara, P. J. Sanchez, T. M. O'Shea, R. N. Goldberg, K. P. Van Meurs, R. G. Faix, D. L. Phelps, I. D. Frantz, 3rd, K. L. Watterberg, S. Saha, A. Das and R. D. Higgins (2010). "Neonatal outcomes of extremely preterm infants from the NICHD Neonatal Research Network." Pediatrics **126**(3): 443-456.

Sucre, J. M., D. Wilkinson, P. Vijayaraj, M. Paul, B. Dunn, J. A. Alva-Ornelas and B. N. Gomperts (2016). "A three-dimensional human model of the fibroblast activation that accompanies bronchopulmonary dysplasia identifies Notch-mediated pathophysiology." Am J Physiol Lung Cell Mol Physiol **310**(10): L889-898.

Sugimoto, K., S. Yoshida, Y. Mashio, N. Toyota, Y. Xing, H. Xu, Y. Fujita, Z. Huang, M. Touma and Q. Wu (2014). "Role of FGF10 on tumorigenesis by MS-K." Genes Cells **19**(2): 112-125.

Tefft, D., M. Lee, S. Smith, D. L. Crowe, S. Bellusci and D. Warburton (2002). "mSprouty2 inhibits FGF10-activated MAP kinase by differentially binding to upstream target proteins." Am J Physiol Lung Cell Mol Physiol **283**(4): L700-706.

Tekin, M., B. O. Hismi, S. Fitoz, H. Ozdag, F. B. Cengiz, A. Sirmaci, I. Aslan, B. Inceoglu, E. B. Yuksel-Konuk, S. T. Yilmaz, O. Yasun and N. Akar (2007). "Homozygous mutations in fibroblast growth factor 3 are associated with a new form of syndromic deafness characterized by inner ear agenesis, microtia, and microdontia." Am J Hum Genet **80**(2): 338-344.

Thebaud, B., F. Ladha, E.D. Michelakis, M. Sawicka, G. Thurston, F. Eaton, K. Hashimoto, G. Harry, A. Haromy, G. Korbutt and S. L. Archer (2005). "Vascular endothelial growth factor gene therapy increases survival, promotes lung angiogenesis, and prevents alveolar damage in hyperoxia-induced lung injury: evidence that angiogenesis participates in alveolarization." Circulation **112**(16), 2477-2486.

Thebaud, B. (2007). "Angiogenesis in lung development, injury and repair: implications for chronic lung disease of prematurity." Neonatology **91**(4): 291-297.

Thebaud, B. and S. H. Abman (2007). "Bronchopulmonary dysplasia: where have all the vessels gone? Roles of angiogenic growth factors in chronic lung disease." American journal of respiratory and critical care medicine **175**(10): 978-985.

Thibeault, D. W., S. M. Mabry, Ekekezie, II and W. E. Truog (2000). "Lung elastic tissue maturation and perturbations during the evolution of chronic lung disease." Pediatrics **106**(6): 1452-1459.

Thibeault, D. W., S. M. Mabry, Ekekezie, II, X. Zhang and W. E. Truog (2003). "Collagen scaffolding during development and its deformation with chronic lung disease." Pediatrics **111**(4 Pt 1): 766-776.

Todd, D. A., M. Earl, J. Lloyd, M. Greenberg and E. John (1998). "Cytological changes in endotracheal aspirates associated with chronic lung disease." Early Hum Dev **51**(1): 13-22.

Tong, L., J. Bi, X. Zhu, G. Wang, J. Liu, L. Rong, Q. Wang, N. Xu, M. Zhong, D. Zhu, Y. Song and C. Bai (2014). "Keratinocyte growth factor-2 is protective in

lipopolysaccharide-induced acute lung injury in rats." Respir Physiol Neurobiol **201**: 7-14.

Torday, J., J. Hua and R. Slavin (1995). "Metabolism and fate of neutral lipids of fetal lung fibroblast origin." Biochimica et biophysica acta **1254**(2): 198-206.

Torday, J. S. and V. K. Rehan (2002). "Stretch-stimulated surfactant synthesis is coordinated by the paracrine actions of PTHrP and leptin." American journal of physiology. Lung cellular and molecular physiology **283**(1): L130-135.

Tordet, C., L. Marin and F. Dameron (1981). "Pulmonary di-and-triacylglycerols during the perinatal development of the rat." Experientia **37**(4): 333-334.

Treutlein, B., D. G. Brownfield, A. R. Wu, N. F. Neff, G. L. Mantalas, F. H. Espinoza, T. J. Desai, M. A. Krasnow and S. R. Quake (2014). "Reconstructing lineage hierarchies of the distal lung epithelium using single-cell RNA-seq." Nature **509**(7500): 371-375.

Vaccaro, C. and J. S. Brody (1978). "Ultrastructure of developing alveoli. I. The role of the interstitial fibroblast." Anat Rec **192**(4), 467-479.

Velten, M., K. M. Heyob, L. K. Rogers and S. E. Welty (2010). "Deficits in lung alveolarization and function after systemic maternal inflammation and neonatal hyperoxia exposure." J Appl Physiol (1985) **108**(5): 1347-1356.

Vicencio A. G, C. G. Lee, S. J. Cho, O. Eickelberg, Y. Chuu, G. G. Haddad, J. A. Elias. "Conditional overexpression of bioactive transforming growth factor-beta1 in neonatal mouse lung: a new model for bronchopulmonary dysplasia?" Am J Respir Cell Mol Biol **31**(6):650-6.

Volckaert, T., A. Campbell, E. Dill, C. Li, P. Minoo and S. De Langhe (2013). "Localized Fgf10 expression is not required for lung branching morphogenesis but prevents differentiation of epithelial progenitors." Development **140**(18): 3731-3742.

Volckaert, T., E. Dill, A. Campbell, C. Tiozzo, S. Majka, S. Bellusci and S. P. De Langhe (2011). "Parabronchial smooth muscle constitutes an airway epithelial stem cell niche in the mouse lung after injury." The Journal of clinical investigation **121**(11): 4409-4419.

Warner, B. B., L. A. Stuart, R. A. Papes and J. R. Wispe (1998). "Functional and pathological effects of prolonged hyperoxia in neonatal mice." Am J Physiol **275**(1 Pt 1): L110-117.

Weinstein, M., X. Xu, K. Ohyama and C. X. Deng (1998). "FGFR-3 and FGFR-4 function cooperatively to direct alveogenesis in the murine lung." Development **125**(18), 3615-3623.

Wendel, D. P., D. G. Taylor, K. H. Albertine, M. T. Keating and D. Y. Li (2000). "Impaired distal airway development in mice lacking elastin." American journal of respiratory cell and molecular biology **23**(3): 320-326.

Weng, T., L. Gao, M. Bhaskaran, Y. Guo, D. Gou, J. Narayanaperumal, N. R. Chintagari, K. Zhang and L. Liu (2009). "Pleiotrophin regulates lung epithelial cell proliferation and differentiation during fetal lung development via beta-catenin and Dlk1." J Biol Chem **284**(41): 28021-28032.

White, K. E., G. Carn, B. Lorenz-Depiereux, A. Benet-Pages, T. M. Strom and M. J. Econs (2001). "Autosomal-dominant hypophosphatemic rickets (ADHR) mutations stabilize FGF-23." Kidney Int **60**(6): 2079-2086.

Willet, K. E., P. Mcmenamin, K. E. Pinkerton, M. Ikegami, A. H. Jobe, L. Gurrin and P. D. Sly (1999). "Lung morphometry and collagen and elastin content: changes during normal development and after prenatal hormone exposure in sheep." Pediatric research **45**(5 Pt 1), 615-625.

Willis, B. C., J. M. Liebler, K. Luby-Phelps, A. G. Nicholson, E. D. Crandall, R. M. du Bois and Z. Borok (2005). "Induction of epithelial-mesenchymal transition in alveolar epithelial cells by transforming growth factor-beta1: potential role in idiopathic pulmonary fibrosis." The American journal of pathology **166**(5): 1321-1332.

Woyda, K., S. Koebrich, I. Reiss, S. Rudloff, S. S. Pullamsetti, A. Ruhlmann, N. Weissmann, H. A. Ghofrani, A. Gunther, W. Seeger, F. Grimminger, R. E. Morty and R. T. Schermuly (2009). "Inhibition of phosphodiesterase 4 enhances lung alveolarisation in neonatal mice exposed to hyperoxia." Eur Respir J **33**(4): 861-870.

9. Supplementary Material

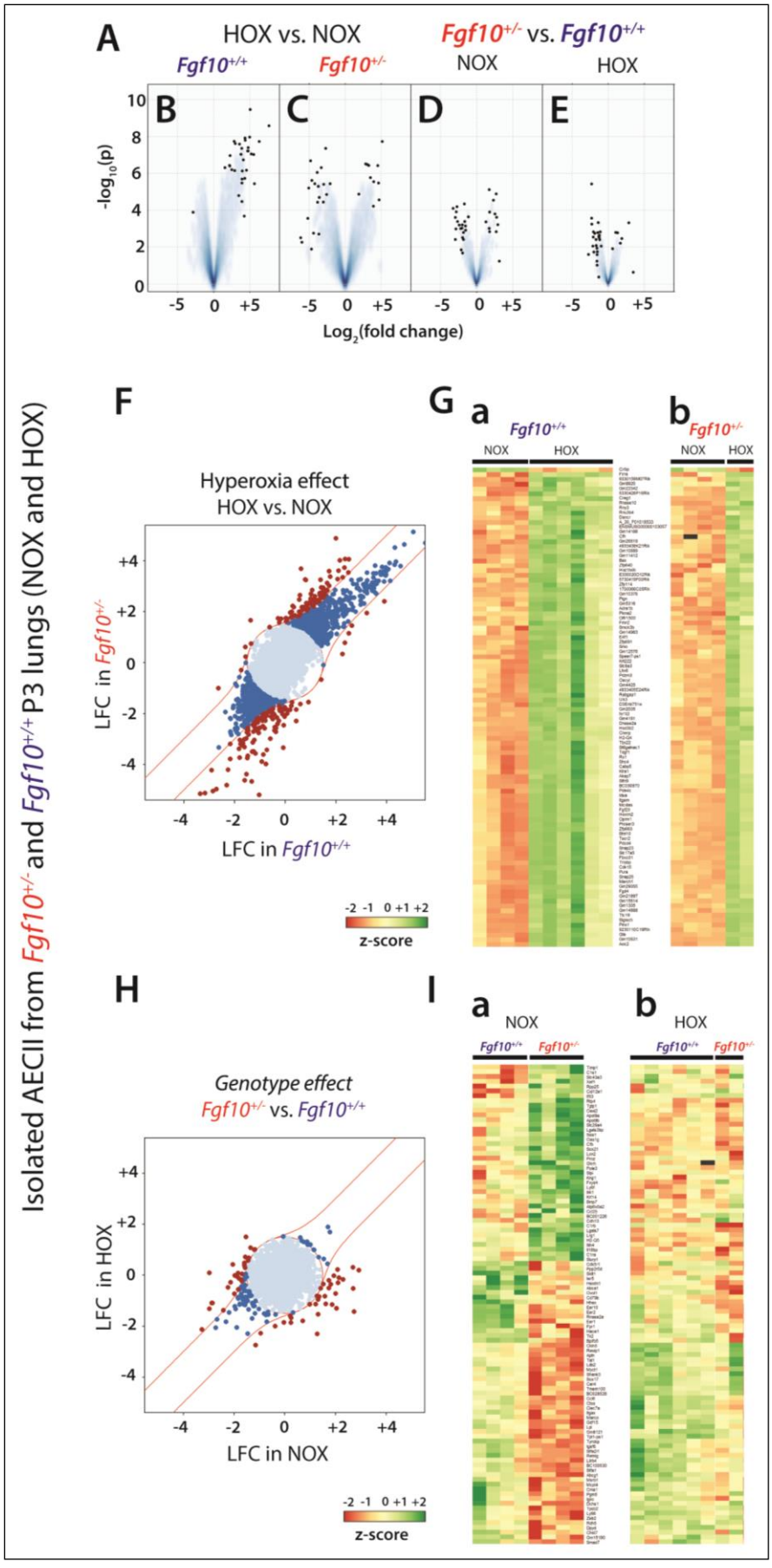

Figure S1. Identification of sets of genes differentially expressed in HOX versus NOX (selected according to their p-values) in isolated AECII cells from WT and *Fgf10*$^{+/-}$.

(**A**) Volcanoplots. (**B**) Volcanoplot for HOX versus NOX in isolated AECII cells from *Fgf10*$^{+/+}$ (WT) lungs. (**C**) Volcanoplot for HOX versus NOX in isolated AECII cells from *Fgf10*$^{+/-}$ lungs. (**D**) Volcanoplot in isolated AECII cells from *Fgf10*$^{+/-}$ versus WT in NOX. (**E**) Volcanoplot in isolated AECII cells from *Fgf10*$^{+/-}$ versus WT in HOX. (**F**) Hyperoxia effect HOX versus NOX. (**G**) (**a**) heat map: top 100 regulated genes selected based on their p value between NOX and Hox in isolated AECII cells from WT lungs. (**b**) heat map: analysis of the same top 100 genes between NOX and HOX in isolated AECII cells from *Fgf10*$^{+/-}$ lungs. (**H**) Genotype effect. (**I**) (**a**) heat map: top 100 regulated genes between isolated AECII cells from *Fgf10*$^{+/-}$ versus WT lungs in NOX. (**b**) heat map: analysis of the same top 100 genes between isolated AECII cells from *Fgf10*$^{+/-}$ versus WT lungs in HOX.

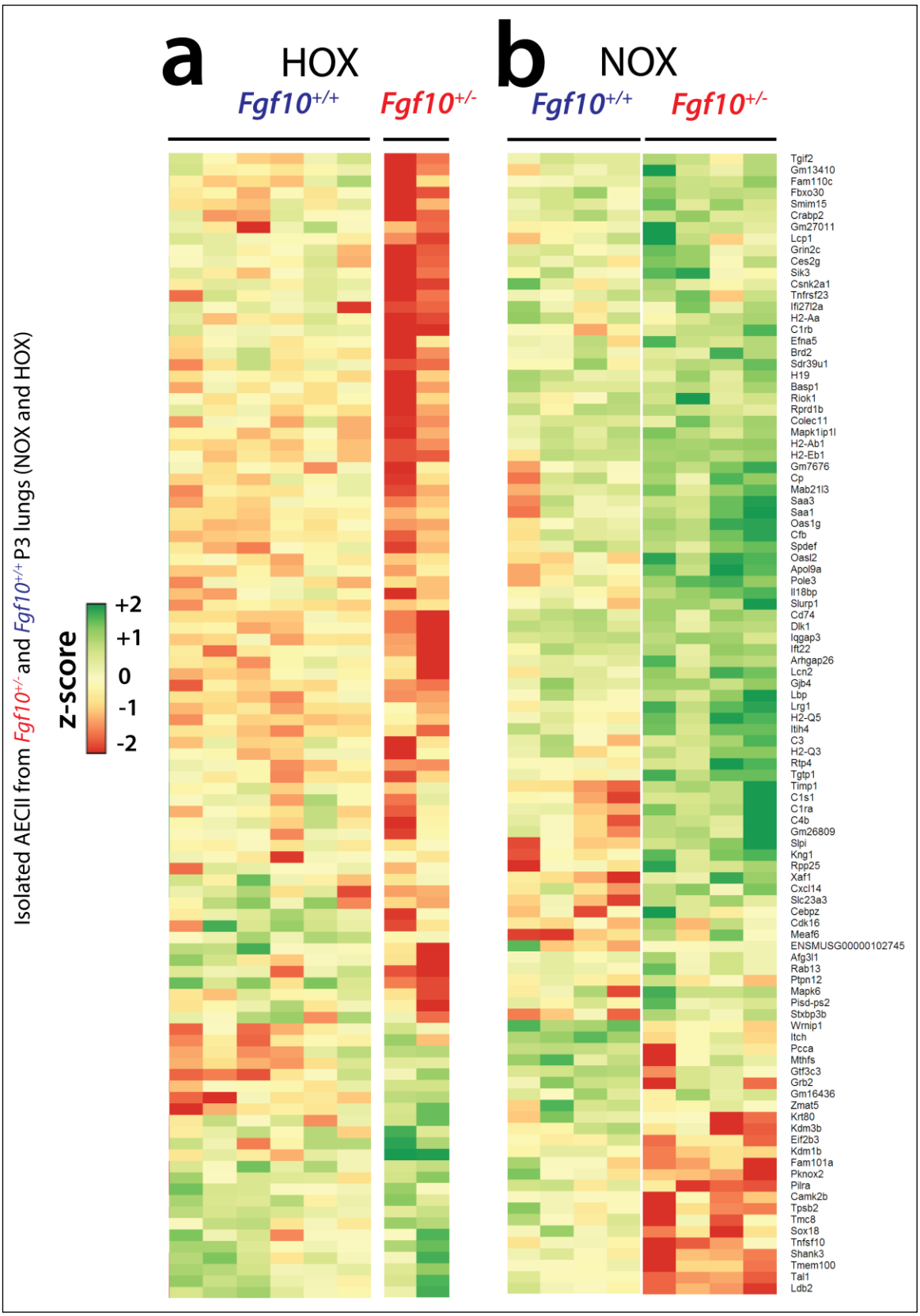

Figure S2. Magnification of the graphs shown in Figure 11Ba,b.

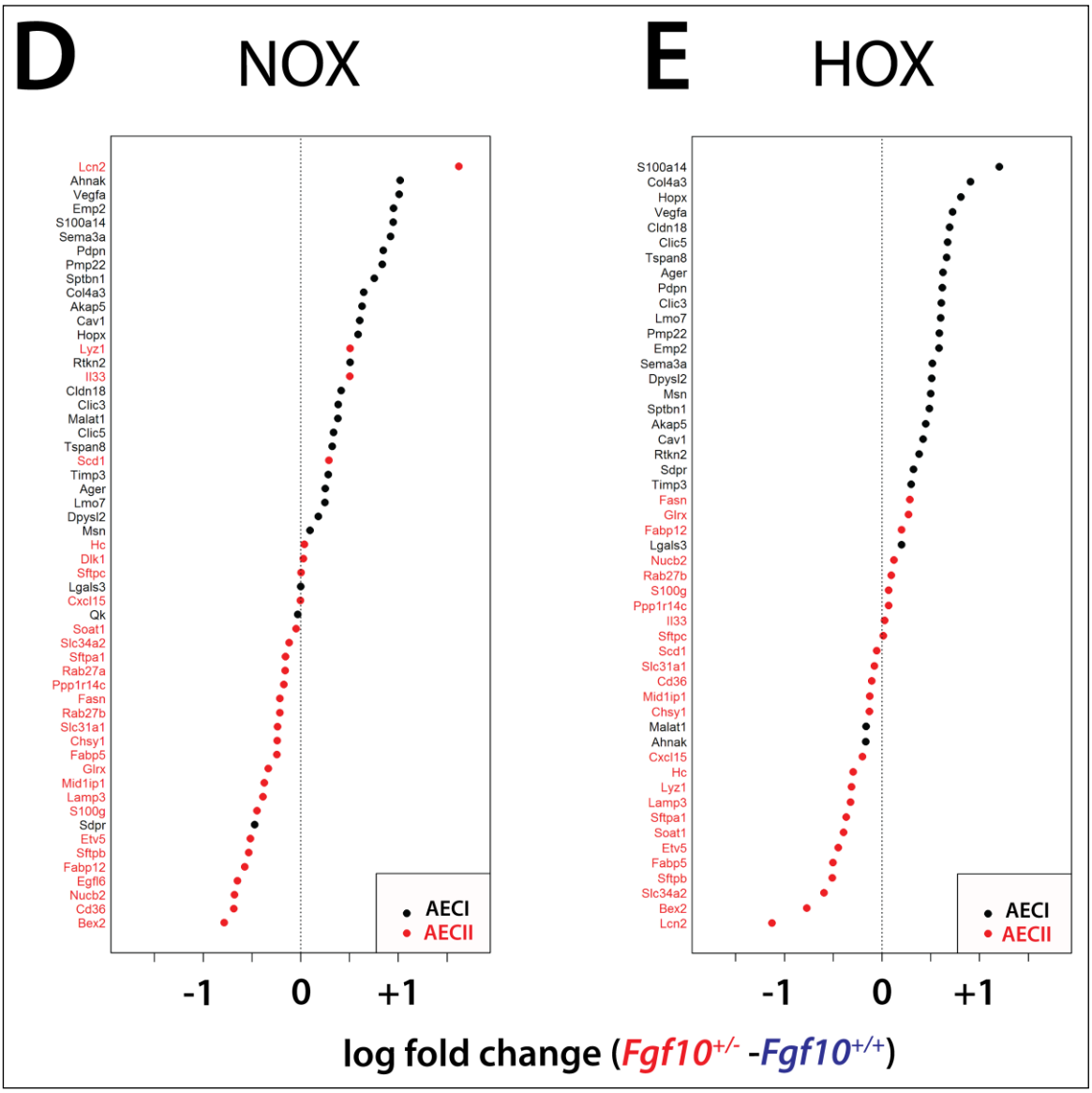

Figure S3. Greater magnification of the graphs shown in Figure 11D,E.

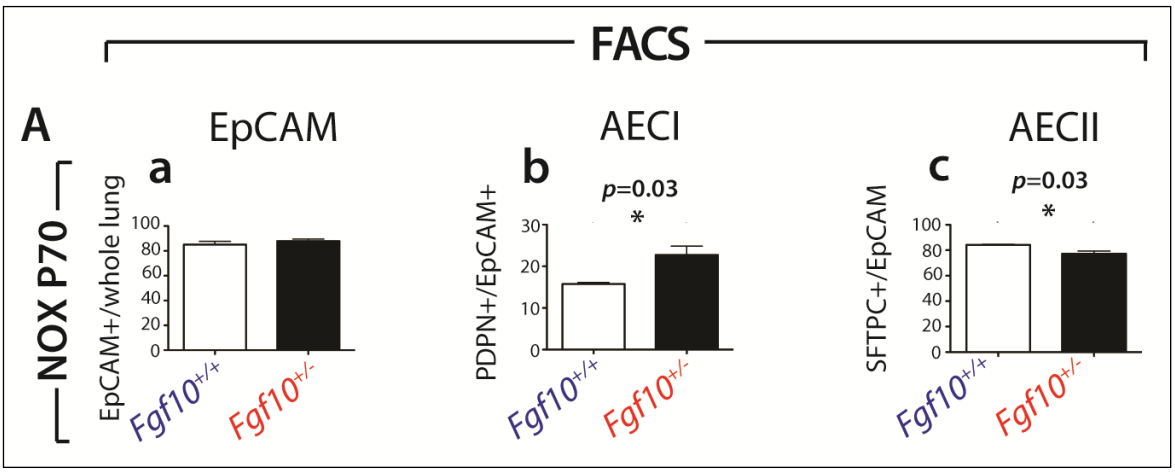

Figure S4. *Fgf10*$^{+/-}$ lungs at P70 in the context of NOX exhibit more AECI but less AECII.

(**A**) Fluorescence Activated Cell Sorting in NOX (**a-c**) of *Fgf10*$^{+/+}$ and *Fgf10*$^{+/-}$ P70 lungs for (**a**) epithelial cells (EpCAM+), (**b**) AECI and (**c**) AECII.

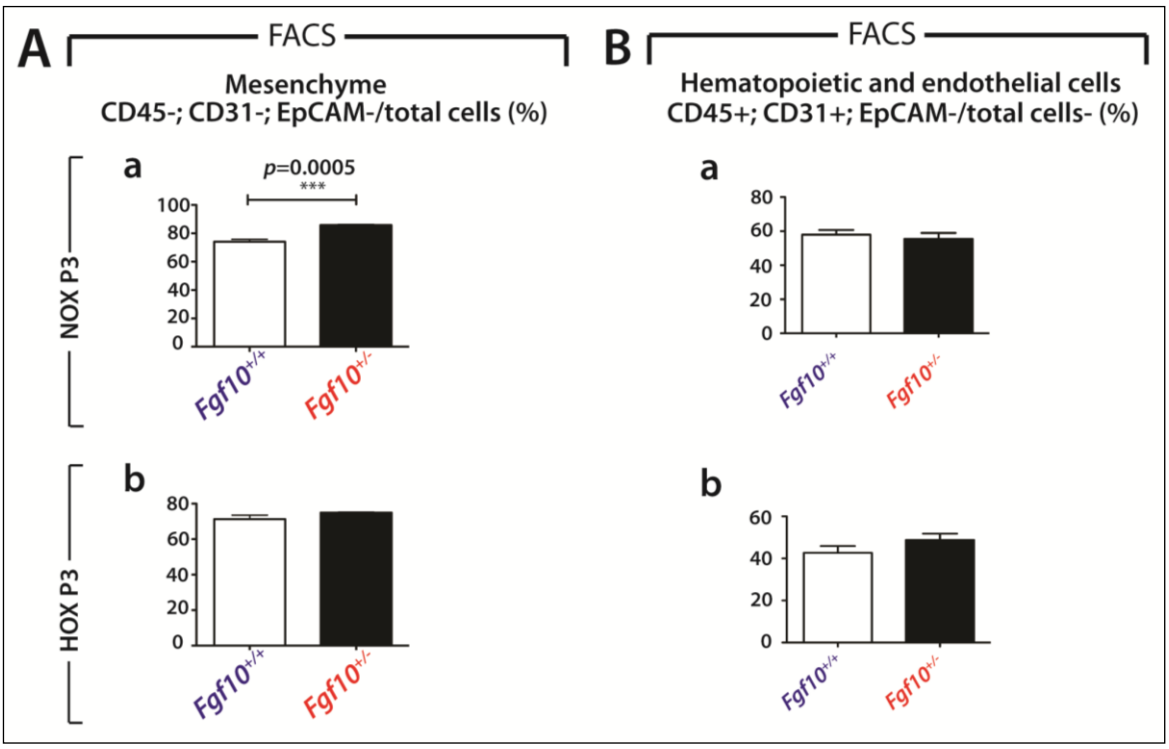

Figure S5. The impact of HOX versus NOX on the mesenchymal, hematopoietic and endothelial cells of *Fgf10*$^{+/-}$ and WT lungs at P3.

(**A**) FACS-based quantification of mesenchymal cells (CD45-;CD31-; EpCAM-) as a percentage of total cells in (**a**) NOX and (**b**) HOX. (**B**) FACS-based quantification of hematopoietic and endothelial cells (CD45+;CD31+; EpCAM-) as a percentage of total cells in (**a**) NOX and (**b**) HOX. *Fgf10*$^{+/-}$ lungs: n=4 and n=5 for HOX versus NOX, respectively. WT lungs: n=4 and n=5 for HOX versus NOX, respectively.

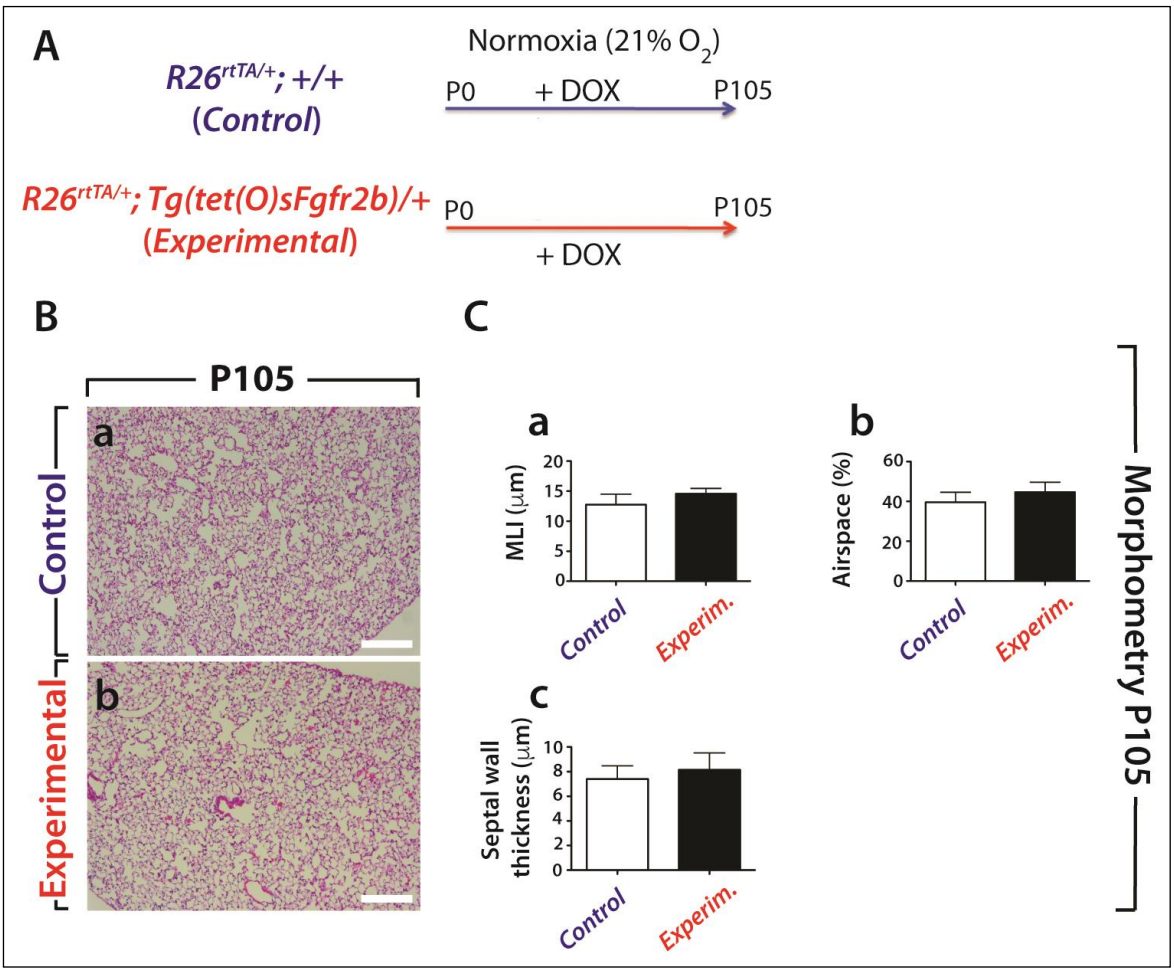

Figure S6. Attenuation of FGFR2B ligands postnatally from P0-P105 in NOX does not lead to changes in lung structure.

(A) Experimental set-up of *R26rtTA/+; +/+* (control group) and *R26rtTA/+; Tg(tet(O)sFgfr2b)/+* (experimental group) animals. All animals are fed with doxycycline-containing food to induce the dominant negative soluble *Fgfr2b* in the experimental group. **(B)** Haematoxylin/eosin staining of **(a)** control or **(b)** experimental lungs at P105. **(C)** Corresponding lung morphometric analysis. Note the absence of differences in **(a)** MLI, **(b)** airspace and **(c)** septal wall thickness. Scale bar for Ba,b: 500 µm.

10. Acknowledgements

First of all, I would like to express my deep gratitude to Prof. Dr. Saverio Bellusci for giving me the chance to join his lab as a part-time clinician. Without his support and enthusiasm throughout the whole time the completion of this doctoral thesis would not be possible. For me, he is more than a teacher who teached me how to do science but also a person whom I deeply respect for his passion, his optimism and his friendliness towards students. In any case and at any time he was available when I needed him for questions and problems. He certainly is the person who inspired me for science and allowed me to grow. His incredible patience and tirelessness in teaching me made me became a clinician scientist step by step.

The same gratitude I would like to express to Prof. Dr. Klaus-Peter Zimmer, my mentor from the University Children´s Hospital, who gave me the opportunity to be a Ph.D. student and a pediatrician working in the hospital at the same time. Always being convinced that the fusion of clinical and scientific knowledge is essential for the advances in future medicine, he gave me all necessary guidance and support to become a clinician scientist. Thank you very much for that!

Secondly, I would like to thank Kerstin and Heike for their friendly administrative help. As a lab manager Kerstin has always been my “target” not only for administrative issues but in many cases for scientific questions as well. “Hey-ke”, I love your exotic personality and your humor.

I would also like to thank Elie and Bre, Saverio´s first two talented postdocs in Germany. Both supported me a lot, especially at the beginning when I joined the lab.

I would also like to acknowledge other students and members in the Bellusci lab, Alena, Amit, Matt, Salma, Jana, Negah, Vahid, Sara, Faady, Zvonimir, Johannes and Jamschid. You all are great colleagues and I am really thankful to get the opportunity to work with you. I would like to express my special thanks to Alena, the person who supported me the most in good, bad and worst times. Especially, I would like to thank Jana and Matt for their help in genotyping many mice. You all contributed to the good working atmosphere in the Bellusci lab in which I love to spend time!

Many thanks also to our collaborators Dr. Jennifer Quantius for her help with FACS measurements, Dr. Jochen Wilhelm for performing gene array analyses and Ewa Bieniek for vascular morphometry analyses. I would also like to thank Prof. Dr. Werner Seeger, Dr. Guillermo Barreto, Dr. Gianni Carraro and Dr. Stijn DeLanghe for their advice and constructive criticism. I would also like to acknowledge Dr. Rory Morty, the director of the MBML program, who spent a lot of efforts in explaining me molecular biology.

I also acknowledge Dr. Daniel Zahner and animal caretakers Christian Eng, Martin Stellwagen and Sabrina Schick for their support. They all taught me a lot about mice.

Finally, I would like to thank my parents who supported me unconditionally in any situations. Thank you for their patience and understanding that I did not spend many many weekends with them together. I would also like to thank my brother and sister, who believed in me.

Lastly, I would like to honor all the mice, who have been sacrificed for science. I deeply wish that their lost lives will be paid off one day by preventing sufferance and death in human with diseases.